

**SENSITIVITY ANALYSIS FOR DESIGN
OPTIMIZATION OF METALLIC MICROWAVE
STRUCTURES WITH THE FINITE-DIFFERENCE
FREQUENCY-DOMAIN METHOD**

**SENSITIVITY ANALYSIS FOR DESIGN
OPTIMIZATION OF METALLIC MICROWAVE
STRUCTURES WITH THE FINITE-DIFFERENCE
FREQUENCY-DOMAIN METHOD**

By

MD ARSHADUDDIN HASIB, B. Sc.

A Thesis

Submitted to the School of Graduate Studies

in Partial Fulfillment of the Requirements

for the Degree

Master of Applied Science

McMaster University

© Copyright by Arshad Hasib, April 2008

MASTER OF APPLIED SCIENCE (2008)
(Electrical and Computer Engineering)

McMASTER UNIVERSITY
Hamilton, Ontario

TITLE: **SENSITIVITY ANALYSIS FOR DESIGN
OPTIMIZATION OF METALLIC STRUCTURES
WITH THE FINITE-DIFFERENCE FREQUENCY-
DOMAIN METHOD**

AUTHOR: MD ARSHADUDDIN HASIB
B. Sc. (Electrical & Electronic Engineering),
Bangladesh University of Engineering & Technology.

SUPERVISOR: Dr. Natalia K. Nikolova, Associate Professor
Department of Electrical and Computer Engineering
Dipl. Eng. (Technical University of Varna)
Ph. D. (University of Electro-Communications, Tokyo)
P. Eng. (Ontario)

NUMBER OF PAGES: xiv, 110

ABSTRACT

This thesis contributes significantly towards the development of a robust algorithm for design sensitivity analysis and the optimization of microwave structures. Based on the frequency-domain finite-element method, the approach provides accurate sensitivity information using both 2-D and 3-D formulations. It also significantly accelerates the optimization process.

The design sensitivity analysis method greatly influences the efficiency and accuracy of gradient-based optimization by providing the response gradient (response Jacobians) for the whole range of parameter values. However, common commercial electromagnetic simulators provide only specific engineering responses, such as Z - or S -parameters. No sensitivity information is made available for further exploration of the design-parameter space. It is common to compute the design sensitivities from the response themselves using finite-difference or higher-order approximations at the response level. Consequently, for each design parameter of interest, at least one additional full-wave analysis is performed. However, when the number of design parameters becomes large, the simulation time becomes prohibitive for electromagnetic design procedures.

The self-adjoint sensitivity analysis (SASA) is so far the most efficient way to extract the sensitivity information for the network parameters with the finite-element method. As an improvement of the adjoint-variable method (AVM), it eliminates the additional (adjoint) system analyses. With one single full-wave analysis, the sensitivities with respect to all design parameters are computed. This significantly improves the efficiency of the sensitivity computations. Through our proposed method, the finite-difference frequency-domain self-adjoint sensitivity analysis (FDFD-SASA), the process is further improved by eliminating the need for exporting the system matrix, thus improving both compatibility and computation time. The only requirement for integrating the sensitivity solver with the commercial EM simulators is the ability to access the field solution at the user-defined grid points. The sensitivity information is obtained by simple manipulation of the field solution as a post-process and hence, it adds little or no overhead to the simulation time.

We explore the feasibility of implementing our newly proposed method using field solutions from a frequency-domain commercial solver HFSS v 11. We confirm the accuracy of the FDFD-SASA for shape parameters of metallic structures. Both 2-D and 3-D examples are presented, where the reference results are provided through the traditional finite-difference approximations. Also, the efficiency of the FDFD-SASA is validated by a filter design example, exploiting gradient-based optimization algorithm.

ACKNOWLEDGEMENTS

The author wishes to express his profound gratitude to Dr. Natalia K. Nikolova for her guidance and supervision during the course of his master's study. Her expert advices, valuable opinions as well as all her patience and understanding have greatly influenced him in his study and research at McMaster University. The author is also deeply indebted to her for taking the time to review this work amidst the stress of teaching duties. Working with her has been a great privilege for the author and her pedagogical personality will be a life-long inspiration for his future endeavors.

The author would also like to acknowledge the collaboration and discussions with his colleagues Xiaying Zhu, Reza Khalaj Amineh, Li Liu, Yunpeng Song and Dr. M. H. Bakr at the Computational Electromagnetics Laboratory. Their co-operation and encouragement contribute to a pleasant environment of teamwork.

Last but not the least, the author would like to express his appreciation to his mother, his family and all his friends for all their love, understanding, and support.

CONTENTS

ABSTRACT	iii
ACKNOWLEDGMENTS	v
LIST OF FIGURES	ix
LIST OF TABLES	xiii
LIST OF ACRONYMS	xiv
CHAPTER 1 INTRODUCTION	1
References.....	8
CHAPTER 2 METHODOLOGY OF THE ADJOINT- VARIABLE METHOD AND SELF-ADJOINT SENSITIVITY ANALYSIS	11
2.1 Introduction.....	11
2.2 Frequency-Domain Adjoint-Variable Method...	15
2.3 Difficulties in the AVM Implementation.....	21
2.4 Computer Resources and the Adjoint-Variable Method.....	21
2.5 Finite-Element Method for EM problems.....	23
2.6 Self-Adjoint Sensitivities for <i>S</i> -parameters in the Finite Element Method.....	27

2.7	General Procedures and Software Requirements for SASA.....	33
	References.....	36
CHAPTER 3	FINITE-DIFFERENCE FREQUENCY-DOMAIN SELF-ADJOINT SENSITIVITY ANALYSIS FOR METALLIC STRUCTURES.....	38
3.1	Introduction.....	38
3.2	Overview of Finite-difference frequency domain self-adjoint sensitivities for S - parameters	41
3.3	Self-Adjoint Sensitivities for S -parameters of Metallic Structures (The 2-D Case).....	47
	3.3.1 Yee-Cell Based Approach.....	47
	3.3.2 Central-Node Based Approach.....	52
3.4	Example.....	54
	3.4.1 Six-Section H-Plane Waveguide Filter	54
3.5	Self-Adjoint Sensitivity Analysis for S - parameters of Metallic Structures (The 3-D Case).....	69
	3.5.1 Metallization.....	70
	3.5.2 De-metallization.....	75
	3.5.3 Algorithm for Software Implementation.....	76
3.6	Example.....	78
	3.6.1 Six-Section H-Plane Waveguide Filter	78
	References.....	83

CHAPTER 4	GRADIENT BASED OPTIMIZATION USING FINITE-DIFFERENCE FREQUENCY-DOMAIN SENSITIVITY ANALYSIS.....	85
	4.1 Introduction.....	85
	4.2 Optimization with 2-D FDFD Self-Adjoint Sensitivities.....	88
	4.3 Example.....	89
	4.3.1 Six-Section H-Plane Waveguide Filter..	89
	4.4 Comparison and Conclusion.....	96
	References.....	99
CHAPTER 5	CONCLUSIONS.....	100
	COMPLETE REFERENCE LIST.....	103

LIST OF FIGURES

Figure 2.1	Basic elements in the FEM mesh: a) one-dimensional, b) two-dimensional, c) three-dimensional.....	25
Figure 3.1	Field mapping technique.....	49
Figure 3.2	Locations where the field is needed for the computation of the derivatives with respect to the length of the object in: (a) metallization and (b) de-metallization case.....	51
Figure 3.3	A 2-D cut of the discretization grid used by the finite-element simulator superimposed with the FD grid used by the sensitivity solver for metallic septum. The vertical field component is recorded at grid points indicated by: (i) crosses – in the Yee cell grid; (ii) dots – in the central-node grid.....	53
Figure 3.4	H-plane waveguide filter.....	55
Figure 3.5	Locations for recording the E_y for the derivatives with respect to L_4 (regardless of whether we assume metallization or de-metallization). Grid cell size of the sensitivity grid is set as $\Delta x = \Delta z = \delta$	56
Figure 3.6	The recorded field locations for the derivatives with respect to S_{11}	57
Figure 3.7	The S -parameters of the H-plane filter.....	60
Figure 3.8	The derivatives of $\text{Re} S_{11}$ and $\text{Im} S_{11}$ with respect to L_4 at 7 GHz for the H-plane filter with Yee-cell grid with assumed forward perturbation.....	60

Figure 3.9	The derivatives of $\text{Re}S_{21}$ and $\text{Im}S_{21}$ with respect to L_4 at 7 GHz for the H-plane filter with Yee-cell grid with assumed forward perturbation.....	61
Figure 3.10	The derivatives of $ S_{11} $ and $ S_{21} $ with respect to L_4 at 7 GHz for the H-plane filter with Yee-cell grid with assumed forward perturbation.....	61
Figure 3.11	The derivative of $\angle S_{11}$ with respect to L_4 at 7 GHz for the H-plane filter with Yee-cell grid with assumed forward perturbation.....	62
Figure 3.12	The derivative of $\angle S_{21}$ with respect to L_4 at 7 GHz for the H-plane filter with Yee-cell grid with assumed forward perturbation.....	62
Figure 3.13	Comparison of the derivatives of $ S_{11} $ with respect to L_4 at 7 GHz for the H-plane filter with Yee-cell grid with both assumed forward and backward perturbation.....	63
Figure 3.14	The derivatives of $\text{Re}S_{11}$ and $\text{Im}S_{21}$ with respect to S_1 at 7 GHz for the H-plane filter with Yee-cell grid with assumed increase of S_1	63
Figure 3.15	The derivatives of $ S_{11} $ and $ S_{21} $ with respect to S_1 at 7 GHz for the H-plane filter Yee-cell grid with assumed increase of S_1	64
Figure 3.16	The derivatives of $\text{Re}S_{11}$ and $\text{Im}S_{11}$ with respect to L_4 at 7 GHz for the H-plane filter with central-node grid for assumed forward perturbation.....	64
Figure 3.17	The derivatives of $\text{Re}S_{21}$ and $\text{Im}S_{21}$ with respect to L_4 at 7 GHz for the H-plane filter with central-node grid for assumed forward perturbation.....	65
Figure 3.18	The derivatives of $ S_{11} $ and $ S_{21} $ with respect to L_4 at 7 GHz for the H-plane filter with central-node grid for assumed forward perturbation.....	65

Figure 3.19	The derivative of $\angle S_{11}$ with respect to L_4 at 7 GHz for the H-plane filter with central-node grid for assumed forward perturbation.....	66
Figure 3.20	The derivative of $\angle S_{21}$ with respect to L_4 at 7 GHz for the H-plane filter with central-node grid for assumed forward perturbation.....	66
Figure 3.21	Comparison of the derivatives of $ S_{11} $ and $ S_{21} $ with respect to L_4 at 7 GHz for the H-plane filter with central-node grid for both assumed forward and backward perturbation.....	67
Figure 3.22	The derivatives of $\text{Re} S_{11}$ and $\text{Im} S_{21}$ with respect to S_1 at 7 GHz for the H-plane filter with central-node grid for assumed increase of S_1	67
Figure 3.23	The derivatives of $ S_{11} $ and $ S_{21} $ with respect to S_1 at 7 GHz for the H-plane filter with central-node grid for assumed increase of S_1	68
Figure 3.24	Comparison of the derivative of $\text{Re} S_{11}$ with respect to S_1 at 7 GHz for the H-plane filter with both Yee-cell and central-node grid for assumed increase of S_1	68
Figure 3.25	Numerical calculation of $D_{zx} E_z$	71
Figure 3.26	Node locations for the numerical calculation of $D_{yy} E_\xi$ ($\xi = x, z$)	72
Figure 3.27	Locations at which the double curl operator \square^2 is affected by change of fields due to metallization in the x direction..	73
Figure 3.28	The derivative of $\text{Re} S_{11}$ and $\text{Im} S_{11}$ with respect to L_4 at 7 GHz for the H-plane filter with 3-D central-node grid for assumed forward perturbation.....	79
Figure 3.29	The derivative of $\text{Re} S_{21}$ and $\text{Im} S_{21}$ with respect to L_4 at 7 GHz for the H-plane filter with 3-D central-node grid for assumed forward perturbation.....	79

LIST OF FIGURES

Figure 3.30	The derivative of $ S_{11} $ and $ S_{21} $ with respect to L_4 at 7 GHz for the H-plane filter with 3-D central-node grid for assumed forward perturbation.....	80
Figure 3.31	The derivative of $\angle S_{11}$ with respect to L_4 at 7 GHz for the H-plane filter with 3-D central-node grid for assumed forward perturbation.....	80
Figure 3.32	The derivative of $\angle S_{21}$ with respect to L_4 at 7 GHz for the H-plane filter with 3-D central-node grid for assumed forward perturbation.....	81
Figure 3.33	Comparison of 3-D sensitivity analyses with forward and backward perturbation.....	81
Figure 4.1	Six-section H-plane filter.....	92
Figure 4.2	$ S_{11} $ with respect to frequency at initial design and optimal design with two parameters	93
Figure 4.3	Parameter step size vs. optimization iterations in the TR-minimax optimization of the H-plane filter with two parameters	93
Figure 4.4	Objective function vs. optimization iterations in the TR-minimax optimization of the H-plane filter with two parameters	94
Figure 4.5	$ S_{11} $ with respect to frequency at initial design and optimal design with four parameters.....	94
Figure 4.6	Parameter step size vs. optimization iterations in the TR-minimax optimization of the H-plane filter with four parameters.....	95
Figure 4.7	Objective function vs. optimization iterations in the TR-minimax optimization of the H-plane filter with four parameters.....	95

LIST OF TABLES

TABLE 2.1	Computational resource comparison between the FD and the AVM.....	23
TABLE 3.1	The nominal design parameter values. (All dimensions in mm).....	55
TABLE 4.1	Optimal designs using different sensitivity analysis methods with TR-minimax (2 variables).....	97
TABLE 4.2	Optimal designs using different sensitivity analysis methods with TR-minimax (4 variables).....	97
TABLE 4.3	Number of iterations and time comparison between the different optimization methods (2 variables).....	97
TABLE 4.4	Number of iterations and time comparison between the different optimization methods (4 variables).....	97

LIST OF ACRONYMS

AVM	Adjoint Variable Method
BFD	Backward Finite-Difference
CFD	Central Finite-Difference
EM	Electromagnetics
FD	Finite-Difference
FDFD	Finite-Difference Frequency-Domain
FDTD	Finite-Difference Time-Domain
FEM	Finite Element Method
FFD	Forward Finite-Difference
MoM	Method of Moment
SASA	Self-adjoint Sensitivity Analysis
SQP	Sequential Quadratic Programming
TLM	Transmission-Line Method
TR	Trust Regions

CHAPTER 1

INTRODUCTION

Since the inception of a variety of numerical techniques, design sensitivity analysis has begun playing an important role in electromagnetic (EM) system analysis due to its importance in improving system performance. The design sensitivity aims at the evaluation of the response derivatives with respect to the design parameters. In microwave design, these are typically shape and constitutive parameters. The sensitivities, together with the responses, greatly extend our knowledge of the system behavior in the design parameter space. The overall design process, including design optimization, yield and tolerance analysis, as well as statistical analysis, can greatly benefit from the knowledge of the sensitivity information [1]. Sensitivity analysis techniques are crucial, especially in numerical microwave problems where analytical sensitivity solutions are impossible. Moreover, when the problem is large, the numerical simulation may become time intensive to an extent, which often makes the design cycle prohibitively slow. To address this problem, we focus on the extraction of the

sensitivities from the field solution with as little computational overhead as possible.

The adjoint-variable method (AVM) is the most efficient method for the sensitivity analysis of complex linear and nonlinear problems [1], [2]. The AVM has a history of applications in the area of control theory [1], as well as in finite-element analysis in structural [1], [3] and electrical [4], [5], [6], [7], [8], [9] engineering. The application of the AVM in the microwave area emerges in the early 1970's with the computation of the network sensitivities based on voltage/current state variables and responses [5], [6], [7], [8], [10]. Yet, the computation is based on Tellegen's theory of circuits, not field solutions.

Recently, an adjoint-variable method has been proposed for the sensitivity computation in numerical electromagnetic (EM) problems both in the time domain (the transmission line method, TLM, [11], and the finite-difference time-domain (FDTD) method, [12]) as well as in the frequency domain (the frequency domain TLM [13], [14], the method of moments, MoM [15], and the finite-element method, FEM [16], [17], [18]). Its efficiency in terms of computer time is orders of magnitude better compared to derivative estimations using finite-difference or higher order approximations at the response level. All traditional AVM techniques require one additional full-wave analysis (the adjoint system analysis) in addition to the original system analysis. Moreover, the excitation in the adjoint system analysis depends on the response and its relation to the solution

of the original problem. This may cause potential difficulties in the formulation of the adjoint analysis, and especially its implementation in the framework of a commercial high-frequency CAD package. This limits applications to specially developed in-house numerical codes. Another major drawback of the traditional exact AVM is the need to compute the system matrix derivatives. The analytical computation of the system matrix derivatives, especially with existing commercial codes, is deemed unfeasible [15]. In frequency-domain applications, the finite-difference approximations of the system matrix derivatives were attained using either finite differences via parameter perturbations [15] or discrete step-wise changes [12], [19].

Recently a method to calculate the so-called adjoint solution directly from the original EM system solution (first discussed in Akel *et al.* [16], in the case of the FEM formulation based on the tetrahedral edge elements) was devised [20], [21]. This method, also called self-adjoint sensitivity analysis, reduces the time for the Jacobian computation by half and at the same time improves applicability by removing the need to perform an adjoint-problem simulation. With this approach, we eliminate the additional (adjoint) system analysis and further improve the efficiency of the sensitivity computation [20], [21]. The computational load is significantly reduced without sacrificing the accuracy.

However, the first self-adjoint formulations [16], [18] pose difficulties in implementation since they need access to the system matrix built by the simulator.

Commercial EM simulators rarely allow such access. Where available, the matrix export is inefficient since large amount of data must be stored on the hard disk. Thus, the last major obstacle in the way of developing a practical EM sensitivity-analysis tool has been the dependence of the sensitivity solver on the discretization scheme and the grid used by the simulator.

In this thesis, the application of a novel self-adjoint sensitivity algorithm based on the finite-difference frequency-domain (FDFD) method, named finite-difference frequency-domain self-adjoint sensitivity analysis (FDFD-SASA), is proposed for the sensitivity analysis of microwave network parameters, i.e., S -parameters, of metallic structures. With a commercial high-frequency FEM solver, this standalone algorithm runs independently of the underlying analysis algorithm. It generates its own uniform finite-difference grid. To obtain the adjoint solutions, it uses the self-adjoint constants given in [20]. The only information it needs is the field solution at specific grid points. Thus, it can be easily integrated into any kind of design automation process with a commercial solver.

In this thesis, for the first time the possibility of using central-node formulation for metallic objects is proposed and investigated. The central-node formulation was first proposed in [22] for the case of dielectric objects and time-domain solutions. There, it was shown that a central-node grid yields more accurate sensitivities in comparison with a finite-difference grid based on the Yee-cell. Later, it was applied to the case of dielectric objects and frequency domain

solutions [23]. In contrast, metallic objects are better fitted to the Yee-cell grid as the boundary conditions for the tangential \mathbf{E} -field components are satisfied exactly. However, the staggered nature of the Yee-cell complicates the implementation in the three-dimensional (3-D) case. In comparison, the central-node grid assumes that all three \mathbf{E} -field components are co-located, which makes the realization much simpler. Here, both the 2-D and 3-D central-node formulations with metallic objects are proposed and investigated.

The most promising application of the SASA is in the area of gradient-based optimization [2], [3], [24]. Gradient-based optimization is widely used to solve nonlinear design and inverse-imaging problems [1], [2], [3]. The optimization process can be significantly accelerated with the Jacobian provided by the SASA, since the computation of the Jacobian and/or Hessian is the bottleneck of the optimization efficiency with full-wave EM solvers.

In this thesis, the advantage of the FDFD-SASA is validated by its application in gradient-based optimization of metallic structures. A metallic bandpass filter has been optimized using FDFD-SASA and forward finite-difference (FFD) Jacobians. The time savings realized by employing FDFD-SASA is demonstrated. The improved accuracy of the Jacobian also leads to improved convergence of the optimization process. Since there is no need to calculate analytical system matrix derivatives and there is no need for an adjoint simulation, the computational load of the Jacobian calculation is practically zero.

Chapter 2 introduces the basics of the adjoint-variable methodology. We review the basic sensitivity expression of the AVM and discuss its implementation in the sensitivity analysis of complex linear systems. The computational overhead of the traditional AVM is analyzed and compared with the overhead of the finite-difference approximation. It also introduces the SASA approach in the frequency domain and comments on its general advantages.

Chapter 3 explores the FDFD-SASA method and its application to S -parameter sensitivity computation for microwave structures using both Yee-cell and central-node approaches. A formulation for 3-D sensitivity analysis of metallic objects is provided for the first time. These algorithms are validated by a rectangular waveguide bandpass filter example. Comparisons with the traditional finite-difference approximation are provided.

Chapter 4 integrates the SASA method with the framework of gradient-based optimization. The FDFD-SASA method is validated through an optimization example. The convergence of the optimization using this method is compared with that using the finite differences at the response level.

An overall conclusion is made in Chapter 5 and suggestions for future developments are given.

The contributions of this research can be summarized as follows:

- (1) Application of the Yee-cell based sensitivity algorithm in the frequency domain with 2-D metallic structures.

- (2) Development of an efficient central-node based sensitivity computation algorithm with the finite-element method that integrates sensitivity calculation for both dielectric and metallic structures in 2-D, i.e., FDFD-SASA [25], [26].
- (3) Development of a central node based algorithm for 3-D sensitivity analysis and hence completing the true applicability of our FDFD-SASA method to all types of structures regardless of shape and material.
- (4) Implementation of the FDFD-SASA algorithm with the commercial finite-element solver HFSS[®] [25], [26], [27].
- (5) Validation of the efficiency of FDFD-SASA through numerical design example [25].
- (6) Application of the sensitivity algorithm in gradient-based optimization [26].

REFERENCES

- [1] D. G. Cacuci, *Sensitivity & Uncertainty Analysis, Volume 1: Theory*. Boca Raton, FL: Chapman & Hall/CRC, 2003.
- [2] A. D. Belegundu and T. R. Chandrupatla, *Optimization Concepts and Applications in Engineering*. Upper Saddle River, NJ: Prentice Hall, 1999.
- [3] E. J. Haug, K. K. Choi and V. Komkov, *Design Sensitivity Analysis of Structural Systems*. Orlando: Academic Press Inc., 1986.
- [4] S. W. Director and R. A. Rohrer, "The generalized adjoint network and network sensitivities," *IEEE Trans. Circuit Theory*, vol. CT-16, pp.318-323, Aug. 1969.
- [5] J. W. Bandler and R. E. Seviora, "Current trends in network optimization," *IEEE Trans. Microwave Theory Tech.*, vol. MTT-18, pp.1159-1170, Dec. 1970.
- [6] V. A. Monaco and P. Tiberio, "Computer-aided analysis of microwave circuits," *IEEE Trans. Microwave Theory Tech.*, vol. MTT-22, pp.249-263, Mar. 1974.
- [7] J. W. Bandler, "Computer-aided circuit optimization," in *Modern Filter Theory and Design*, G. C. Temes and S. K. Mitra, Eds. New York: Wiley, ch. 6, 1973.
- [8] K. C. Gupta, R. Garg, and R. Chadha, *Computer-Aided Design of Microwave Circuits*. Norwood, MA: Artech House, 1981.
- [9] J. Vlach and K. Singhal, *Computer Methods for Circuit Analysis and Design*. New York: Van Nostrand, 1983.
- [10] J. W. Bandler and R. E. Seviora, "Wave sensitivities of networks," *IEEE Trans. Microwave Theory Tech.*, vol. MTT-20, pp. 138-147, Feb. 1972.
- [11] M. H. Bakr and N. K. Nikolova, "An adjoint variable method for time-domain TLM with wide-band Johns matrix boundaries," *IEEE Trans. Microwave Theory Tech.*, vol. 52, pp. 678-685, Feb. 2004.
- [12] N. K. Nikolova, H. W. Tam, and M. H. Bakr, "Sensitivity analysis with the FDTD method on structured grids," *IEEE Trans. Microwave Theory Tech.*, vol. 52, pp. 1207-1216, Apr. 2004.
- [13] M. H. Bakr and N. K. Nikolova, "An adjoint variable method for frequency domain TLM problems with conducting boundaries," *IEEE Microwave and Wireless Component Letters*, vol. 13, pp. 408-410, Sept. 2003.

- [14] S. M. Ali, N. K. Nikolova, and M. H. Bakr, "Central adjoint variable method for sensitivity analysis with structured grid electromagnetic solvers," *IEEE Trans. Magnetics*, vol. 40, pp. 1969-1971, Jul. 2004.
- [15] N. K. Georgieva, S. Glavic, M. H. Bakr, and J. W. Bandler, "Feasible adjoint sensitivity technique for EM design optimization," *IEEE Trans. Microwave Theory Tech.*, vol. 50, pp. 2751-2758, Dec. 2002.
- [16] H. Akel and J. P. Webb, "Design sensitivities for scattering-matrix calculation with tetrahedral edge elements," *IEEE Trans. Magnetics*, vol. 36, pp. 1043-1046, Jul. 2000.
- [17] Hong-bae Lee and T. Itoh, "A systematic optimum design of waveguide-to-microstrip transition," *IEEE Trans. Microwave Theory Tech.*, vol. 45, pp. 803-809, May 1997.
- [18] N. K. Nikolova, J. Zhu, D. Li, M. Bakr, and J. Bandler, "Sensitivities of network parameters with electromagnetic frequency domain simulator," *IEEE Trans. Microwave Theory Tech.* vol. 54, pp. 670-681, Feb. 2006.
- [19] S. M. Ali, N. K. Nikolova and M. H. Bakr, "Recent advances in sensitivity analysis with frequency-domain full-wave EM solvers," *Appl. Comput. Electromagn. Soc. J.*, vol. 19, pp. 147-154, Nov. 2004.
- [20] N. K. Nikolova, J. Zhu, D. Li, M. Bakr, and J. Bandler, "Sensitivities of network parameters with electromagnetic frequency domain simulator," *IEEE Trans. Microwave Theory Tech.* vol. 54, pp. 670-681, Feb. 2006.
- [21] N. K. Nikolova, Ying Li, Yan Li, and M. H. Bakr, "Sensitivity analysis of scattering parameters with electromagnetic time-domain simulators," *IEEE Trans. Microw. Theory Tech.*, vol. 54, pp. 1589-1610, Apr. 2006.
- [22] Y. Song and N. K. Nikolova, "Central-node approach for accurate self-adjoint sensitivity analysis of dielectric structures," *IEEE MTT-S Int. Microwave Symposium*, pp. 895-898, June 2007.
- [23] X. Zhu, A. Hasib, and N. K. Nikolova, "Electromagnetic sensitivity analysis of scattering parameters based on the FDFD method," *Int. Symp. on Signals, Systems, and Electronics (ISSSE 2007)*, pp. 165-168, July-Aug. 2007.
- [24] N. K. Nikolova, R. Safian, E. A. Soliman, M. H. Bakr and J. Bandler, "Accelerated gradient based optimization using adjoint sensitivities," *IEEE Trans. Antenna Propagat.*, vol. 52, pp. 2147-2157, Aug. 2004.
- [25] N. K. Nikolova, A. Hasib, and X. Zhu, "Independent sensitivity solver based on the frequency domain finite difference method," *The 24th Int. Review of Progress in Applied Computational Electromagnetics (ACES 2008)*, pp. 1024-1029, March-Apr. 2008.

- [26] X. Zhu, A. Hasib, N. K. Nikolova and M. H. Bakr, "Efficient electromagnetic optimization using self-adjoint jacobian computation based on a central-node FDFD method," *Int. Microwave Symposium (IMS 2008)*, June 2008.
- [27] Ansoft HFSS ver. 11, Ansoft Corporation, 225 West Station Square Drive, Suite 200, Pittsburgh, PA 15219, USA, 2006, www.ansoft.com.

CHAPTER 2

METHODOLOGY OF THE ADJOINT VARIABLE METHOD AND SELF ADJOINT SENSITIVITY ANALYSIS

2.1 INTRODUCTION

The importance of the design sensitivity analysis of distributed systems stems from the need to improve their performance or to know their uncertainties. The design sensitivity comprises the response derivatives with respect to shape or material parameters. Manufacturing and yield tolerances, design of experiments and models, design optimization, etc., are aspects of the overall design, which can greatly benefit from the availability of the response sensitivity.

Commercial high-frequency electromagnetic (EM) solvers usually do not compute sensitivity information, i.e., the Jacobian of the objective function, with respect to the design parameters. For design purposes, when sensitivity

information is required, a finite-difference approximation at the response level is usually performed as a simple although inefficient way to obtain the response derivatives. The finite-difference approximation is highly inefficient in numerical computations, since it requires at least $N+1$ additional full system analyses for a problem with N designable parameters [1]. With higher-order approximations, the number of analyses increases. The feasibility of this approach becomes questionable when the design-variable space is large.

The adjoint-variable method (AVM) is proved to be the most efficient method for sensitivity analysis [2], [3], [4] as it requires only one additional system analysis to compute all sensitivities. The additional analysis is known as adjoint system analysis, with the adjoint system matrix being the transpose of the system matrix of the original problem [1], [3], [4]. Thus, the AVM improves the efficiency of the sensitivity computation by a factor of N in comparison with the forward or backward finite-difference approximations. The performance of the AVM has been validated in control theory [2], [3], structural engineering [3], [4], and in circuit and computational EM applications in electrical engineering [5]. Yet, feasible implementations remain a challenge. The reason lies mainly in the complexity of these techniques.

A simpler and more versatile approach has been adopted in [6], [7], [8] for analyses in the frequency domain. The effort to formulate analytically the system matrix derivative — an essential component of the sensitivity formula — was

abandoned as impractical for a general purpose sensitivity solver. Instead, approximations of the system-matrix derivatives are employed using finite differences [8] or step-wise parameter changes in conjunction with a 2nd-order sensitivity formula [6], [7]. Neither the accuracy nor the computational speed are sacrificed.

All of the above approaches require the analysis of an adjoint problem whose excitation is response dependent. Not only does this mean one additional full-wave simulation but it also requires modification of the electromagnetic (EM) analysis engine due to the specifics of the adjoint-problem excitation. Notably, Akel *et al.* [9] have pointed out that in the case of the FEM with tetrahedral edge elements, the sensitivity of the S -matrix can be derived without an adjoint simulation.

In this chapter, we give a brief introduction into the methodology of the AVM, especially its applications with frequency-domain numerical EM solvers. Most of the discussion in this chapter and in the rest of the thesis focuses on applications with the finite-element method (FEM). We also discuss a general self-adjoint approach to the sensitivity analysis of network parameters of the linear problem in the frequency domain, which is at the core of a number of commercial high-frequency simulators. These standalone algorithms can be incorporated in an automated design to perform optimization, modeling, or

tolerance analysis of high-frequency structures with any commercial solver, which exports the system matrix and the solution vector.

In Section 2.2, we present the concept of the frequency-domain AVM for linear systems followed by a general discussion on the sensitivity analysis of complex linear systems. Section 2.3 discusses the difficulties in the implementation of the AVM with commercial solvers. The efficiency and the required computational resources are discussed in Section 2.4 along with a comparison with the finite-difference approximation at the response level. The advantages and the drawbacks of the AVM are also discussed. In Section 2.5, we briefly introduce the formulation of the finite-element method. Then in Section 2.6, we introduce the definition of a self-adjoint problem and show the self-adjoint formulas for network-parameter sensitivity calculations, particularly for the S -parameter sensitivities, based on the finite-element method. Section 2.7 outlines the features of the commercial FEM solvers, which enable independent network-parameter sensitivity analysis, and gives a general procedure for the implementation of the SASA with commercial software.

2.2 FREQUENCY-DOMAIN ADJOINT-VARIABLE METHOD

After proper discretization, a time-harmonic linear EM problem (by linear, we refer to the fact that the problem has linear material properties) can be written as a linear system of equations [6]:

$$\mathbf{A}\mathbf{x}=\mathbf{b}. \quad (2.1)$$

Here, \mathbf{A} is the M by M system matrix, \mathbf{x} is the 1 by M state variable vector, e.g., the \mathbf{E} -field solution vector, and \mathbf{b} is the 1 by M excitation vector, which can be derived from the electromagnetic sources and the inhomogeneous boundary conditions. The system matrix is a function of the vector of design (shape or material) parameters \mathbf{p} , i.e., $\mathbf{A}(\mathbf{p})$. Thus, the field solution \mathbf{x} is an implicit function of \mathbf{p} .

For sensitivity analysis purposes, we need to determine the gradient of a user defined response function $f(\mathbf{p},\mathbf{x}(\mathbf{p}))$ with respect to \mathbf{p} at the field solution \mathbf{x} of (2.1):

$$\nabla_{\mathbf{p}}f(\mathbf{p},\mathbf{x}(\mathbf{p})) \text{ subject to } \mathbf{A}\mathbf{x}=\mathbf{b}. \quad (2.2)$$

Here, the gradient of the response function $f(\mathbf{p},\mathbf{x}(\mathbf{p}))$ is defined as a row vector [4], [6]

$$\nabla_{\mathbf{p}}f=\left[\frac{\partial f}{\partial p_1} \quad \frac{\partial f}{\partial p_2} \quad \dots \quad \frac{\partial f}{\partial p_N}\right]. \quad (2.3)$$

Note that the response function $f(\mathbf{p}, \mathbf{x}(\mathbf{p}))$ is formulated so that it may have an explicit dependence on the design variables in addition to its implicit dependence on \mathbf{p} through \mathbf{x} . In some situations, both dependencies exist.

We first constrain our problem as a real-number problem, i.e., both the system matrix $\mathbf{A}(\mathbf{p})$ and the response function $f(\mathbf{p}, \mathbf{x}(\mathbf{p}))$ are real. The sensitivity analysis with complex numbers is discussed next.

According to [10], an AVM sensitivity expression can be formulated as:

$$\nabla_{\mathbf{p}} f = \nabla_{\mathbf{p}}^e f + \hat{\mathbf{x}}^T [\nabla_{\mathbf{p}} \mathbf{b} - \nabla_{\mathbf{p}} (\mathbf{A}\bar{\mathbf{x}})]. \quad (2.4)$$

where $\bar{\mathbf{x}}$ is the system solution. The ‘bar’ emphasizes that $\bar{\mathbf{x}}$ is not subject to differentiation in the $\nabla_{\mathbf{p}} (\mathbf{A}\bar{\mathbf{x}})$ term. Here, we divide the gradient of the response function into two parts:

$$\nabla_{\mathbf{p}} f = \nabla_{\mathbf{p}}^e f + \nabla_{\mathbf{x}} f \cdot \nabla_{\mathbf{p}} \mathbf{x}. \quad (2.5)$$

$\nabla_{\mathbf{p}}^e f$ stands for the explicit dependence of the response function f on the design variables \mathbf{p} , and $\nabla_{\mathbf{x}} f \cdot \nabla_{\mathbf{p}} \mathbf{x}$ reflects the implicit dependence on \mathbf{p} through the field solution \mathbf{x} . $\nabla_{\mathbf{p}} \mathbf{x}$ is defined as:

$$\nabla_{\mathbf{p}} \mathbf{x} = \begin{bmatrix} \frac{\partial x_1}{\partial p_1} & \dots & \frac{\partial x_1}{\partial p_N} \\ \dots & \dots & \dots \\ \frac{\partial x_M}{\partial p_1} & \dots & \frac{\partial x_M}{\partial p_N} \end{bmatrix}. \quad (2.6)$$

The vector $\hat{\mathbf{x}}$ is the adjoint solution, which is the solution of the adjoint system of equations [4], [10]:

$$\mathbf{A}^T \hat{\mathbf{x}} = [\nabla_{\mathbf{x}} f]^T. \quad (2.7)$$

The adjoint system excitation is

$$\hat{\mathbf{b}} = [\nabla_{\mathbf{x}} f]^T. \quad (2.8)$$

Here, we need to compute the original system solution $\bar{\mathbf{x}}$, the adjoint system solution $\hat{\mathbf{x}}$, and the derivative of the system matrix with respect to each design variable $\partial \mathbf{A} / \partial p_i$, $i=1, \dots, N$. Thus, with only two full-wave simulations, namely, the original system simulation and the adjoint system simulation, we can compute the sensitivities.

It is important to notice that we need to compute the system matrix derivative with respect to each design parameter $\partial \mathbf{A} / \partial p_i$, $i=1, \dots, N$. In some rare cases, the matrix derivatives may be analytically available [12], [13]. Then, the sensitivities are exact. According to [12], the time needed for the analytical computation of one system matrix derivative is comparable with one system matrix fill. Thus, the sensitivity computation of a problem with N design parameters leads to an overhead of N matrix fills in addition to the original and adjoint system analyses.

For most of the full-wave EM analysis methods, the system matrix derivatives are either not analytically available or too complicated to be

analytically derived for general design software. In these cases, the system matrix derivatives are computed by the finite-difference approximation [14]:

$$\frac{\partial \mathbf{A}(\mathbf{p})}{\partial p_i} = \frac{\mathbf{A}(\mathbf{p} + \Delta p_i \cdot \mathbf{e}_i) - \mathbf{A}(\mathbf{p})}{\Delta p_i}, \quad i = 1, \dots, N. \quad (2.9)$$

Here, \mathbf{e}_i is the unit vector whose i th element equals 1 and all others equal 0:

$$\mathbf{e}_i = \begin{bmatrix} 0 \\ \vdots \\ 1 \\ \vdots \\ 0 \end{bmatrix} \text{ } i\text{th element} \quad (2.10)$$

and Δp_i is the finite-difference perturbation of the i th design variable. This approximation also requires N additional matrix fills, similarly to the exact method. Our studies have shown that the accuracy for the sensitivity computation using this system-matrix-level finite-difference approximation is satisfactory, with a relative error well below 1%, compared with the exact sensitivity computation [1].

The derivations in the above section apply to real-number problems only. However, in electromagnetic frequency-domain sensitivity analysis, the system equations are complex, and, often, the responses are complex, too. It can be shown that the sensitivity formula in the complex case can be derived from the real-number sensitivity formula.

A complex linear system of equations in the form of (2.1) can be reformulated in a real-valued form [14]:

$$\begin{bmatrix} \Re A & -\Im A \\ \Im A & \Re A \end{bmatrix} \begin{bmatrix} \Re x \\ \Im x \end{bmatrix} = \begin{bmatrix} \Re b \\ \Im b \end{bmatrix}. \quad (2.11)$$

Here, \Re and \Im stand for the real and the imaginary parts of a matrix, respectively. We can re-write (2.11) as

$$\mathbf{A}_r \mathbf{x}_r = \mathbf{b}_r \quad (2.12)$$

where

$$\mathbf{A}_r = \begin{bmatrix} \Re A & -\Im A \\ \Im A & \Re A \end{bmatrix}, \quad \mathbf{x}_r = \begin{bmatrix} \Re x \\ \Im x \end{bmatrix}, \quad \mathbf{b}_r = \begin{bmatrix} \Re b \\ \Im b \end{bmatrix}. \quad (2.13)$$

The size of the real-valued system of equations is twice the size of the complex-valued one.

With this real-valued system of equations, the AVM sensitivity expression for a real-valued response f becomes:

$$\nabla_p f = \nabla_p^e f + \hat{\mathbf{x}}_r^T [\nabla_p \mathbf{b}_r - \nabla_p (\mathbf{A}_r \bar{\mathbf{x}}_r)]. \quad (2.14)$$

Here, $\hat{\mathbf{x}}_r$ is the solution of the corresponding adjoint system of equations

$$\mathbf{A}_r^T \hat{\mathbf{x}}_r = \hat{\mathbf{b}}_r = [\nabla_{\mathbf{x}_r} f]^T. \quad (2.15)$$

The real-valued adjoint system excitation $\hat{\mathbf{b}}_r$ is

$$[\nabla_{\mathbf{x}_r} f]^T = [\nabla_{\Re x} f \quad \nabla_{\Im x} f]^T. \quad (2.16)$$

The adjoint system of equations can be written in a complex form as

$$\mathbf{A}^H \hat{\mathbf{x}} = \hat{\mathbf{b}} = [\nabla_{\mathbf{x}} f]^H \quad (2.17)$$

where $\nabla_{\mathbf{x}} f = \nabla_{\Re x} f + j \nabla_{\Im x} f$.

Note that here we use the Hermitian transpose of \mathbf{A} , which is the complex conjugate transpose. For complex matrices, the Hermitian transpose has analogous properties as those of the direct transpose for real-number matrices. Thus, with equation (2.17), we can write the AVM sensitivity expression in its complex form [6]:

$$\nabla_{\mathbf{p}} f = \nabla_{\mathbf{p}}^e f + \Re\{\hat{\mathbf{x}}^H [\nabla_{\mathbf{p}} \mathbf{b} - \nabla_{\mathbf{p}} (\mathbf{A}\bar{\mathbf{x}})]\}. \quad (2.18)$$

Usually, the response function is also complex, i.e.

$$f = f_R + jf_I. \quad (2.19)$$

Here, f_R and f_I represent the real and imaginary parts of f . In most of the cases, the response function is analytic, i.e., it satisfies the Cauchy-Riemann equations [15]:

$$\begin{aligned} \nabla_{\Re \mathbf{x}} f_R &= \nabla_{\Im \mathbf{x}} f_I = \Re \nabla_{\mathbf{x}} f \\ -\nabla_{\Im \mathbf{x}} f_R &= \nabla_{\Re \mathbf{x}} f_I = \Im \nabla_{\mathbf{x}} f. \end{aligned} \quad (2.20)$$

In these cases, the AVM sensitivity formula becomes [6], [10]:

$$\nabla_{\mathbf{p}} f = \nabla_{\mathbf{p}}^e f + \hat{\mathbf{x}}^H [\nabla_{\mathbf{p}} \mathbf{b} - \nabla_{\mathbf{p}} (\mathbf{A}\bar{\mathbf{x}})]. \quad (2.21)$$

Still, as in the real-number cases, we only require one additional adjoint system analysis to compute the full sensitivity information.

In some rare cases, the response functions are complex but not analytic [6]. In this situation [8], we must perform two separate AVM sensitivity analyses for the real and the imaginary parts of the response function:

$$\nabla_{\mathbf{p}} f_R = \nabla_{\mathbf{p}}^e f_R + \Re \left\{ \hat{\mathbf{x}}_R^H \left[\nabla_{\mathbf{p}} \mathbf{b} - \nabla_{\mathbf{p}} (A\bar{\mathbf{x}}) \right] \right\} \quad (2.22)$$

$$\nabla_{\mathbf{p}} f_I = \nabla_{\mathbf{p}}^e f_I + \Re \left\{ \hat{\mathbf{x}}_I^H \left[\nabla_{\mathbf{p}} \mathbf{b} - \nabla_{\mathbf{p}} (A\bar{\mathbf{x}}) \right] \right\} \quad (2.23)$$

where $\hat{\mathbf{x}}_R$ is the solution of the real-part adjoint problem,

$$A^H \hat{\mathbf{x}}_R = \nabla_{\Re \mathbf{x}} f \quad (2.24)$$

and $\hat{\mathbf{x}}_I$ is the solution of the imaginary-part adjoint problem,

$$A^H \hat{\mathbf{x}}_I = \nabla_{\Im \mathbf{x}} f. \quad (2.25)$$

2.3 DIFFICULTIES IN THE AVM IMPLEMENTATION

As stated above, commercial EM solvers cannot compute sensitivities. The major difficulty that prevents the integration of the AVM in commercial full-wave EM solvers is the unavailability of the system matrix derivatives with respect to the design parameters $\partial A / \partial p_i$, $i=1, \dots, N$. The computation of the system matrix derivatives involves complicated manipulation of the mesh structure even when using a finite-difference approximation.

2.4 COMPUTER RESOURCES AND THE ADJOINT-VARIABLE METHOD

The sensitivity analysis using response level finite-difference approximations is equivalent to N additional full-wave analyses. Each full-wave analysis consists of two stages of calculations. The first stage involves the matrix

fill, and the second one involves solving the system of equations (2.1). The latter often involves the LU decomposition of the system matrix and the forward and backward substitutions. Iterative linear-system solvers are preferred when the system matrix is very large. Each of these stages is repeated N times if forward (or backward) finite-difference approximations are used at the response level for the purpose of sensitivity analysis.

For sensitivity analysis using the AVM, only one additional full-wave analysis is performed. For this additional adjoint system analysis, a matrix fill is not required, as the system matrix of the adjoint problem is the transpose of the original one. The computational time required to transpose a matrix is negligible. Thus, the overhead related to this additional analysis is only the time and memory required to solve (2.17). This overhead may actually be minimal if the original problem (2.1) has already been solved by LU decomposition and the L and U factors are re-used in the solution of (2.17) [10].

The remaining overhead of the AVM is to compute the sensitivity with respect to each design parameters using (2.21). This also involves two steps: 1) the computation of the system matrix derivatives using (2.9), which is equivalent to a matrix fill for each perturbed system of equations, i.e. $A(\mathbf{p} + \Delta p_i \cdot \mathbf{e}_i)$, and 2) the calculation of the AVM sensitivity expression (2.21).

We compare the overhead of the sensitivity analysis using the traditional finite-difference (FD) approximation at the response level, and that of the AVM, for a problem with N design parameters in Table 2.1.

TABLE 2.1
COMPUTATIONAL RESOURCE COMPARISON BETWEEN THE FD
METHOD AND THE AVM

Method	Matrix fills	System solutions	Sensitivity formula computation
FD	N	N	0
AVM	N	1	N

For problems with FEM formulation, the system matrix is often sparse due to the nature of the numerical method. Thus, the time required by a matrix fill is usually far less than the time required by a system solution, especially for an electrically large problem. Also, the time required for the calculation of the sensitivity formula (2.21) is negligible compared with the other two computations. Thus, the AVM is significantly more efficient than the traditional FD method.

2.5 FINITE-ELEMENT METHOD FOR EM PROBLEMS

The FEM is a numerical technique for obtaining approximate solutions to boundary-value problems of mathematical physics. The FEM was first introduced in the 1950's, mainly in the structural design area. Through more than 50 years of development, FEM has been widely applied in all kinds of areas such as

mechanical engineering, structural engineering, thermal dynamic engineering, as well as electrical engineering. The FEM has been recognized as a general method widely applicable to engineering and physics problems.

The FEM was first used to solve electromagnetic problems in 1965, by O. C. Zienkiewicz and Y. K. Cheung [16], by discretizing 2-D problems and using Poisson's equation. Since then, FEM has been developed as a major numerical method in computational electromagnetics and has been applied to a wide variety of problems for different frequency bands.

The FEM implementation mainly consists of four stages [17]: 1) domain discretization, 2) selection of interpolation functions, 3) system equation formulation, and 4) system equation solution.

In the first stage, the whole computational domain, denoted as Ω , is subdivided into a number of small domains, or the "elements", as Ω^e , $e=1,2,\dots,K$, where K is the number of the elements. A typical element can be a line segment in one-dimensional domains, a triangle or a rectangle in two-dimensional domains, and a tetrahedron, a triangular prism or a rectangular brick in three-dimensional domains, as Figure 2.1 shows [17].

In the scalar FEM, the problem is formulated in terms of the unknown function ϕ computed at the nodes of each element, while in the vector FEM it is computed at the edge of each element. In electromagnetics, ϕ is the field solution. The complete description of an element node in the FEM includes the coordinates

of the node, its local position in the element and its global position in the entire system (referred to as “local number” and “global number”).

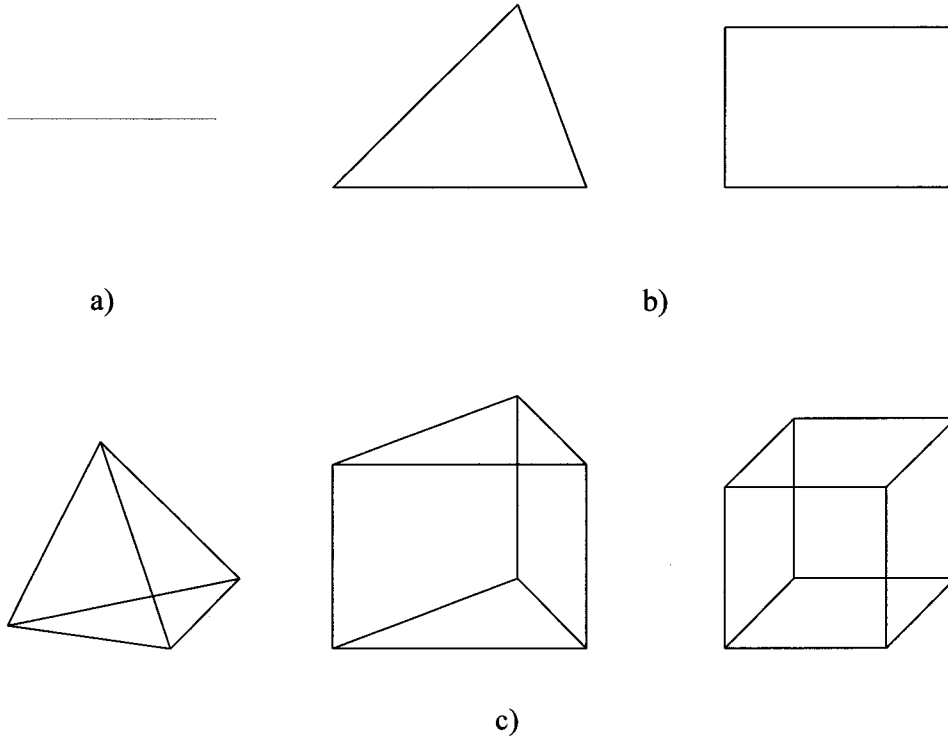


Figure 2.1 Basic elements in the FEM mesh: a) one-dimensional, b) two-dimensional, c) three-dimensional.

The second stage is to select an interpolation function, which provides an approximation of the solution at coordinates other than the element nodes (scalar FEM), or the element edges (vector FEM). The interpolation function can be a polynomial, which is linear, quadratic, or higher-order. Thus, the solution anywhere in an element can be expressed as:

$$\tilde{\phi}^e = \sum_{j=1}^n N_j^e \phi_j^e . \quad (2.26)$$

Here, n is the number of the nodes in one element, ϕ_j^e is the value of ϕ at the j th node, and N_j^e is the interpolation coefficient for the j th node. The latter equals 1 at the j th node and 0 at all other nodes of the element.

After proper discretization and interpolation, we can formulate the system of equations using the Ritz method or the Galerkin method, both of which solve the boundary value problem

$$\mathcal{L}\phi = f. \quad (2.27)$$

Here, \mathcal{L} is the integro-differential operator, and f is the function determined by the excitation or the boundary conditions.

The Ritz method or the Galerkin method cast (2.27) in the general matrix form:

$$\mathbf{K}\boldsymbol{\phi} = \mathbf{b}. \quad (2.28)$$

Here, \mathbf{K} is an M by M matrix where M is the number of the total nodes (or edges), $\boldsymbol{\phi}$ is an M by 1 vector of the solution values at the nodes, \mathbf{b} is an M by 1 vector computed from the desired excitation f and the boundary conditions.

For consistency of notations, in this thesis, the solution vector $\boldsymbol{\phi}$ is expressed as the field solution vector \mathbf{x} , and \mathbf{K} is expressed as the system matrix \mathbf{A} . Then, equation (2.28) has exactly the same form as equation (2.1).

2.6 SELF-ADJOINT SENSITIVITIES FOR S -PARAMETERS IN THE FINITE-ELEMENT METHOD

The AVM needs an additional adjoint system analysis for the sensitivity computation. It is well known that this adjoint system analysis is hard to set up and carry out in commercial EM software. This limits the practical applications of the AVM.

In this section, we give a detailed derivation of the self-adjoint sensitivity analysis (SASA) for the scattering matrix, i.e., the S -parameters. We show that SASA needs only the original system analysis to compute the sensitivity information [18]. We also comment on how to use SASA to compute other network parameter sensitivities.

Recall the AVM sensitivity formula (2.4). For network parameter sensitivity, the gradients $\nabla_p \mathbf{b}$ and $\nabla_p^e F$ in (2.4) vanish, and the formula becomes:

$$\nabla_p F = -\hat{\mathbf{x}}^T \cdot \nabla_p (\mathbf{A}\bar{\mathbf{x}}). \quad (2.29)$$

In (2.29), $\bar{\mathbf{x}}$ is fixed, and only \mathbf{A} is differentiated.

To obtain the full scattering matrix of a K -port structure for a particular mode ν , K solutions of the system of equations (2.1) are carried out with one of the ports being excited while the rest of the ports are matched. We assume that the j th port is excited and define the S_{kj} parameters as

$$S_{kj}^{(\nu)} = \frac{\iint_{k\text{-port}} (\mathbf{a}_n \times \mathbf{E}_j^{(\nu)}) \cdot (\mathbf{a}_n \times \mathbf{e}_k^{(\nu)}) ds_k}{\iint_{j\text{-port}} (\mathbf{a}_n \times \mathbf{E}_j^{(\nu)inc}) \cdot (\mathbf{a}_n \times \mathbf{e}_j^{(\nu)}) ds_j} - \delta_{kj}, \quad \delta_{kj} = \begin{cases} 1, & k = j \\ 0, & k \neq j \end{cases}. \quad (2.30)$$

Here, $\mathbf{E}_j^{(\nu)inc}$ is the incident field of the ν mode at the j th port, $\mathbf{E}_j^{(\nu)}$ is the resulting \mathbf{E} -field solution, \mathbf{a}_n is the unit normal to the respective port surface, and $\mathbf{e}_\xi^{(\nu)}$, $\xi = j, k$, are the orthonormal modal vectors representing the ν -mode \mathbf{E} -field distribution across the respective ports. The vectors $\mathbf{e}_\xi^{(\nu)}$ form an orthonormal basis:

$$\iint_{\xi\text{-port}} (\mathbf{e}_\xi^{(\nu)} \cdot \mathbf{e}_\xi^{(\nu')}) ds_\xi = \delta_{\nu\nu'} \quad (2.31)$$

where $\delta_{\nu\nu'} = 1$ if the modes ν and ν' are the same, and $\delta_{\nu\nu'} = 0$ otherwise. They are obtained either analytically or numerically [17], [19]. The analytical expressions for the modes $\mathbf{e}^{(\nu)}$ of a rectangular waveguide can be found in [17].

We note that if the S -parameters in (2.30) are computed at planes different from their respective ports, de-embedding is applied. It is in the form of an additional exponential factor; e.g., for the reflection coefficient, it is $e^{2\gamma L_d}$ where γ is the propagation constant and L_d is the distance between the port and the plane of de-embedding. This factor is parameter-independent and does not change the derivations which follow. It is omitted for the sake of simpler notations.

The formulation (2.30) uses the approach in [17] where the output power wave in the k th port is obtained by projecting the transverse components of the transmitted/reflected \mathbf{E} -field onto the transverse components of the port modal vector $\mathbf{e}_k^{(\nu)}$. In the denominator, the input power wave in the j th port is obtained in the same manner. For a single-mode analysis, the typical incident field setup is $\mathbf{E}_j^{(\nu)inc} = E_{0j}\mathbf{e}_j^{(\nu)}$ where E_{0j} is a user defined magnitude. Usually, $E_{0j} = 1$. Note that an alternative formulation, see, e.g., [19], uses the orthonormal set (2.31) as well as its dual (\mathbf{H} -field) vector set. Both S -parameter definitions lead to the same final sensitivity result. We choose to work with (2.30).

Since we consider the S -parameter sensitivities of a single mode, for simpler notations, the superscript (ν) is omitted but implied in all formulas hereafter. Thus, with the j th port being excited, the respective right-hand side of (2.1) is denoted by \mathbf{b}_j , and its respective solution vector is \mathbf{x}_j . It represents the field solution \mathbf{E}_j . K such field solutions $\bar{\mathbf{x}}_j$, $j = 1, \dots, K$, are available from the S -parameter analysis of the structure.

In the FEM, within each surface element s at a port, the field \mathbf{E}^s is approximated via the \mathbf{E} -field components x_i^s , $i = 1, \dots, n_s$, tangential to the n_s edges of the element [17]:

$$\mathbf{a}_n^s \times \mathbf{E}^s = \sum_{i=1}^{n_s} \mathbf{B}_i^s x_i^s = (\mathbf{x}^s)^T \cdot \{\mathbf{B}^s\} = \{\mathbf{B}^s\}^T \cdot \mathbf{x}^s. \quad (2.32)$$

Here, \mathbf{a}_n^s is the unit normal to the surface element, $\mathbf{x}^s = [x_1^s \cdots x_{n_s}^s]^T$, and \mathbf{B}_i^s are the vector basis functions of the element. The column $\{\mathbf{B}^s\}$ has the \mathbf{B}_i^s vectors as its elements, $\{\mathbf{B}^s\} = [\mathbf{B}_1^s \cdots \mathbf{B}_{n_s}^s]^T$. Note that the vector of edge field components \mathbf{x}^s is a subset of the solution \mathbf{x} of (2.1).

If S_{kj} is the response whose sensitivities we need, i.e., $F = S_{kj}$, we must consider the solution of the adjoint problem:

$$\mathbf{A}^T \hat{\mathbf{x}} = [\nabla_{\mathbf{x}} f]^T \quad (2.33)$$

where the respective adjoint excitation becomes $\hat{\mathbf{b}}_{kj} = [\nabla_{\mathbf{x}} S_{kj}]^T$. Instead of dealing with the global adjoint excitation vector $[\nabla_{\mathbf{x}} S_{kj}]^T$ we can consider its elemental subset $[\nabla_{\mathbf{x}^s} S_{kj}]^T$.

From (2.30), we see that S_{kj} is a linear and, therefore, analytic function of the field solution \mathbf{E}_j , and, therefore, of \mathbf{x}_j , as implied by the linear relation (2.32). Then the analysis with (2.29) and (2.33) applies. We first write (2.30) in terms of the field of the surface elements of the k th port:

$$S_{kj} = \frac{\sum_{s_k \text{-element}} \iint (\mathbf{a}_n^s \times \mathbf{E}_j^s) \cdot (\mathbf{a}_n^s \times \mathbf{e}_k) ds_{s_k}}{\iint_{j\text{-port}} (\mathbf{a}_n \times \mathbf{E}_j^{inc}) \cdot (\mathbf{a}_n \times \mathbf{e}_j) ds_j} - \delta_{kj} \quad (2.34)$$

where δ_{kj} has been already defined in (2.30). Making use of (2.32),

$$S_{kj} = \frac{\sum_{s_k} \iint_{s_k\text{-element}} (\{\mathbf{B}^{s_k}\}^T \cdot \mathbf{x}^{s_k}) \cdot (\mathbf{a}_n^{s_k} \times \mathbf{e}_k) ds_{s_k}}{\iint_{j\text{-port}} (\mathbf{a}_n \times \mathbf{E}_j^{inc}) \cdot (\mathbf{a}_n \times \mathbf{e}_j) ds_j} - \delta_{kj}. \quad (2.35)$$

From (2.35), we find the derivatives of S_{kj} with respect to the edge field components of the s_k element at the k th port:

$$\frac{\partial S_{kj}}{\partial x_i^{s_k}} = \frac{\iint_{s_k\text{-element}} \mathbf{B}_i^{s_k} \cdot (\mathbf{a}_n^{s_k} \times \mathbf{e}_k) ds_{s_k}}{\iint_{j\text{-port}} (\mathbf{a}_n \times \mathbf{E}_j^{inc}) \cdot (\mathbf{a}_n \times \mathbf{e}_j) ds_j}, i = 1, \dots, n_{s_k} \quad (2.36)$$

where n_{s_k} is the number of edges of the s_k element. In gradient notation, (2.36)

becomes

$$[\nabla_{\mathbf{x}^{s_k}} S_{kj}]^T = \frac{\iint_{s_k\text{-element}} \{\mathbf{B}^{s_k}\} \cdot (\mathbf{a}_n^{s_k} \times \mathbf{e}_k) ds_{s_k}}{\iint_{j\text{-port}} (\mathbf{a}_n \times \mathbf{E}_j^{inc}) \cdot (\mathbf{a}_n \times \mathbf{e}_j) ds_j}. \quad (2.37)$$

After the assembly of the FEM equations, each of the elements of $[\nabla_{\mathbf{x}^{s_k}} S_{kj}]^T$

becomes an element of the global adjoint excitation vector $\hat{\mathbf{b}}_{kj} = [\nabla_{\mathbf{x}} S_{kj}]^T$.

We now compare the elements of the adjoint excitation (2.37) with the elements of the excitation for the s_k element of the k th port in the original FEM problem [17]:

$$\mathbf{b}^{s_k} = \iint_{s_k\text{-element}} \{\mathbf{B}^{s_k}\} \cdot (\mathbf{U}_k^{inc} \times \mathbf{a}_n^{s_k}) ds_{s_k} \quad (2.38)$$

where

$$\mathbf{U}_k^{inc} = -2\gamma_k E_{0k} \mathbf{e}_k \quad (2.39)$$

for a single-mode incident field. Here, \mathbf{e}_k is the normalized modal vector, E_{0k} is a user defined magnitude (usually set as 1), and γ_k is the modal propagation constant of the port. The comparison reveals a simple linear relationship between the original and adjoint excitation vectors, \mathbf{b}_k and $\hat{\mathbf{b}}_{kj}$:

$$\hat{\mathbf{b}}_{kj} = \frac{1}{2\gamma_k E_{0k} \iint_{j\text{-port}} (\mathbf{a}_n \times \mathbf{E}_j^{inc}) \cdot (\mathbf{a}_n \times \mathbf{e}_j) ds_j} \cdot \mathbf{b}_k. \quad (2.40)$$

Both \mathbf{b}_k and $\hat{\mathbf{b}}_{kj}$ are obtained from their respective elemental excitations, \mathbf{b}^{sk} and $[\nabla_{\mathbf{x}^{sk}} S_{kj}]^T$, through identical system-assembly procedures.

Next, we turn to the adjoint solutions $\hat{\mathbf{x}}_{kj}$ resulting from $\hat{\mathbf{b}}_{kj}$ ($k, j = 1, \dots, K$). We note that the FEM system matrix \mathbf{A} is symmetric (see, e.g., [17]),

$$\mathbf{A} = \mathbf{A}^T. \quad (2.41)$$

From (2.40) and (2.41), we conclude that all adjoint solutions $\hat{\mathbf{x}}_{kj}$ needed for the S -parameter sensitivities can be calculated from the K original solution vectors \mathbf{x}_k , $k = 1, \dots, K$, by a simple multiplication with a known complex constant:

$$\hat{\mathbf{x}}_{kj} = \kappa_{kj} \cdot \mathbf{x}_k, \quad \kappa_{kj} = \frac{1}{2\gamma_k E_{0k} \iint_{j\text{-port}} (\mathbf{a}_n \times \mathbf{E}_j^{inc}) \cdot (\mathbf{a}_n \times \mathbf{e}_j) ds_j}. \quad (2.42)$$

They are then substituted in (2.29) where F can be any of the elements of the S -matrix.

The self-adjoint nature of the solution derived above shows that the information necessary to compute the S -parameter sensitivities is already contained in the full-wave solution provided by the FEM simulator. The sensitivity analysis is thus reduced to a relatively simple and entirely independent post-process, which does not require additional full-wave solutions.

As a conclusion, we state the sensitivity formula for the self-adjoint S -parameter problem:

$$\nabla_{\mathbf{p}} S_{kj} = -\kappa_{kj} (\bar{\mathbf{x}}_k)^T \cdot \nabla_{\mathbf{p}} (A \bar{\mathbf{x}}_j), \quad j, k = 1, \dots, K. \quad (2.43)$$

Here, κ_{kj} is a constant, which depends on the power of the waves incident upon the j th and k th ports.

We also notice that the S -parameters relate to all other types of network parameters through known analytical formulas. Thus, the S -parameter sensitivities can be converted to any other type of network-parameter sensitivities using chain differentiation.

2.7 GENERAL PROCEDURES AND SOFTWARE REQUIREMENTS FOR SASA

Assume that the basic steps in the EM structure analysis have already been carried out. These include: 1) a geometrical model of the structure has been built through the graphic user interface of the simulator, 2) a mesh has been generated,

3) the system matrix \mathbf{A} has been assembled, 4) the system equations have been solved for all K port excitations, and the original solution vectors $\bar{\mathbf{x}}_k$, $k = 1, \dots, K$, of the nominal structure have been found with sufficient accuracy. The self-adjoint sensitivity analysis is then carried out with the following steps:

(1) *Parameterization*: Identify design parameters p_i , $i = 1, \dots, N$.

(2) *Generation of Matrix Derivatives*: For each p_i , perturb the structure slightly (with about 1 % of the nominal p_i value) while keeping the other parameters at their nominal values. Re-generate the system matrix $\mathbf{A}_i = \mathbf{A}(\mathbf{p} + \Delta p_i \cdot \mathbf{u}_i)$, where \mathbf{u}_i is a $N \times 1$ vector whose elements are all zero except the i th one, $u_i = 1$. Compute the N derivatives of the system matrix via finite differences:

$$\frac{\partial \mathbf{A}}{\partial p_i} \approx \frac{\Delta \mathbf{A}}{\Delta p_i} = \frac{\mathbf{A}_i - \mathbf{A}}{\Delta p_i}, i = 1, \dots, N. \quad (2.44)$$

Note that (2.44) is applicable only if \mathbf{A} and \mathbf{A}_i are of the same size, i.e., the two respective meshes contain the same number of nodes and elements. Moreover, the numbering of these nodes and elements must correspond to the same locations (within the prescribed perturbation) in the original and perturbed structures.

(3) *Sensitivity Computations*: Use (2.43) with the proper constant κ .

The above steps show that the EM simulator must have certain features, which enable the self-adjoint sensitivity analysis. First, it must be able to export the system matrix so that the user can compute the system matrix derivatives with

(2.44). Second, it must allow the control over the mesh generation so that (2.44) is physically meaningful. Third, it must export the field/current solution vector \bar{x} so that we can compute the sensitivities with (2.43). The second and third features are available with practically all commercial EM simulators. The first feature deserves more attention. The system matrix is typically very large. Fortunately, in the FEM it is usually sparse and can be compressed and further stored in the computer RAM or in a disk file without excessive time delay. Only a few of the commercial simulators give access to the generated system matrices. Hence, the necessity for a self-adjoint formulation without requiring elaborate manipulation of system matrix is greatly felt.

REFERENCES

- [1] N. K. Nikolova, *et al.*, "Accelerated gradient based optimization using adjoint sensitivities," *IEEE Trans. Antenna Propagat.*, vol. 52, pp. 2147-2157, Aug. 2004.
- [2] D. G. Cacuci, *Sensitivity & Uncertainty Analysis, Volume 1: Theory*. Boca Raton, FL: Chapman & Hall/CRC, 2003.
- [3] A. D. Belegundu and T. R. Chandrupatla, *Optimization Concepts and Applications in Engineering*. Upper Saddle River, NJ: Prentice Hall, 1999.
- [4] E. J. Haug, K. K. Choi and V. Komkov, *Design Sensitivity Analysis of Structural Systems*. Orlando: Academic Press Inc., 1986.
- [5] J. W. Bandler, "Computer-aided circuit optimization," in *Modern Filter Theory and Design*, G. C. Temes and S. K. Mitra, Eds. New York: Wiley, 1973, ch. 6.
- [6] S. M. Ali, N. K. Nikolova, and M. H. Bakr, "Recent advances in sensitivity analysis with frequency-domain full-wave EM solvers," *Applied Computational Electromagnetics Society Journal*, vol. 19, pp. 147-154, Nov. 2004.
- [7] M. H. Bakr and N. K. Nikolova, "An adjoint variable method for frequency domain TLM problems with conducting boundaries," *IEEE Microwave and Wireless Components Letters*, vol. 13, pp. 408-410, Sept. 2003.
- [8] N. K. Georgieva, S. Glavic, M. H. Bakr, and J. W. Bandler, "Feasible adjoint sensitivity technique for EM design optimization," *IEEE Trans. Microwave Theory Tech.*, vol. 50, pp. 2751-2758, Dec. 2002.
- [9] H. Akel and J. P. Webb, "Design sensitivities for scattering-matrix calculation with tetrahedral edge elements," *IEEE Trans. Magnetics*, vol. 36, pp. 1043-1046, July 2000.
- [10] N. K. Nikolova, J. W. Bandler, and M. H. Bakr, "Adjoint techniques for sensitivity analysis in high-frequency structure CAD," *IEEE Trans. Microwave Theory Tech.*, vol. 52, No. 1, pp. 403-419, Jan. 2004.

- [11] M. D. Greenberg, *Advanced Engineering Mathematics*. Upper Saddle River, NJ: Prentice Hall, 1998, pp. 605.
- [12] J. Ureel and D. De Zutter, "Shape sensitivities of capacitances of planar conducting surfaces using the method of moments," *IEEE Trans. Microwave Theory Tech.*, vol. 44, pp. 198-207, Feb. 1996.
- [13] J. Ureel and D. De Zutter, "A new method for obtaining the shape sensitivities of planar microstrip structures by a full-wave analysis," *IEEE Trans. Microwave Theory Tech.*, vol. 44, pp. 249-260, Feb. 1996.
- [14] N. K. Georgieva, S. Glavic, M. H. Bakr, and J. W. Bandler, "Feasible adjoint sensitivity technique for EM design optimization," *IEEE Trans. Microwave Theory Tech.*, vol. 50, pp. 2751-2758, Dec. 2002.
- [15] E. B. Saff and A. D. Snider, *Fundamentals of Complex Analysis*. Englewood Cliffs, NJ: Prentice Hall, Inc., 1976.
- [16] O. C. Zienkiewicz and Y. K. Cheung, "Finite elements in the solution of field problems," *The Engineer*, vol. 200, pp. 507-510, 1965.
- [17] J. Jin, *The Finite Element Method in Electromagnetics*, 2nd ed. New York: John Wiley & Sons, 2002.
- [18] N. K. Nikolova, J. Zhu, D. Li, M. H. Bakr, and J. W. Bandler, "Sensitivity analysis of network parameter with electromagnetic frequency-domain simulators," *IEEE Trans. Microwave Theory Tech.*, vol. 54, pp. 670-681, Feb. 2006.
- [19] M. Salazar-Palma, T. K. Sarkar, L.-E. García-Castillo, T. Roy, A. Djordjević, *Iterative and Self-Adaptive Finite-Elements in Electromagnetic Modeling*. Norwood, MA: Artech, 1998, pp. 465-466.
- [20] E. A. Soliman, M. H. Bakr, and N. K. Nikolova, "Accelerated gradient-based optimization of planar circuits," *IEEE Trans. Antennas Propagat.*, vol. 53, pp. 880-883, Feb. 2005.

CHAPTER 3

FINITE-DIFFERENCE FREQUENCY- DOMAIN SELF-ADJOINT SENSITIVITY ANALYSIS FOR METALLIC STRUCTURES

3.1 INTRODUCTION

The goal of the design of a multi-port electromagnetic structure is obtaining the optimal values of optimizable parameters such that responses satisfy the specifications over the desired frequency range. The adjoint-variable method (AVM) is known to be the most efficient approach to design sensitivity analysis for problems of high complexity where the number of state variables is much greater than the number of the required response derivatives [1], [2], [3]. Yet, feasible implementations remain a challenge. The reason lies mainly in the complexity of these techniques. They require the analysis of an adjoint problem whose excitation is response dependent. Not only does this mean one additional

full-wave simulation but it also requires modification of the electromagnetic (EM) analysis engine due to the specifics of the adjoint-problem excitation. Techniques complementary to the finite-element method (FEM) have been developed in electrical engineering [4], [5]. A simpler and more versatile approach has been adopted [6], [7], [8], [9] for analyses in the frequency domain, which is described in Chapter 2. Instead of analytical formulations, approximations of the system-matrix derivatives are employed using finite differences or the iterative Broyden update [9].

When the design requirements involve the S -parameters, the traditional EM sensitivity analysis often determines the N derivatives for the N design parameters by approximations at the response level. The structure is perturbed for each designable parameter and a system analysis is performed. With central finite differences, such an approach would require $2N+1$ system analyses to compute the objective function and its gradient. If N is large, this approach may easily become impractical. Generally, the AVM requires two simulations, the original and the adjoint simulations, to compute the derivatives. It is hard to set up and carry out the adjoint simulation in commercial EM softwares. On the other hand, the self-adjoint sensitivity analysis (SASA) [8] needs only one simulation to obtain all derivatives regardless of their number together with the response itself.

In general, both the conventional adjoint-variable method and the self-adjoint method require access to the system matrix built by the simulator.

Commercial simulators, however, rarely allow such access due to copyright protection. Where available, the matrix export is inefficient since large amount of space is required to store the data on the hard disk and this is quite time-consuming.

In this chapter, a self-adjoint approach to the 2-D and 3-D sensitivity analysis of network parameters using structured grids with finite-element EM solvers is formulated and validated in the case of metallic objects. The S -parameter derivatives are computed as an independent post-process, which has negligible computational requirements compared to a full-wave system analysis. It requires neither an adjoint problem nor system matrix derivatives. We focus on the linear problem in the frequency domain, which is at the core of a number of commercial high-frequency simulators. Thus, for the first time, we suggest practical and fast sensitivity solutions realized entirely outside the framework of the EM solver. These standalone algorithms can be incorporated in an automated design to perform optimization, modeling, or tolerance analysis of high-frequency structures with any commercial solver, which exports the field solution.

In our work, we investigate self-adjoint problems solved using Ansoft's high-frequency structure simulator (HFSS) [10] for waveguide structures with metallic boundaries. Both Yee-cell and central-node techniques are tested and compared for accuracy. An H-plane waveguide filter is used to validate the proposed methods.

In Section 3.2, we introduce the formulation of the finite-difference frequency-domain sensitivity analysis method for network-parameter sensitivity calculations, particularly for the S -parameter sensitivities. Then in Section 3.3, we outline the two approaches for metallic objects. Section 3.4 provides a validation example and compares the Yee-cell and central-node approaches applied with different design parameters. Section 3.5 discusses the 3-D sensitivity analysis with regard to metallic objects. Section 3.6 provides verification of our proposed 3-D method with an example.

3.2 OVERVIEW OF FINITE-DIFFERENCE FREQUENCY-DOMAIN SELF-ADJOINT SENSITIVITIES FOR S -PARAMETERS

In this section, we provide an overview of self-adjoint sensitivity analysis based on the finite-difference frequency-domain technique. A description of SASA developed for the FEM is provided in Chapter 2. The proposed finite-difference frequency-domain SASA enhances this application by replacing the need for system matrix export with the introduction of a solver-independent finite-difference grid. This approach not only improves the time required by the overall sensitivity analysis but also ensures better software portability for a variety of frequency-domain simulators.

An EM problem in a linear medium can be described by the vector wave equation for the \mathbf{E} field

$$\nabla \times \boldsymbol{\mu}_r^{-1} \nabla \times \mathbf{E} + \mu_0 \boldsymbol{\varepsilon}_0 \boldsymbol{\varepsilon}_r \frac{\partial^2 \mathbf{E}}{\partial t^2} + \mu_0 \boldsymbol{\sigma} \frac{\partial \mathbf{E}}{\partial t} = -\mu_0 \frac{\partial \mathbf{J}}{\partial t} \quad (3.1)$$

where ε_0 , μ_0 are the permittivity and permeability of vacuum, while $\boldsymbol{\varepsilon}_r$, $\boldsymbol{\mu}_r$, $\boldsymbol{\sigma}$ are the medium relative permittivity, permeability, and conductivity, respectively. In general, $\boldsymbol{\varepsilon}_r$, $\boldsymbol{\mu}_r$, $\boldsymbol{\sigma}$ are tensors. Here, we assume an isotropic medium for simplicity. In the frequency domain, (3.1) can be written as

$$\nabla \times \boldsymbol{\mu}_r^{-1} \nabla \times \mathbf{E} - \mu_0 \boldsymbol{\varepsilon}_0 \boldsymbol{\varepsilon}_r \omega^2 \mathbf{E} + j\omega \mu_0 \boldsymbol{\sigma} \mathbf{E} = -j\omega \mu_0 \mathbf{J}. \quad (3.2)$$

One of the conditions for the problem described by (3.2) to be self-adjoint is that these tensors are symmetric or Hermitian. The finite-difference discretization of (3.2) leads to

$$\square^2 \mathbf{E} + \boldsymbol{\alpha} \cdot \mathbf{E} = \mathbf{G} \quad (3.3)$$

where

$$\boldsymbol{\alpha} = k_0^2 \left(\boldsymbol{\varepsilon}_r - j \frac{\boldsymbol{\sigma}}{\omega \boldsymbol{\varepsilon}_0} \right) \Delta h^2, \quad \mathbf{G} = \beta \mathbf{J}, \quad \beta = j\omega \mu_0 \Delta h^2. \quad (3.4)$$

Here, $k_0 = \omega \sqrt{\mu_0 \boldsymbol{\varepsilon}_0}$ and Δh is the discretization step. The finite-difference operator \square^2 has three vector components. It corresponds to the double-curl operator in (3.2) (with a minus sign). For example, in a magnetically isotropic medium, and on a Yee-cell grid, the x -component is [11]:

$$(\square^2 \mathbf{E})_x = h_y^2 D_{yy}^\mu E_x + h_z^2 D_{zz}^\mu E_x - h_y h_x D_{yx}^\mu E_y - h_z h_x D_{zx}^\mu E_z \quad (3.5)$$

where

$$h_x = \frac{\Delta h}{\Delta x}, \quad h_y = \frac{\Delta h}{\Delta y}, \quad h_z = \frac{\Delta h}{\Delta z} \quad (3.6)$$

and

$$D_{yy}^\mu E_x(x_0, y_0, z_0) = \frac{E_x(x_0, y_0 + \Delta y, z_0)}{\mu_r(x_0, y_0 + \Delta y/2, z_0)} + \frac{E_x(x_0, y_0 - \Delta y, z_0)}{\mu_r(x_0, y_0 - \Delta y/2, z_0)} - \left[\frac{1}{\mu_r(x_0, y_0 + \Delta y/2, z_0)} + \frac{1}{\mu_r(x_0, y_0 - \Delta y/2, z_0)} \right] \cdot E_x(x_0, y_0, z_0) \quad (3.7)$$

$$D_{yx}^\mu E_y(x_0, y_0, z_0) = \frac{E_y(x_0 + \Delta x/2, y_0 + \Delta y/2, z_0) - E_y(x_0 - \Delta x/2, y_0 + \Delta y/2, z_0)}{\mu_r(x_0, y_0 + \Delta y/2, z_0)} - \frac{E_y(x_0 + \Delta x/2, y_0 - \Delta y/2, z_0) - E_y(x_0 - \Delta x/2, y_0 - \Delta y/2, z_0)}{\mu_r(x_0, y_0 - \Delta y/2, z_0)}. \quad (3.8)$$

$D_{zx}E_z$ and $D_{zz}E_x$ are derived similarly.

The EM response in the frequency-domain sensitivity analysis is a functional of the field solution which can be written as

$$F(\mathbf{E}, \mathbf{p}) = \iiint_{\Omega} f(\mathbf{E}, \mathbf{p}) d\Omega. \quad (3.9)$$

Here, Ω is the computational volume and $\mathbf{p} = [p_1 \dots p_N]^T$ contains the design variables, which relate to the shape and the materials of the structure.

Using an approach similar to that in the time domain [11] and bearing in mind that the S -parameters are functions of the field solution at the ports, the discrete sensitivity formula for N shape parameters is obtained from (3.9) as

$$\frac{\partial S_{jk}}{\partial p_n} \approx -\kappa_{jk} \iiint_{\Omega} (\bar{\mathbf{E}}_j)_n \cdot \frac{\Delta_n R(\bar{\mathbf{E}}_k)}{\Delta p_n} d\Omega, \quad j, k = 1, \dots, N_p. \quad (3.10)$$

Here, N_p denotes the total number of ports. The optimizable shape parameter p_n ($n=1, \dots, N$) can assume only discrete values snapped to the finite-difference grid of the sensitivity solver whose step is Δh . Thus, $\Delta p_n = \pm \Delta h$. We emphasize that the grid of the sensitivity solver is independent of that of the simulator and Δh is usually chosen to be equal or less than the length of the smallest edge of the perturbed shape (but not smaller than the shortest grid edge of the simulation grid at the object). $\bar{\mathbf{E}}_k$ denotes the field solution resulting from the simulation of the original structure with port k being excited. A distinct feature of the discrete formula is that the adjoint field solution, $(\hat{\mathbf{E}}_{jk})_n = \kappa_{jk}(\bar{\mathbf{E}}_j)_n$, corresponds to the n th perturbed state of the structure, i.e., the structure in which p_n is perturbed by Δp_n while all other parameters are kept at their nominal values. $(\bar{\mathbf{E}}_j)_n$ is obtained from $\bar{\mathbf{E}}_j$ through a simple field-mapping procedure. The expressions for the self-adjoint constants κ_{jk} for S -parameters computed by an FEM solver can be found in [8]. Further, the term $\Delta_n R(\bar{\mathbf{E}})$ is computed as

$$\Delta_n R(\bar{\mathbf{E}}) = \Delta_n \square^2 \cdot \bar{\mathbf{E}} + \Delta_n \alpha \cdot \bar{\mathbf{E}} - \Delta_n \mathbf{G} \quad (3.11)$$

where $\Delta_n \square^2$ and $\Delta_n \alpha$ are the changes of the frequency-domain finite-difference (FDFD) system coefficients arising from the changes in the material/shape

parameters of grid cells affected by the perturbation $\Delta p_n = \pm \Delta h$. The FDFD source term \mathbf{G} may also be affected by shape perturbations, which is reflected by $\Delta_n \mathbf{G}$.

The S -parameter sensitivity formula for material parameters is exact in the sense that the system coefficient derivatives are analytical and the material parameters such as permittivity and conductivity belong to a continuous (not discrete) space :

$$\frac{\partial S_{jk}}{\partial p_n} = -\kappa_{jk} \iiint_{\Omega} \bar{\mathbf{E}}_j \cdot \frac{\partial R(\bar{\mathbf{E}}_k)}{\partial p_n} d\Omega, \quad j, k = 1, \dots, N_p \quad (3.12)$$

where

$$\frac{\partial R(\bar{\mathbf{E}}_k)}{\partial p_n} = \frac{\partial \alpha}{\partial p_n} \cdot \bar{\mathbf{E}}_k \quad \text{and} \quad \frac{\partial \alpha}{\partial p_n} = \begin{cases} k_0^2 \Delta h^2, & \text{if } p_n = \varepsilon_r \\ -j \frac{k_0^2 \Delta h^2}{\omega \varepsilon_0}, & \text{if } p_n = \sigma. \end{cases} \quad (3.13)$$

Note that the exact formula requires that the adjoint field $\hat{\mathbf{E}}_{jk} = \kappa_{jk} \bar{\mathbf{E}}_j$ corresponds to the structure's nominal (unperturbed) state. Field mapping is not needed.

The shape sensitivity formula (3.10) can be discretized as:

$$\frac{\partial S_{jk}}{\partial p_n} = - \sum_{P \in \mathcal{S}_n} \left((\hat{\mathbf{E}}_j)_n \cdot \frac{\Delta_n R(\bar{\mathbf{E}}_k)}{\Delta p_n} \cdot \Delta x \Delta y \Delta z \right)_P \quad (3.14)$$

where

$$\frac{\Delta_n R(\bar{\mathbf{E}}_k)}{\Delta p_n} = \frac{\Delta_n \square^2}{\Delta p_n} \bar{\mathbf{E}}_k + \frac{\Delta_n \alpha}{\Delta p_n} \bar{\mathbf{E}}_k - \frac{\Delta_n (\beta \bar{\mathbf{J}}_k)}{\Delta p_n}. \quad (3.15)$$

In the FEM, the self-adjoint constant κ_{jk} is derived as [8] :

$$\kappa_{jk} = \frac{1}{2\gamma_j E_{0j} \iint_{k\text{-port}} (\mathbf{a}_n \times \mathbf{E}_k^{inc}) \cdot (\mathbf{a}_n \times \mathbf{e}_k) dS_k}. \quad (3.16)$$

Here, γ_j is the modal propagation constant of the j th port, E_{0j} is a user defined magnitude at the j th port, \mathbf{E}_k^{inc} is the incident field at the k th port, \mathbf{a}_n is the unit normal to the respective port surface, and \mathbf{e}_k is the orthonormal modal vector. We apply our theory to sensitivity analysis with field solutions obtained with Ansoft's HFSS [10]. In HFSS, when the k th port is excited by a wave port, absorbing boundary conditions are applied at all other ports.

To summarize, we state the sensitivity formula for the self-adjoint S -parameter problem:

$$\frac{\partial S_{jk}}{\partial p_n} = -\kappa_{jk} \sum_{p \in S_n} \left[(\bar{\mathbf{E}}_j)_n \cdot \frac{\Delta_n R(\bar{\mathbf{E}}_k)}{\Delta p_n} \cdot \Delta x \Delta y \Delta z \right]_p, \quad n = 1, \dots, N. \quad (3.17)$$

The only points needed for shape sensitivity analysis are those near the boundary of perturbed structures [11]. With shape parameters, we need to apply our mapping technique [11] in order to obtain the field solution in the n -th perturbed state from the field solution in the nominal (unperturbed) state. The implementation of the field mappings in 2-D and 3-D analyses are explained in detail in the next sections.

3.3 SELF-ADJOINT SENSITIVITIES FOR S-PARAMETERS OF METALLIC STRUCTURES (THE 2-D CASE)

3.3.1 Yee-Cell Based Approach

Yee-cell FD grid was originally used for the time-domain sensitivity analysis of both dielectric and metallic objects [11]. Here, we apply it for the first time to the frequency-domain sensitivity analysis of metallic structures. Due to the structured nature of the grid, the implementation is rather straightforward and, at the same time, computationally efficient since it eliminates the calculation of the system matrix derivatives.

For a 2-D TM_y problem in a magnetically homogeneous medium, (3.2)

reduces to

$$\frac{\partial^2 E_y}{\partial^2 x} + \frac{\partial^2 E_y}{\partial^2 z} + \left(\frac{\omega}{c}\right)^2 \epsilon_r \mu_r E_y - j\omega\mu_0\mu_r\sigma E_y = j\omega\mu_0\mu_r J_y. \quad (3.18)$$

Here, c is the speed of light in vacuum. Applying central finite differences to (3.18), we obtain [11]

$$\square^2 E_y + \alpha E_y = \mathbf{G} \quad (3.19)$$

where

$$\alpha = k_0^2 \left(\epsilon_r - j \frac{\sigma}{\omega \epsilon_0} \right) \Delta h^2, \mathbf{G} = \beta \mathbf{J}_y, \beta = j\omega\mu_0 \Delta h^2 \quad (3.20)$$

$$\square^2 E_y = h_x^2 D_{xx} E_y + h_z^2 D_{zz} E_y \quad (3.21)$$

$$h_x = \frac{\Delta h}{\Delta x}, \quad h_z = \frac{\Delta h}{\Delta z}. \quad (3.22)$$

The difference operators in (3.21) are as follows:

$$D_{xx}E_y = E_y(x_0 + \Delta x) + E_y(x_0 - \Delta x) - 2E_y(x_0) \quad (3.23)$$

$$D_{zz}E_y = E_y(z_0 + \Delta z) + E_y(z_0 - \Delta z) - 2E_y(z_0). \quad (3.24)$$

To recapitulate, we state the sensitivity formula for the self-adjoint S -parameter problem for 2-D TM_y case in a discretized form:

$$\frac{\partial S_{jk}}{\partial p_n} = -\kappa_{jk} \sum_{P \in \mathcal{S}_n} \left[(\bar{\mathbf{E}}_j)_n \cdot \frac{\Delta_n R(\bar{\mathbf{E}}_k)}{\Delta p_n} \cdot \Delta x \Delta z \right]_P. \quad (3.25)$$

For the computation of shape sensitivities, only the field points around the perturbed object boundary are needed. The adjoint field values are approximated by shifting the original-field coordinates in space in the direction of the assumed n th parameter perturbation [11]. Figure 3.1 illustrates how the mapping technique works in a 2-D problem. There, the dark area represents the original structure. In order to compute the adjoint field $\hat{\mathbf{E}}_n$ for a perturbation in the parameter p_n , we imagine a perturbation of the structure one cell further along the p_n direction (the light-gray area). The points where the adjoint field of the perturbed problem is needed are the square points. They are approximated by the adjoint field of the unperturbed problem at the circle points. Following this methodology, all N perturbed adjoint field solutions for the computation of the N parameter sensitivities can be obtained from only one unperturbed system simulation. The

total number of system analyses for the response and its sensitivities is one, compared with $2N+1$ system analyses if central finite differences at the response level are used.

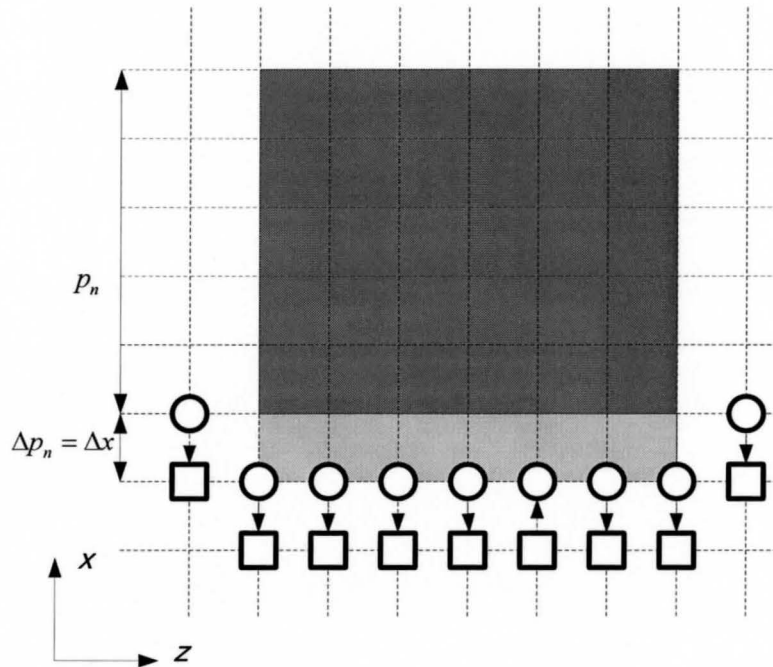


Figure 3.1 Field mapping technique.

When the design parameters relate to the shape, the derivatives of the system coefficients $\mathbf{\Gamma}^2$, α , and \mathbf{G} cannot be mathematically defined [11]. In this case, we resort to finding the differences of the system coefficients in two system states: the nominal (unperturbed) state and the n th perturbed state. In the n th perturbed state, the parameter p_n changes to $p_n + \Delta p_n$ while all other parameters

are kept at their nominal values. The change Δp_n is usually chosen to be one cell, which is the smallest possible on-grid change. As a consequence, the system coefficients in (3.19) at the perturbation grid point change.

The perturbation grid points are the points where either the original or the adjoint field values are needed for the sensitivity computation. For example, for the computation of the shape sensitivities of a perfect metallic object, the perturbation grid points are those being metallized or de-metallized during the perturbation as well as their neighbors.

In the case of metallization, of the three system coefficients, only the double curl operator \square^2 is affected. This is because the tangential electric field components become zero at the edges of all metallized grid cells. Correspondingly, the components of \square^2 multiplying these electric field components become zero.

If the object is de-metallized, the only contribution to the $\Delta_n R(\bar{\mathbf{E}}_k)$ term is due to $\Delta_n(\beta \bar{\mathbf{J}}_n)$ in (3.15). The implicit current term \mathbf{G} , which in the unperturbed structure is not zero on the metallic surface, now becomes zero [11].

Figure 3.2 shows the locations of points where fields are recorded for a perturbation in the $\pm x$ direction. At the points marked with squares in Figure 3.2, both the term $\Delta_n R(\bar{\mathbf{E}}_y)$ and the adjoint field $(\hat{\mathbf{E}}_y)_n$ are not zero. These points

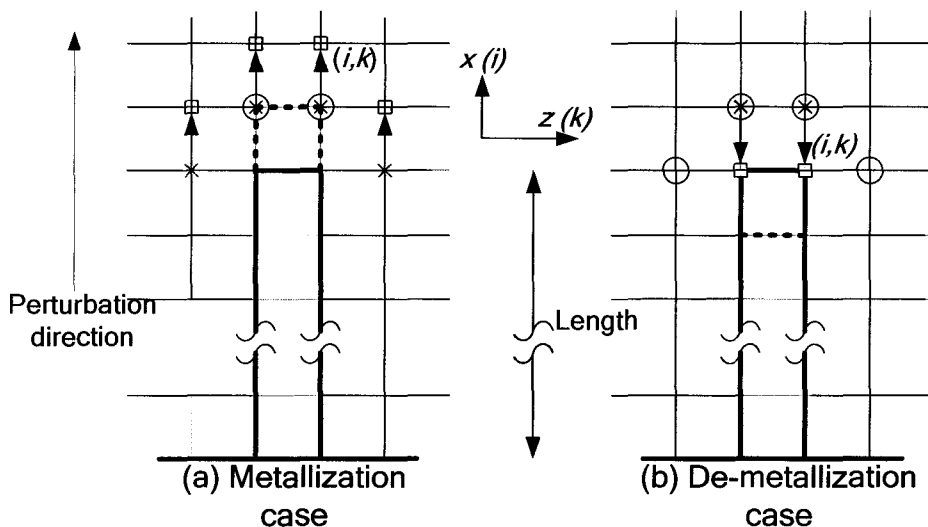


Figure 3.2 Locations where the field is needed for the computation of the derivatives with respect to the length of the object in: (a) metallization and (b) de-metallization case. The original and adjoint field values are needed at the points marked with circles and squares, respectively. The arrows denote the field mapping used to obtain the adjoint field of the perturbed problem from the adjoint field of the unperturbed problem (recorded at points indicated by crosses). Since both adjoint and original field values are obtained from the original problem simulation only, the actual locations where the field is recorded are: (a) at crosses; (b) at circles.

surround the grid cells, which are ‘metallized’ as a result of a perturbation

$\Delta L = +\Delta x$. At point (i, k) in Figure 3.2 (a), the $\Delta_n R(\bar{\mathbf{E}}_y)$ term is calculated as [11]:

$$\Delta_n R(\bar{\mathbf{E}}_y) = -h_x^2 \bar{\mathbf{E}}_y(i-1, k). \quad (3.26)$$

To calculate all “metallization” contributions to the sensitivity formula (3.25), we need the adjoint field at the points marked by a square. These are obtained by the field mapping, i.e., assuming that the field at crosses is same as the field at

squares upon perturbation. The fields at points marked by circles are used to calculate $\Delta_n R(\bar{\mathbf{E}}_y)$.

Non-zero contribution to the sensitivity formulation is also generated in the ‘de-metallized’ region. At the point (i, k) in Figure 3.2 (b), which illustrates the demetallization case, $\Delta_n R(\bar{\mathbf{E}}_y)$ is [11]:

$$\Delta_n R(\bar{\mathbf{E}}_y) = -h_x^2 (\bar{\mathbf{E}}_y)_{i+1,k} - h_z^2 (\bar{\mathbf{E}}_y)_{i,k+1}. \quad (3.27)$$

3.3.2 Central-node Based Approach

In the time-domain sensitivity algorithm [11], [12], the Yee-cell is adopted. This is the grid traditionally employed by the finite-difference time-domain (FDTD) method. There, the field components are staggered by half a step in space. We apply and verify this same approach with metallic objects using solutions provided by the frequency-domain FEM. Figure 3.3 shows with crosses some of the points where the vertical \mathbf{E} -field component is recorded on a Yee-cell grid.

Recently, we have shown [14] that a central-node finite-difference grid, where all three field components are co-located, improves the accuracy of the derivative calculations significantly in the case of structures involving high-contrast dielectric interfaces. Later, this approach was applied to the case of dielectric objects and frequency-domain solutions [15]. In contrast, metallic objects are better fitted to the Yee-cell grid as the boundary conditions for the

tangential \mathbf{E} -field components are satisfied exactly. Here, for the 1st time, we present results in implementing the central-node approach for derivative calculations with respect to the shapes of metallic objects.

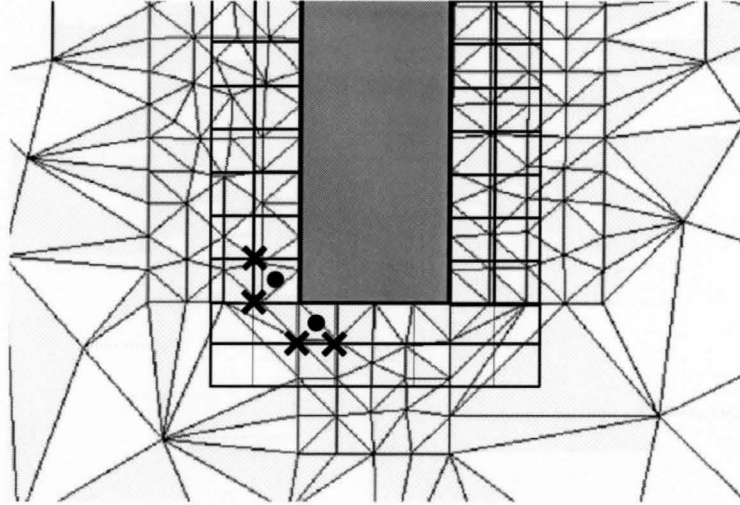


Figure 3.3 A 2-D cut of the discretization grid used by the finite-element simulator superimposed with the FD grid used by the sensitivity solver for metallic septum. The vertical field component is recorded at grid points indicated by: (i) crosses – in the Yee cell grid; (ii) dots – in the central-node grid.

The central-node FD cell is characterized by a single node where all three \mathbf{E} -field components are calculated. The central-node grid cannot impose vanishing tangential \mathbf{E} -field exactly at the surface of a metallic object. Instead, it assumes that all three field components vanish in the object's interior [16]. Like the Yee cell, its faces coincide with material interfaces and its edges follow the edges of objects. The points at which vertical \mathbf{E} -field is recorded in the central-node grid for 2-D case are illustrated in Figure 3.3 by black dots. Mapping techniques

similar to those of the Yee-cell approach are used to determine the field values in the perturbed state. The method of the derivative computations and the changes in the system coefficients remain the same.

3.4 EXAMPLE

We compute the network-parameter sensitivities with our self-adjoint formula based on finite-difference frequency-domain technique and compare the results with those obtained by a central finite-difference approximation applied directly at the level of the S -parameter response. This second approach requires an additional full-wave simulation for each designable parameter.

3.4.1 Six-Section H-Plane Waveguide Filter

A six-septum metallic H-plane filter is used to test the accuracy of both the Yee-cell and the central-node approaches as compared to the response-level finite-difference approach. The sensitivities of this structure have already been investigated for an energy-type response with the TLM method [12] and time-domain FDTD method [11], [12].

Figure 3.4 shows the geometry and the nominal design parameter values of the H-plane filter. We consider the derivatives of the S -parameters with respect to L_4 and S_1 . The computational domain of the structure has the dimensions $(56 \times 26 \times 700)\Delta h$. Because of the symmetry of the dominant mode, only half the

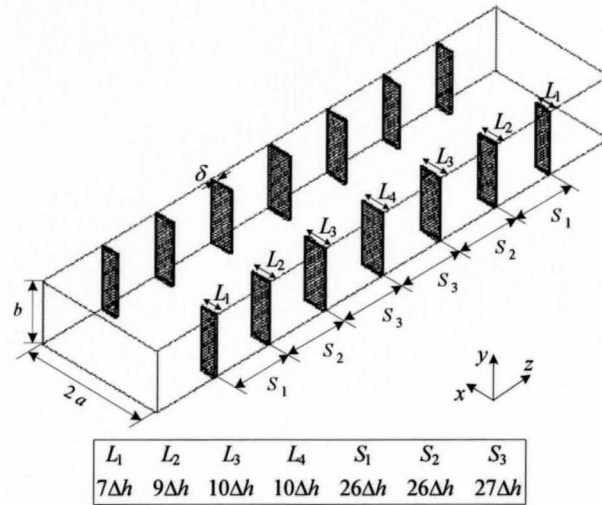


Figure 3.4 H-plane waveguide filter [17].

Table 3.1 The nominal design parameter values. (All dimensions in mm)

a	17.4244
b	15.7988
δ	0.62230
L_1	4.35610
L_2	5.60070
L_3	6.22300
L_4	6.22300
S_1	16.1798
S_2	16.1798
S_3	16.8021

computational domain in the x -direction is simulated by using a magnetic boundary. The analysis is performed at $f_0 = 7$ GHz where only the dominant TE_{10} mode propagates. The maximum mesh convergence error for the S -parameters is set as 0.009. We set the step size of the sensitivity grid as $\Delta h = \delta = 0.6223$ mm.

The port symmetry of the filter can be used in both HFSS simulation and the post-processing. We do not need to export field values when port 2 is excited because it is fully symmetric to the one when port 1 is excited where the plane of symmetry is mid-way along the filter. However, due to the minor effect of extra field exporting on the overall simulation time for sensitivity analysis, this symmetry was not used in the present implementation. In the case of the parameter L_4 , we compute the sensitivities for both the metallization (the forward perturbation and the de-metallization case (the backward perturbation). The fields

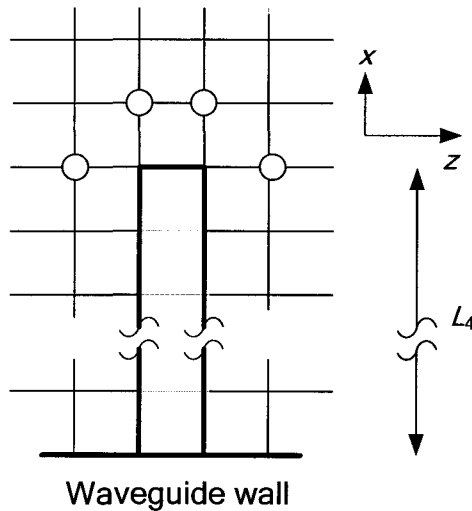


Figure 3.5 Locations for recording E_y for the derivatives with respect to L_4 (regardless of whether we assume metallization or de-metallization). Grid cell size of the sensitivity grid is set as $\Delta x = \Delta z = \delta$.

we need to record are the ones adjacent to the perturbed boundary, see Figure 3.5. The field E_y is recorded at points indicated by circles. Note that these locations are in accordance with the illustration in Figure 3.2.

For the derivatives with respect to S_1 , the perturbation grid points are shown in Figure 3.6. A perturbation of S_1 by Δz involves simultaneously the metallization of cells on one side of the septum and the de-metallization of cells on other side of the septum. Here, we assume a shift of the structure to the left, so that the cells on the left are metallized while the right-hand cells are de-metallized. In Figure 3.6, the points with a cross are the actual points where we record the fields; the points with a square are the adjoint field points and those with a circle are the original field points.

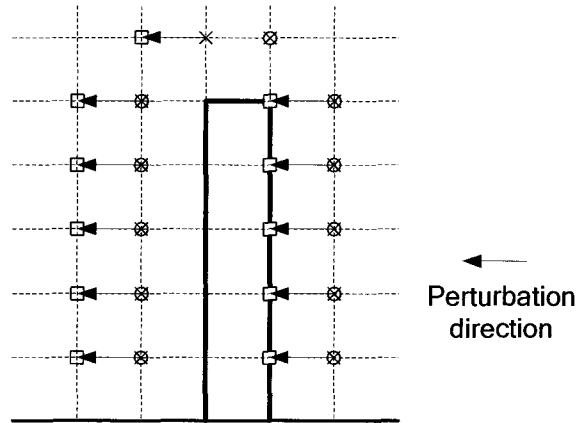


Figure 3.6 The recorded field locations for the derivatives with respect to S_1 . The points, at which the field is recorded, are marked with a cross. The original field and the adjoint field values are needed at the points marked with circles and squares, respectively. The arrows denote the field mapping we use to obtain the adjoint field of the perturbed problem.

The S -parameter derivatives are computed with our FDFD-based self-adjoint sensitivity analysis technique and are compared with the derivatives obtained via response-level central finite differences (CFD). In all plots, our results are marked with FDFD-SASA (for finite-difference frequency-domain self-adjoint sensitivity analysis), while the results obtained through direct finite differencing are marked with CFD. Both the field solution and the S -parameters are obtained with a commercial FEM solver [10].

First, we plot the S -parameters in Figure 3.7. Figures 3.8 to 3.12 show the derivatives of $\text{Re}S_{11}$, $\text{Im}S_{11}$, $|S_{11}|$, $\angle S_{11}$, $\text{Re}S_{21}$, $\text{Im}S_{21}$, $|S_{21}|$ and $\angle S_{21}$ with respect to the septum length L_4 for a sweep of L_4 from $6\Delta h = 3.7338$ mm to $15\Delta h = 9.3345$ mm for forward perturbation. The Yee-cell approach is employed in all cases. The rest of the variables are kept at their nominal values (see Table 3.1).

We note that FDFD-SASA yields identical derivatives for assumed forward (metallization) and backward (de-metallization) perturbations. Hence, we can employ either of the formulations to compute the S -parameter Jacobians. Figure 3.13 shows a comparison of the two cases. In contrast, forward finite-difference (FFD) and backward finite-difference (BFD) derivative estimates consistently display some differences, which sometimes are very significant.

The derivatives of the reflection and insertion losses with respect to the resonator length S_1 are shown in Figure 3.14 and Figure 3.15 for a sweep of S_1 from $21\Delta h = 13.0683$ mm to $30\Delta h = 18.669$ mm.

The agreement between the CFD and the FDFD-SASA curves is generally very good. Also, it is evident that the FDFD-SASA derivatives suffer less from the numerical noise of the EM simulation than the CFD derivatives and are more reliable.

We next employ the central-node approach and confirm its validity by comparing with the CFD approach. Figures 3.16 to 3.20 provide comparison of the derivatives of S -parameters with respect to the septum length L_4 . Figure 3.21 shows the comparison of forward and backward perturbation. Likewise, Figure 3.22 and Figure 3.23 compare the derivatives with respect to the resonator length S_1 .

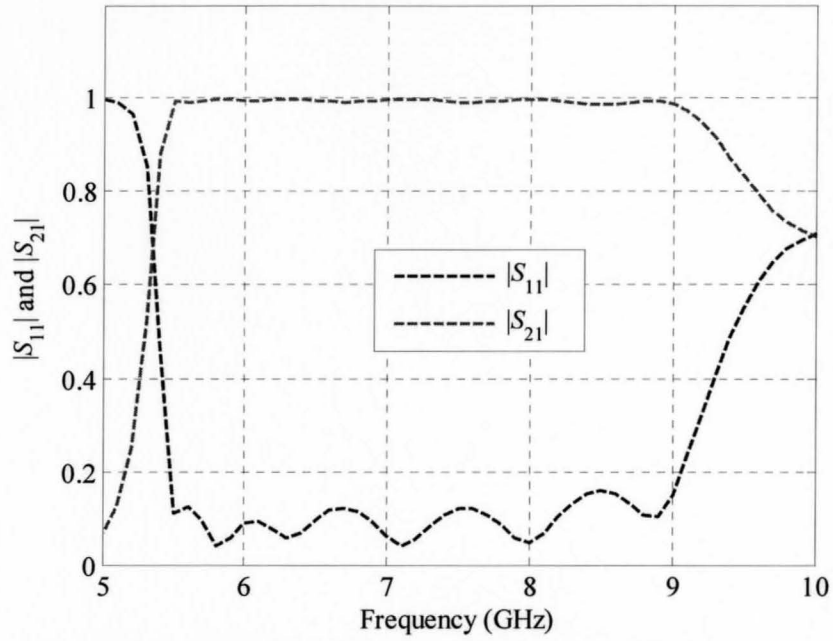


Figure 3.7 The S -parameters of the H-plane filter.

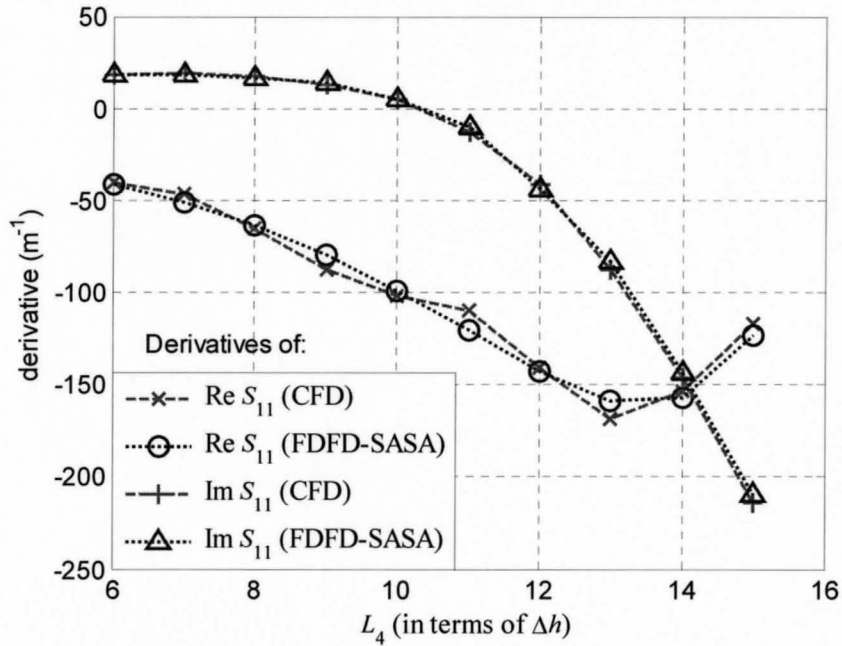


Figure 3.8 The derivatives of $\text{Re } S_{11}$ and $\text{Im } S_{11}$ with respect to L_4 at 7 GHz for the H-plane filter with Yee-cell grid with assumed forward perturbation.

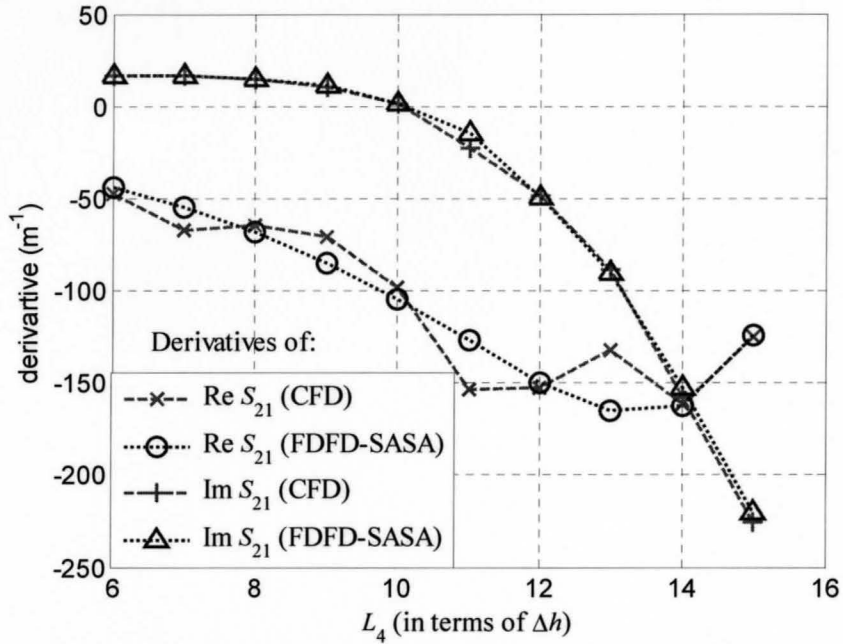


Figure 3.9 The derivatives of $Re S_{21}$ and $Im S_{21}$ with respect to L_4 at 7 GHz for the H-plane filter with Yee-cell grid with assumed forward perturbation.

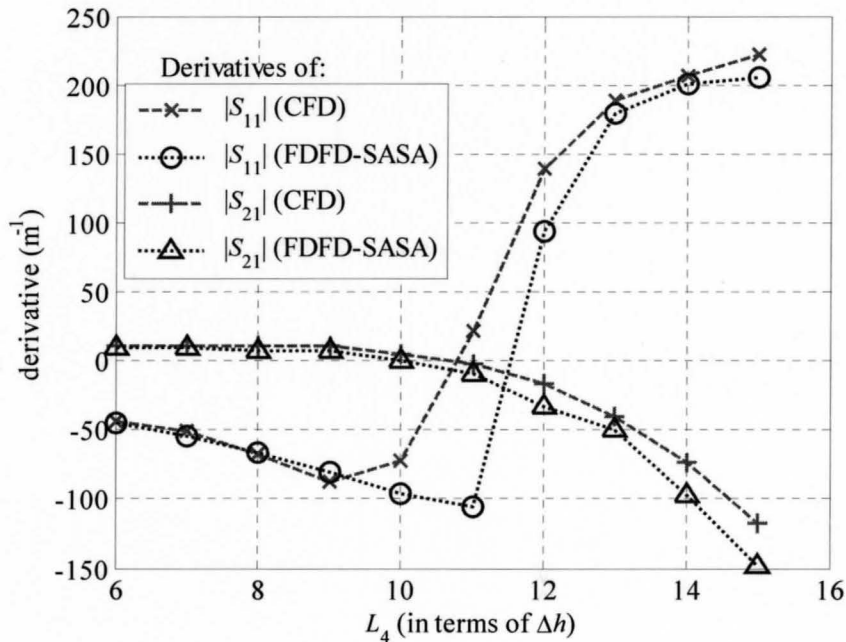


Figure 3.10 The derivatives of $|S_{11}|$ and $|S_{21}|$ with respect to L_4 at 7 GHz for the H-plane filter with Yee-cell grid with assumed forward perturbation.

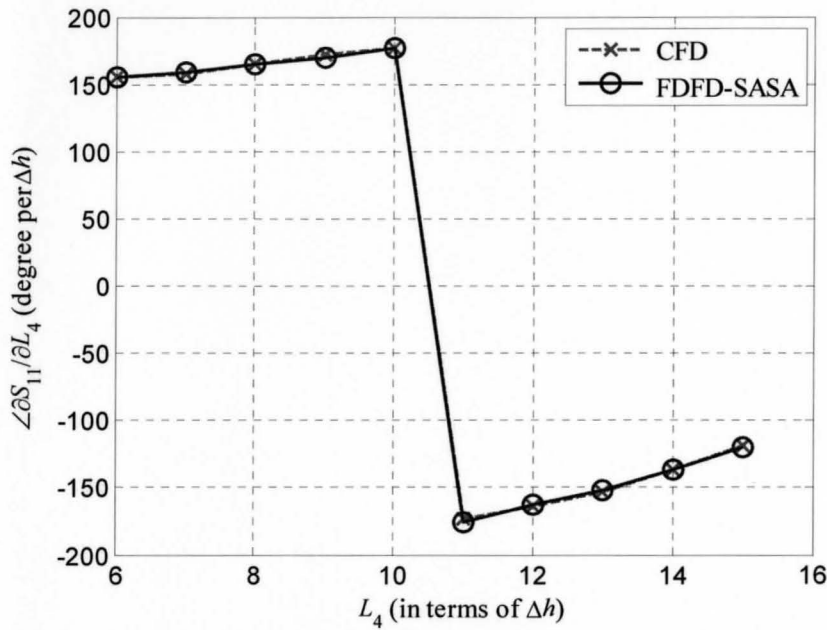


Figure 3.11 The derivative of $\angle S_{11}$ with respect to L_4 at 7 GHz for the H-plane filter with Yee-cell grid with assumed forward perturbation.

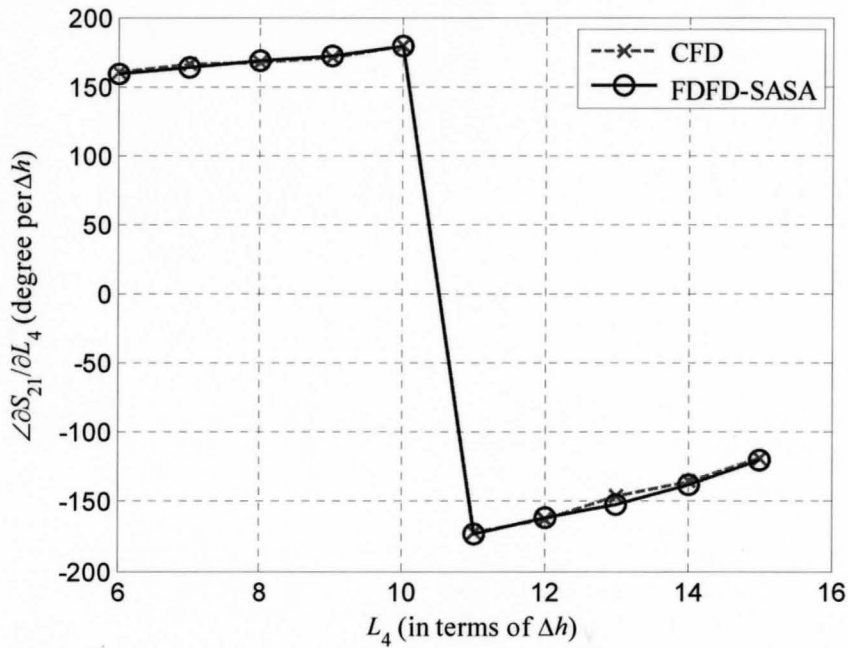


Figure 3.12 The derivative of $\angle S_{21}$ with respect to L_4 at 7 GHz for the H-plane filter with Yee-cell grid with assumed forward perturbation.

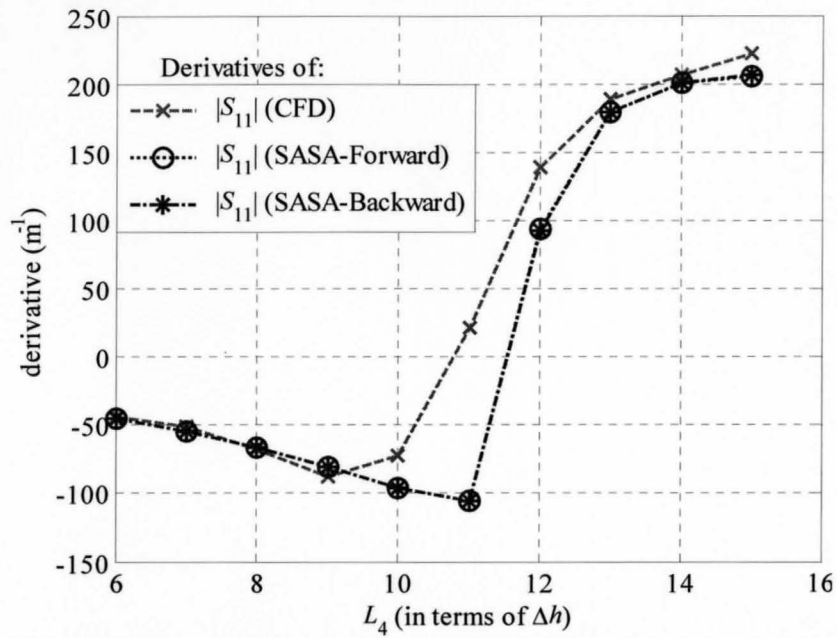


Figure 3.13 Comparison of the derivatives of $|S_{11}|$ with respect to L_4 at 7 GHz for the H-plane filter with Yee-cell grid with assumed forward and backward perturbation.

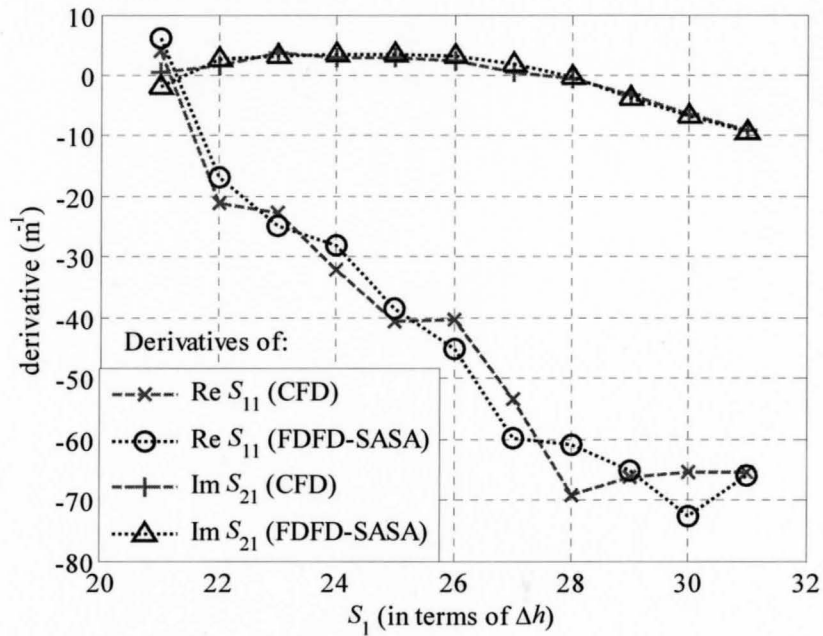


Figure 3.14 The derivatives of $\text{Re } S_{11}$ and $\text{Im } S_{21}$ with respect to S_1 at 7 GHz for the H-plane filter with Yee-cell grid with assumed increase of S_1 .

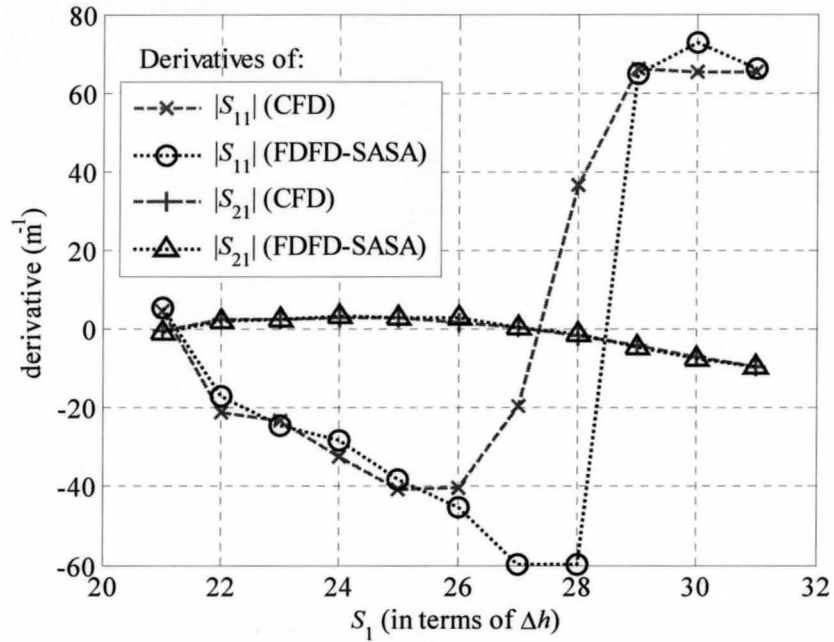


Figure 3.15 The derivatives of $|S_{11}|$ and $|S_{21}|$ with respect to S_1 at 7 GHz for the H-plane filter Yee-cell grid with assumed increase of S_1 .

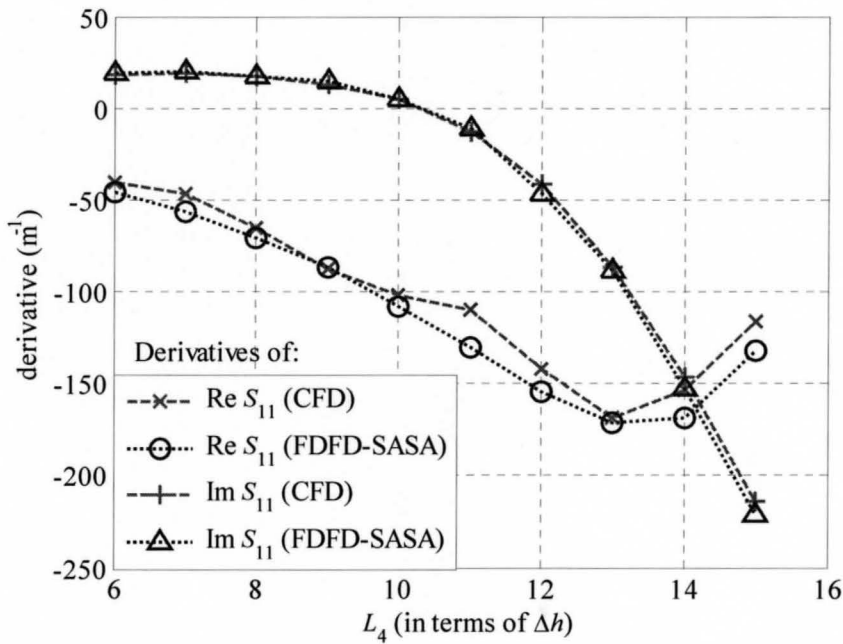


Figure 3.16 The derivatives of $\text{Re } S_{11}$ and $\text{Im } S_{11}$ with respect to L_4 at 7 GHz for the H-plane filter with central-node grid for assumed forward perturbation.

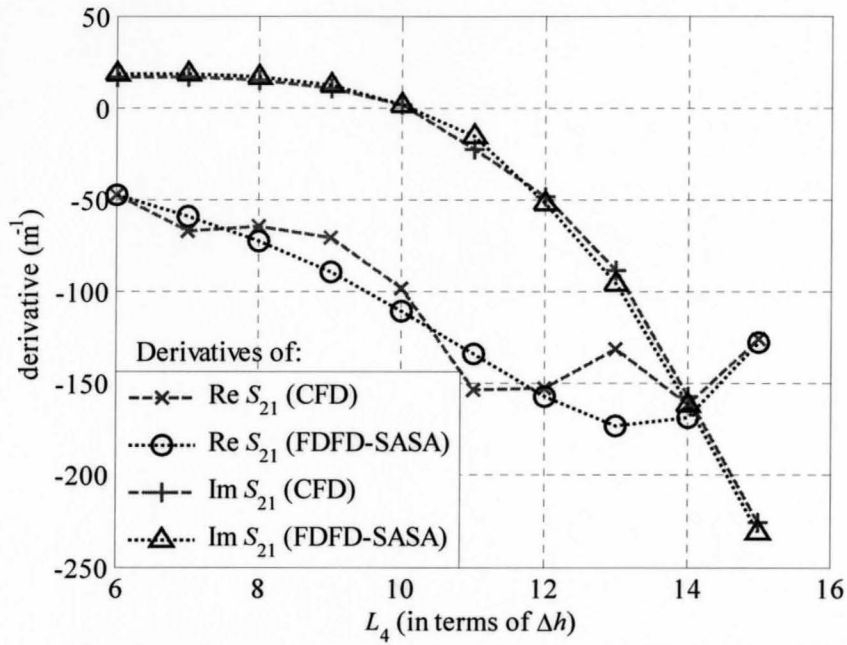


Figure 3.17 The derivatives of $Re S_{21}$ and $Im S_{21}$ with respect to L_4 at 7 GHz for the H-plane filter with central-node grid for assumed forward perturbation.

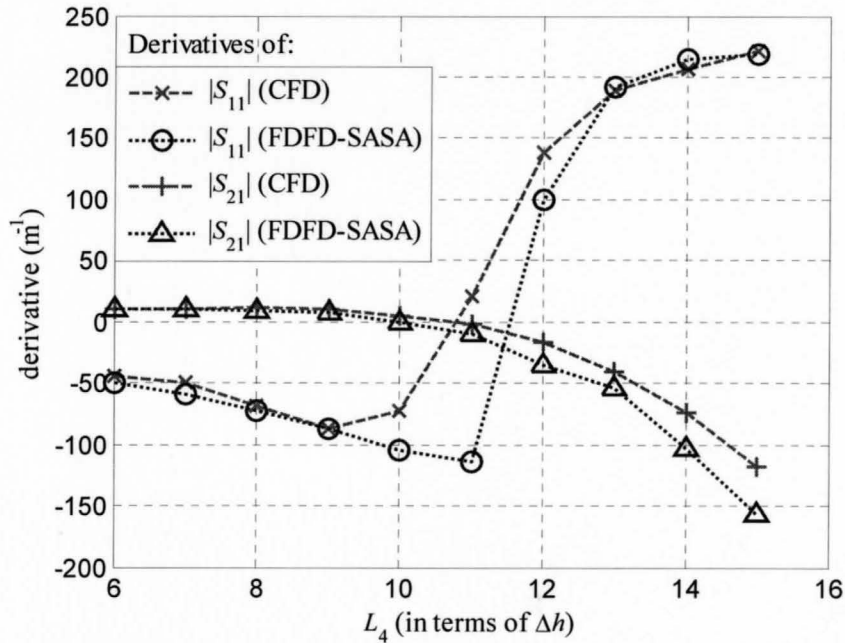


Figure 3.18 The derivatives of $|S_{11}|$ and $|S_{21}|$ with respect to L_4 at 7 GHz for the H-plane filter with central-node grid for assumed forward perturbation.

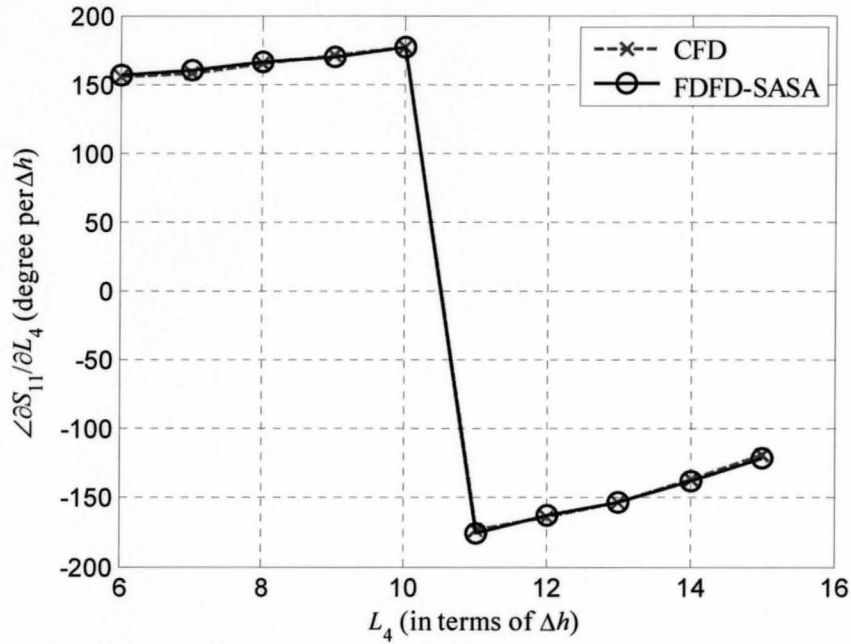


Figure 3.19 The derivative of $\angle S_{11}$ with respect to L_4 at 7 GHz for the H-plane filter with central-node grid for assumed forward perturbation.

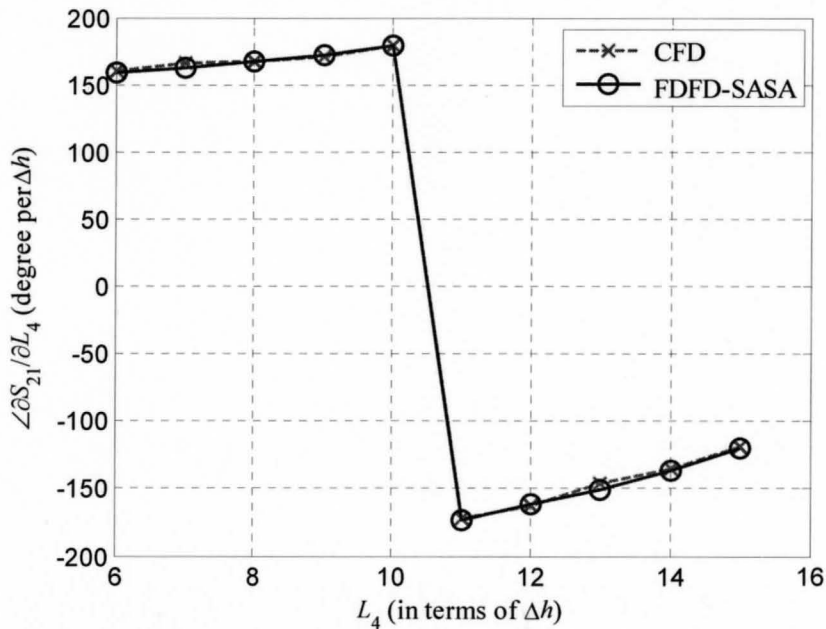


Figure 3.20 The derivative of $\angle S_{21}$ with respect to L_4 at 7 GHz for the H-plane filter with central-node grid for assumed forward perturbation.

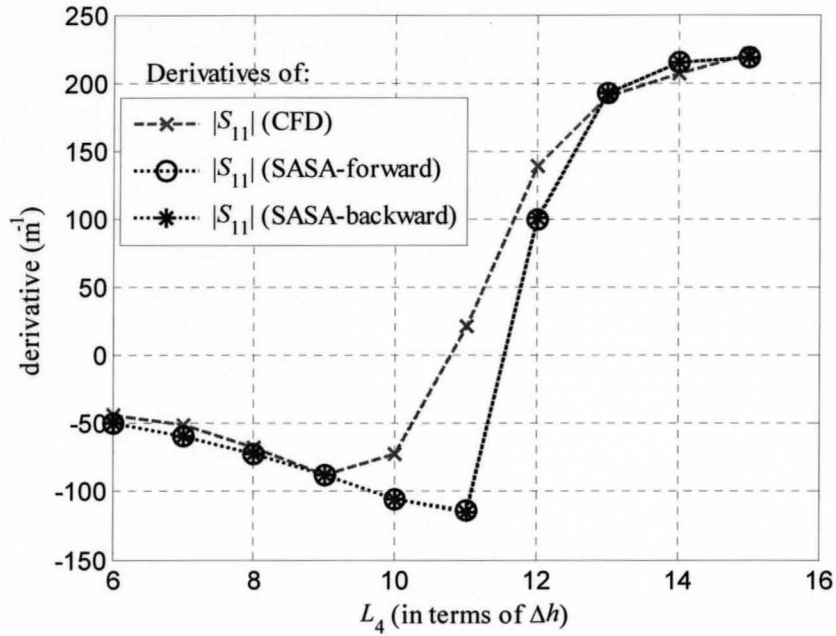


Figure 3.21 Comparison of the derivatives of $|S_{11}|$ and $|S_{21}|$ with respect to L_4 at 7 GHz for the H-plane filter with central-node grid for assumed forward and backward perturbation.

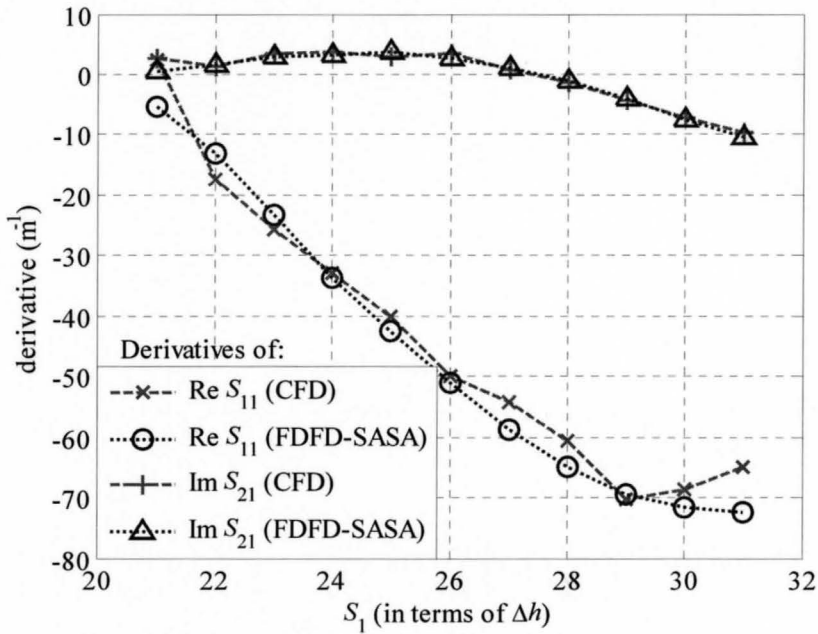


Figure 3.22 The derivatives of $\text{Re } S_{11}$ and $\text{Im } S_{21}$ with respect to S_1 at 7 GHz for the H-plane filter with central-node grid for assumed increase of S_1 .

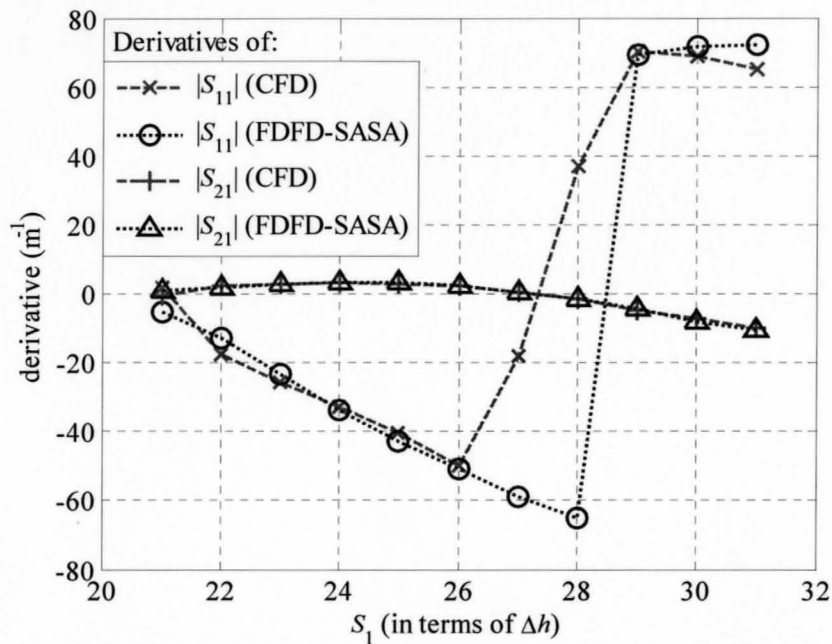


Figure 3.23 The derivatives of $|S_{11}|$ and $|S_{21}|$ with respect to S_1 at 7 GHz for the H-plane filter with central-node grid for assumed increase of S_1 .

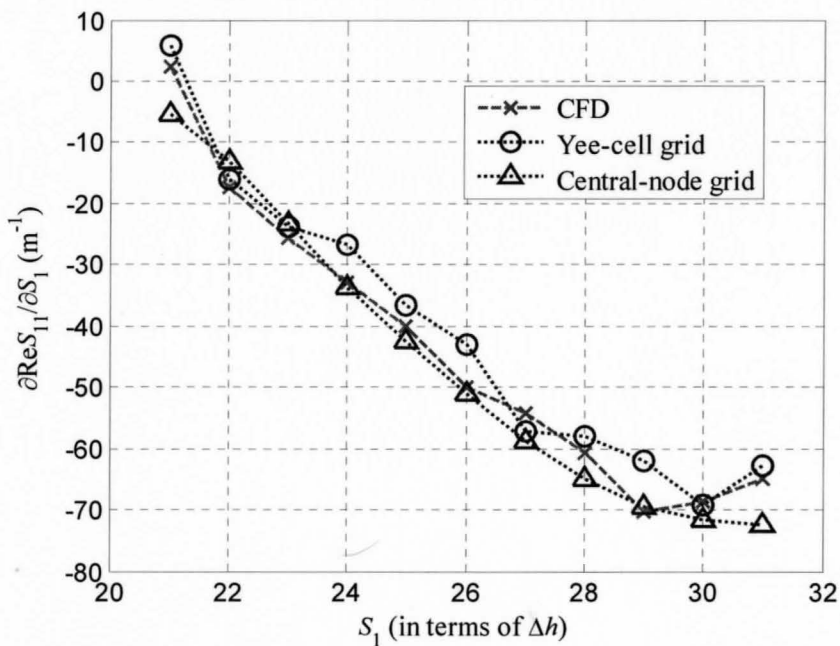


Figure 3.24 Comparison of the derivative of $\text{Re} S_{11}$ with respect to S_1 at 7 GHz for the H-plane filter with both Yee-cell and central-node grid for assumed increase of S_1 .

Finally, Figure 3.24 compares all three approaches to sensitivity analysis, i.e., finite-difference, Yee-cell and central-node for the derivative of $\text{Re}S_{11}$ with respect to the resonator length S_1 . Good agreement is observed among all three curves. The central-node approach provides the smoothest curve, i.e., the least numerical noise. We find that the central-node grid is suitable for sensitivity analysis of metallic objects—there is no loss of accuracy compared to the Yee-cell grid [18].

3.5 SELF-ADJOINT SENSITIVITIES FOR S-PARAMETERS OF METALLIC STRUCTURES (THE 3-D CASE)

The theoretical formulation and the software implementation of a 3-D sensitivity algorithm are complicated on a Yee-cell grid because of the staggered locations of the three \mathbf{E} -field components. Due to the abundance of shapes encountered in microwave structures, a simpler method for 3-D sensitivity analysis is very much needed. We have already verified the central-node grid in the sensitivity analysis of 2-D problems. This approach can also be applied on a 3-D grid where all \mathbf{E} -field components are co-located at the center of each 3-D cell cuboid. This assumption drastically reduces the number of locations to be taken into account, hence simplifying the 3-D sensitivity analysis to a great extent. The central-node grid provides a convenient method for sensitivity analysis of 3-D

metallic objects while bringing together the algorithms for both metallic and dielectric microwave structures.

3.5.1 Metallization

Recall that the sensitivity formula for the S -parameters is:

$$\nabla_p S_{jk} = -\kappa_{jk} \sum_{P \in S_n} \left[(\bar{\mathbf{E}}_j) \cdot \frac{\Delta_n R(\bar{\mathbf{E}}_k)}{\Delta p_n} \cdot \Delta x \Delta y \Delta z \right]_P. \quad (3.28)$$

The residual operator $\Delta_n R(\bar{\mathbf{E}}_k)$ is now calculated in 3-D space. When the assumed perturbation involves the metallization of cells, the difference residual operator is:

$$\frac{\Delta_n R(\bar{\mathbf{E}}_k)}{\Delta p_n} = \frac{\Delta_n \square^2}{\Delta p_n} \bar{\mathbf{E}}_k. \quad (3.29)$$

The operator \square^2 involves finite-difference expressions in 3-D space corresponding to the double-curl operator with a minus sign.

A sample procedure for obtaining the finite-difference expressions for the 2nd order derivatives with respect to two different spatial variables is described in below. Figure 3.25 indicates the relative locations of the points required for the calculation of 2nd order mixed derivative $\partial^2 E_z / \partial x \partial z$ and the respective difference operator $D_{xz} E_z$ at $(0, 0, 0)$. This derivative is obtained as:

$$\left. \frac{\partial^2 E_z}{\partial x \partial z} \right|_{(0,0,0)} \approx \frac{1}{2\Delta z} \left[f^{(0,0,1)} - f^{(0,0,-1)} \right] \quad (3.30)$$

where

$$f^{(0,0,1)} \approx \frac{1}{2\Delta x} \left[E_z^{(1,0,1)} - E_z^{(-1,0,1)} \right] \quad (3.31)$$

$$f^{(0,0,-1)} \approx \frac{1}{2\Delta x} \left[E_z^{(1,0,-1)} - E_z^{(-1,0,-1)} \right] \quad (3.32)$$

Therefore,

$$\begin{aligned} \frac{\partial^2 E_z}{\partial x \partial z} &\approx \frac{1}{4\Delta x \Delta z} \left[E_z^{(1,0,1)} + E_z^{(-1,0,-1)} - E_z^{(-1,0,1)} - E_z^{(1,0,-1)} \right] \\ &= \frac{1}{4\Delta x \Delta z} D_{xz} E_z. \end{aligned} \quad (3.33)$$

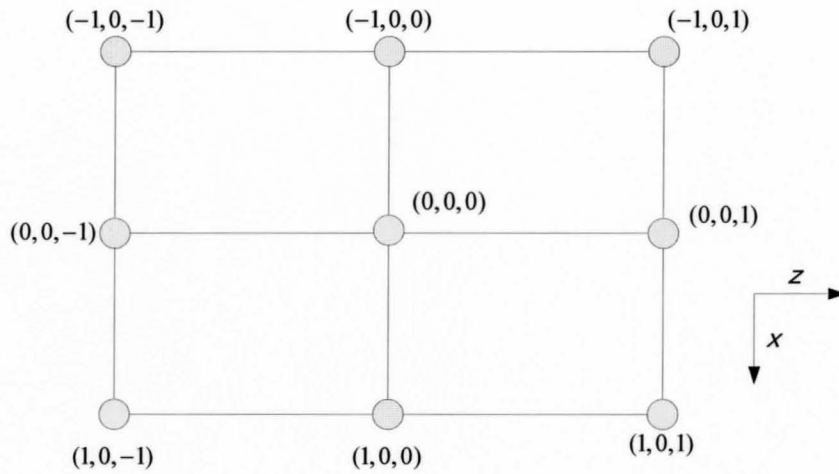
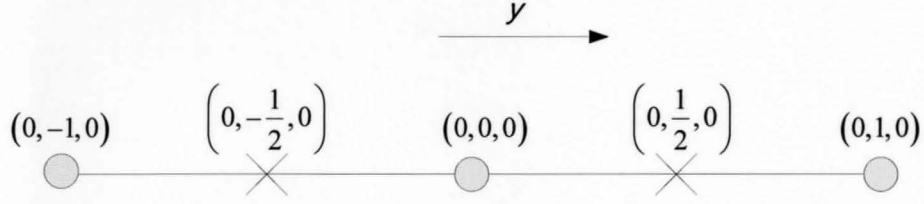


Figure 3.25 Numerical calculation of $D_{xz} E_z$

For calculating 2nd order derivatives with respect to a single variable, the procedure is straightforward. Figure 3.26 shows the locations of the nodes used in the computation.


 Figure 3.26 Node locations for the numerical calculation of $D_{yy}E_\xi$ ($\xi = x, z$)

The central-difference expression is derived as

$$\frac{\partial^2 E_\xi}{\partial y^2} \approx \frac{1}{\Delta y} \left[f^{(0, \frac{1}{2}, 0)} - f^{(0, -\frac{1}{2}, 0)} \right], \quad \xi = x, z \quad (3.34)$$

where

$$f^{(0, \frac{1}{2}, 0)} \approx \frac{1}{\Delta y} \left[E_\xi^{(0, 1, 0)} - E_\xi^{(0, 0, 0)} \right] \quad (3.35)$$

$$f^{(0, -\frac{1}{2}, 0)} \approx \frac{1}{\Delta y} \left[E_\xi^{(0, 0, 0)} - E_\xi^{(0, -1, 0)} \right]. \quad (3.36)$$

Therefore,

$$\begin{aligned} \frac{\partial^2 E_\xi}{\partial y^2} &\approx \frac{1}{\Delta y^2} \left[E_\xi^{(0, 1, 0)} + E_\xi^{(0, -1, 0)} - 2E_\xi^{(0, 0, 0)} \right] \\ &= \frac{1}{\Delta y^2} D_{yy} E_\xi, \quad \xi = x, z. \end{aligned} \quad (3.37)$$

Following similar procedures, we can compute each of the 2nd-order derivative terms in the expressions for the double-curl operator \square^2 . The general expressions for the three components of \square^2 are:

$$\left(\square^2 \mathbf{E}\right)_x = h_y^2 D_{yy} E_x + h_z^2 D_{zz} E_x - \frac{1}{4} \left[h_y h_x D_{yx} E_y - h_z h_x D_{zx} E_z \right] \quad (3.38)$$

$$\left(\square^2 \mathbf{E}\right)_y = h_z^2 D_{zz} E_y + h_x^2 D_{xx} E_y - \frac{1}{4} \left[h_z h_y D_{zy} E_z - h_x h_y D_{yx} E_x \right] \quad (3.39)$$

$$\left(\square^2 \mathbf{E}\right)_z = h_x^2 D_{xx} E_z + h_y^2 D_{yy} E_z - \frac{1}{4} \left[h_x h_z D_{xz} E_x - h_y h_z D_{yz} E_y \right] \quad (3.40)$$

Note that $\Delta_n \square^2$ operates on the original problem solution, which always corresponds to the nominal state.

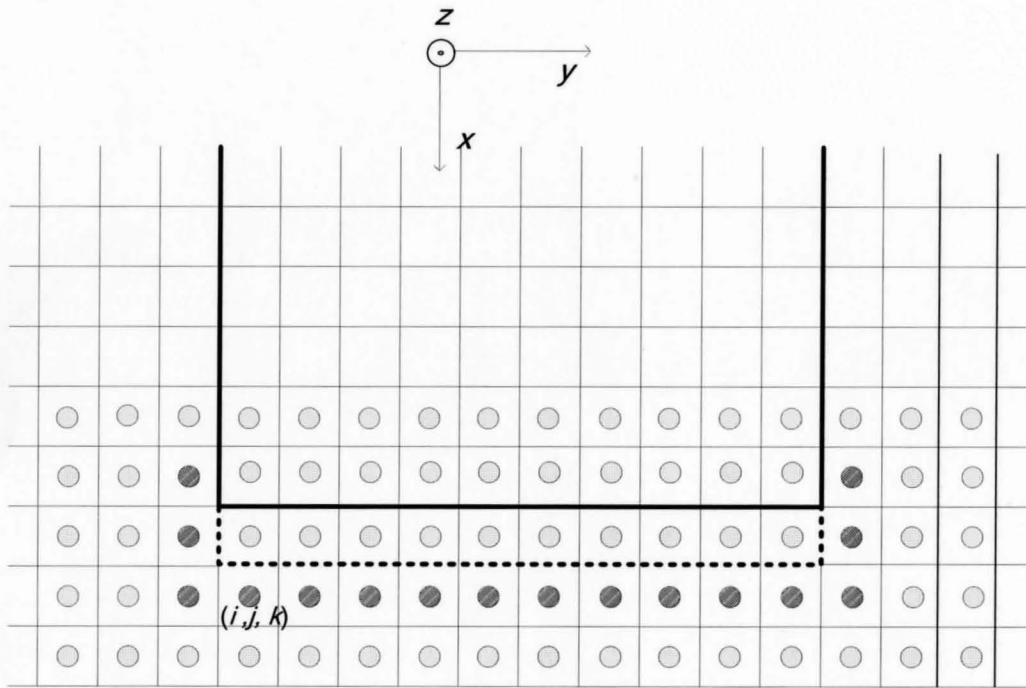


Figure 3.27 Locations at which the double curl operator \square^2 is affected by change of fields due to metallization in the x direction.

Figure 3.27 shows the required field sampling points in the case of a perturbation in the x direction for a rectangular 3-D object. The double-curl

operator \square^2 is affected at all locations marked with dark circles by the perturbation indicated by the dash line.

Consider as an example the point (i, j, k) in Figure 3.27. This point is at an edge of the metallic structure which runs along z . The x component of the \square^2 operator is :

$$\left(\square^2 \bar{\mathbf{E}}\right)_x = h_y^2 D_{yy} E_x + h_z^2 D_{zz} E_x - \frac{1}{4} \left[h_y h_x D_{yx} E_y - h_z h_x D_{zx} E_z \right] \quad (3.41)$$

where

$$D_{yy} E_x = E_x^{(i,j+1,k)} + E_x^{(i,j-1,k)} - 2 \cdot E_x^{(i,j,k)} \quad (3.42)$$

$$D_{zz} E_x = E_x^{(i,j,k+1)} + E_x^{(i,j,k-1)} - 2 \cdot E_x^{(i,j,k)} \quad (3.43)$$

$$D_{xy} E_y = E_y^{(i+1,j+1,k)} + E_y^{(i-1,j-1,k)} - \underline{E_y^{(i-1,j+1,k)}} - E_y^{(i+1,j-1,k)} \quad (3.44)$$

$$D_{zx} E_z = E_z^{(i+1,j,k+1)} + \underline{E_z^{(i-1,j,k-1)}} - \underline{E_z^{(i-1,j,k+1)}} - E_z^{(i+1,j,k-1)}. \quad (3.45)$$

The y component of $\square^2 \bar{\mathbf{E}}$ is:

$$\left(\square^2 \bar{\mathbf{E}}\right)_y = h_z^2 D_{zz} E_y + h_x^2 D_{xx} E_y - \frac{1}{4} \left[h_z h_y D_{zy} E_z - h_x h_y D_{xy} E_x \right] \quad (3.46)$$

where

$$D_{xx} E_y = E_y^{(i+1,j,k)} + \underline{E_y^{(i-1,j,k)}} - 2 \cdot E_y^{(i,j,k)} \quad (3.47)$$

$$D_{zz} E_y = E_y^{(i,j,k+1)} + E_y^{(i,j,k-1)} - 2 \cdot E_y^{(i,j,k)} \quad (3.48)$$

$$D_{xy} E_x = E_x^{(i+1,j+1,k)} + E_x^{(i-1,j-1,k)} - \underline{E_x^{(i-1,j+1,k)}} - E_x^{(i+1,j-1,k)} \quad (3.49)$$

$$D_{yz} E_z = E_z^{(i,j+1,k+1)} + E_z^{(i,j-1,k-1)} - E_z^{(i,j-1,k+1)} - E_z^{(i,j+1,k-1)}. \quad (3.50)$$

Finally, the z component is:

$$\left(\square^2 \bar{\mathbf{E}}\right)_z = h_x^2 D_{xx} E_z + h_y^2 D_{yy} E_z - \frac{1}{4} \left[h_x h_z D_{xz} E_x - h_y h_z D_{yz} E_y \right] \quad (3.51)$$

where

$$D_{xx} E_z = E_z^{(i+1,j,k)} + \underline{E_z^{(i-1,j,k)}} - 2 \cdot E_z^{(i,j,k)} \quad (3.52)$$

$$D_{yy} E_z = E_z^{(i,j+1,k)} + \underline{E_z^{(i,j-1,k)}} - 2 \cdot E_z^{(i,j,k)} \quad (3.53)$$

$$D_{zx} E_x = E_x^{(i+1,j,k+1)} + \underline{E_x^{(i-1,j,k-1)}} - \underline{E_x^{(i-1,j,k+1)}} - E_x^{(i+1,j,k-1)} \quad (3.54)$$

$$D_{yz} E_y = E_y^{(i,j+1,k+1)} + \underline{E_y^{(i,j-1,k-1)}} - \underline{E_y^{(i,j-1,k+1)}} - E_y^{(i,j+1,k-1)}. \quad (3.55)$$

The field components calculated at positions affected by the perturbation are underlined. These terms result in the change of \square^2 . The difference can therefore be calculated from \square^2 in the nominal and the n -th perturbed states. $\Delta_n \square^2$ can be calculated for other points in a similar manner. The n -th perturbed state is used to obtain the n -th adjoint field solution $(\hat{\mathbf{E}}_j)_n$ which multiplies the $\Delta_n R(\bar{\mathbf{E}}_k)$ term.

3.5.2 De-metallization

In the demetallization case, a similar procedure is employed. The residual operator in this case is:

$$\frac{\Delta_n R(\bar{\mathbf{E}})}{\Delta p_n} = -\mathbf{G} \quad (3.56)$$

where $\mathbf{G} = \Delta_n(\beta \mathbf{J}) / \Delta p_n$.

As follows from the discretized Helmholtz equation (3.3) at points where the \mathbf{E} - field component vanishes, the induced current density is:

$$\mathbf{G} = \frac{\square^2}{\Delta p_n} \bar{\mathbf{E}}. \quad (3.57)$$

Therefore,

$$\frac{\Delta_n R(\bar{\mathbf{E}})}{\Delta p_n} = - \frac{\square^2}{\Delta p_n} \bar{\mathbf{E}}. \quad (3.58)$$

3.5.3 Algorithm for software implementation

The central-node grid in 3-D sensitivity analysis not only provides a unified approach for complex metallic-dielectric designs but also paves the way for easy error-free software implementation. Using the field mapping technique already illustrated in the 2-D case, we can determine the field solution for the nominal and all perturbed states in 3-D problems as well. General procedures for software implementation of both metallization and de-metallization cases are outlined below.

Step 1: Generate 3-D matrices for the local E_x, E_y and E_z solutions around the perturbed area at the object of interest.

Step 2: a) Metallization: Generate mapped 3-D solution matrices for the n -th shape parameter $(E_x)_n, (E_y)_n$, and $(E_z)_n$ by incrementing respective coordinate (x, y, z) by respective step $(\pm\Delta x, \pm\Delta y$ or $\pm\Delta z)$.

b) Demetallization: go to Step 4.

Step 3: For metallization case, generate auxiliary field matrices

$(E_\xi)_n^a$, ($\xi = x, y, z$) according to the rule:

unperturbed cells: if $[(E_\xi)^{(i,j,k)} \neq 0. \text{ and } .(E_\xi)_n^{(i,j,k)} \neq 0]$

then

$$(E_\xi)_n^{a(i,j,k)} = 0$$

metallized cells: if $[(E_\xi)^{(i,j,k)} \neq 0. \text{ and } .(E_\xi)_n^{(i,j,k)} = 0]$

then

$$(E_\xi)_n^{a(i,j,k)} = -(E_\xi)^{(i,j,k)}$$

Step 4: a) Metallization: calculate $\square_\xi^2(\bar{\mathbf{E}}_n^a)$ everywhere in the perturbation

domain and assign to $\Delta_n \square_\xi^2(\bar{\mathbf{E}})$. This is the $\Delta_n R(\bar{\mathbf{E}}_k)$ term.

b) De-metallization: calculate $\square_\xi^2(\bar{\mathbf{E}})$ at perturbed points, i.e., where

$(E_\xi)_n^a$ is not zero, and multiply by -1. This is the $\Delta_n R(\bar{\mathbf{E}}_k)$ term for

demetallization.

Step 5: Multiply $\Delta_n R(\bar{\mathbf{E}}_k)$ by respective component of $(E_\xi)_n$ and add to

sensitivity summation (see (3.28)).

3.6 EXAMPLE

3.6.1 Six-Section H-Plane Waveguide Filter

A six-section H-plane waveguide filter similar to that of Figure 3.4 is used for verifying our 3-D approach. The only difference is in the width of the middle septum. The width of this septum is set to $4 \cdot \Delta h$ instead of Δh to test the 3-D nature of our algorithm. The analysis is performed at $f_0 = 7$ GHz where only the dominant TE_{10} mode propagates. We set the step size of the sensitivity grid as $\Delta h = \delta = 0.6223$ mm in the x and z directions and to 0.631952 mm in the y direction. Figures 3.28 to 3.32 show the derivatives of $\text{Re}S_{11}$, $\text{Im}S_{11}$, $|S_{11}|$, $\angle S_{11}$, $\text{Re}S_{21}$, $\text{Im}S_{21}$, $|S_{21}|$ and $\angle S_{21}$ with respect to the septum length L_4 for a sweep of L_4 from $6\Delta h = 3.7338$ mm to $15\Delta h = 9.3345$ mm for both assumed forward and backward perturbations. The rest of the variables are at their nominal values (see Table 3.1). As before, in all plots, our results are marked with FDFD-SASA, while the results obtained through direct finite differencing are marked with CFD.

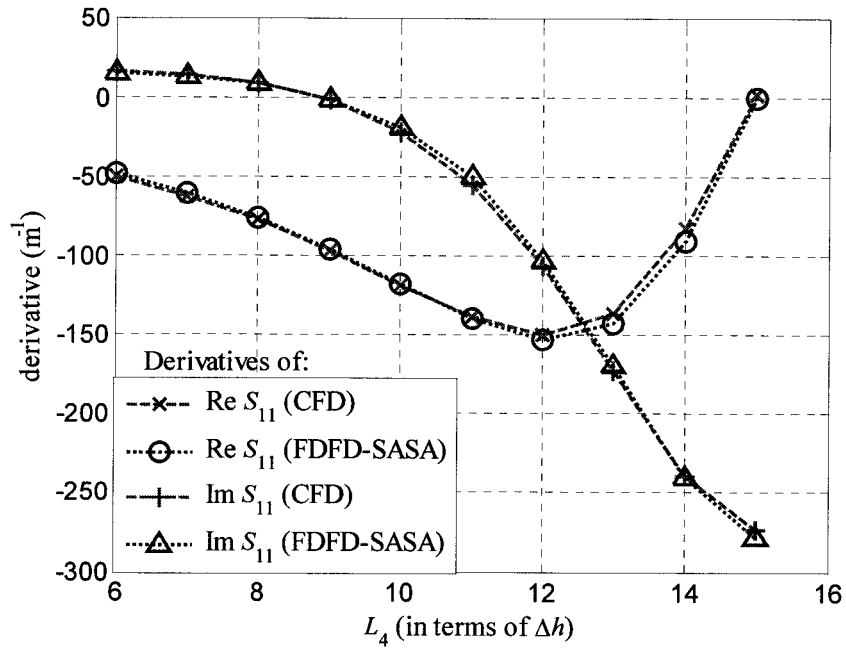


Figure 3.28 The derivatives of $Re S_{11}$ and $Im S_{11}$ with respect to L_4 at 7 GHz for the H-plane filter with 3-D central-node grid for assumed forward perturbation.

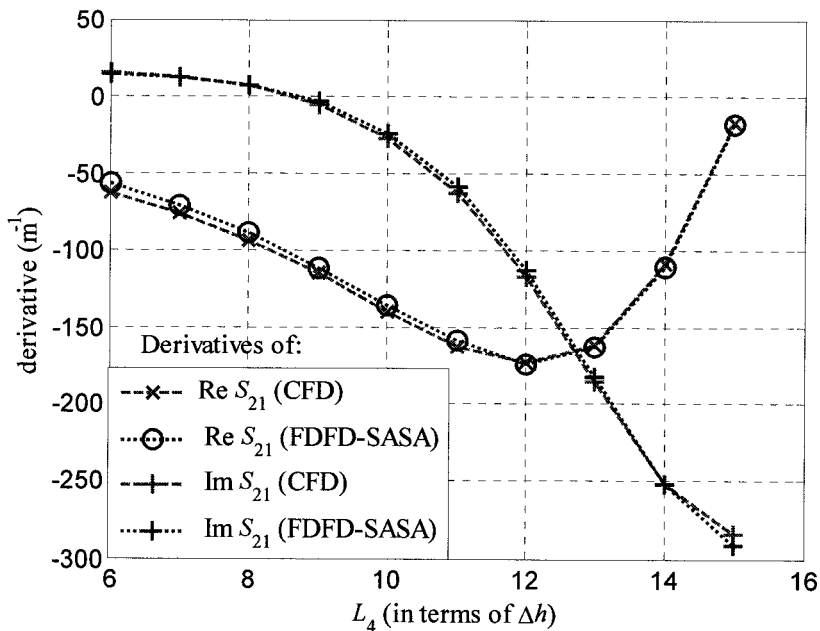


Figure 3.29 The derivatives of $Re S_{21}$ and $Im S_{21}$ with respect to L_4 at 7 GHz for the H-plane filter with 3-D central-node grid for assumed forward perturbation.

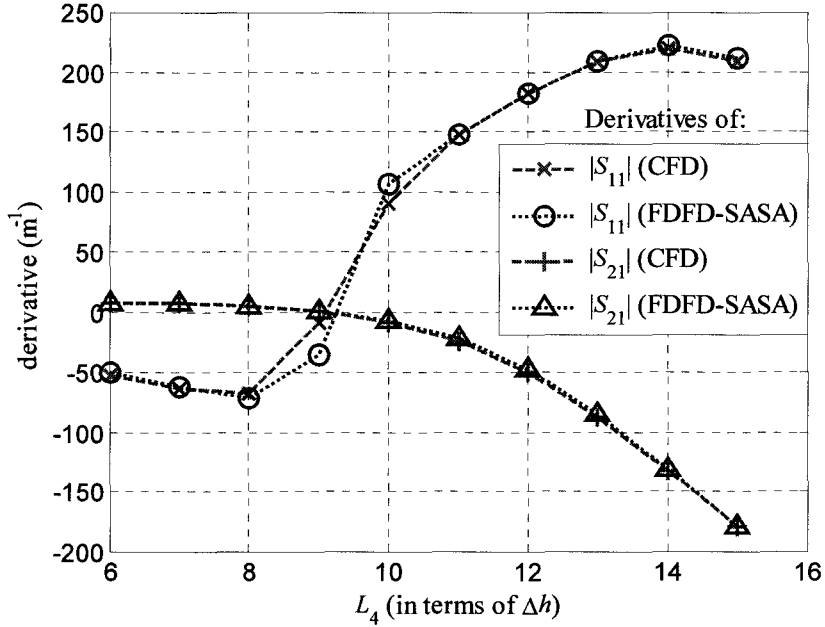


Figure 3.30 The derivatives of $|S_{11}|$ and $|S_{21}|$ with respect to L_4 at 7 GHz for the H-plane filter with 3-D central-node grid for assumed forward perturbation.

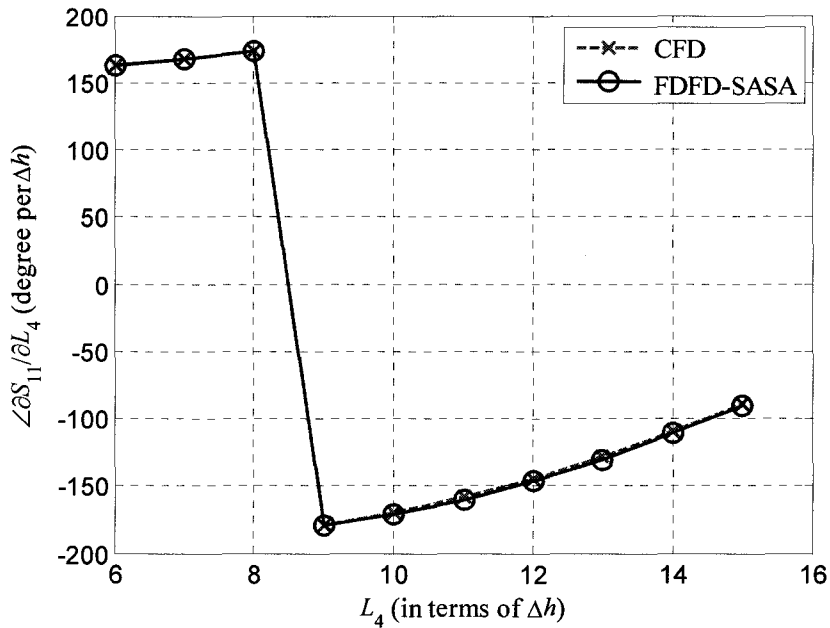


Figure 3.31 The derivative of $\angle S_{11}$ with respect to L_4 at 7 GHz for the H-plane filter with 3-D central-node grid for assumed forward perturbation.

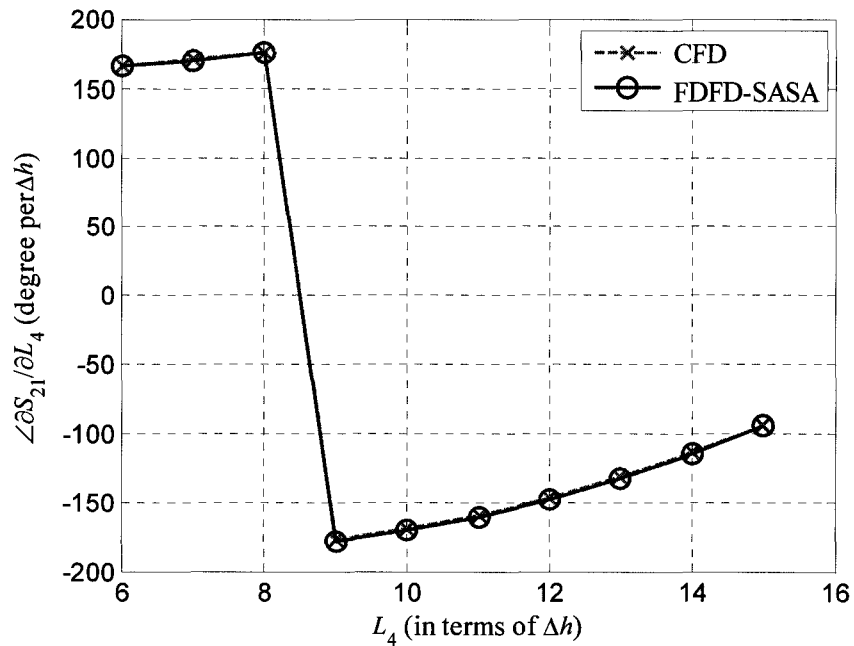


Figure 3.32 The derivative of $\angle S_{21}$ with respect to L_4 at 7 GHz for the H-plane filter with 3-D central-node grid for assumed forward perturbation.

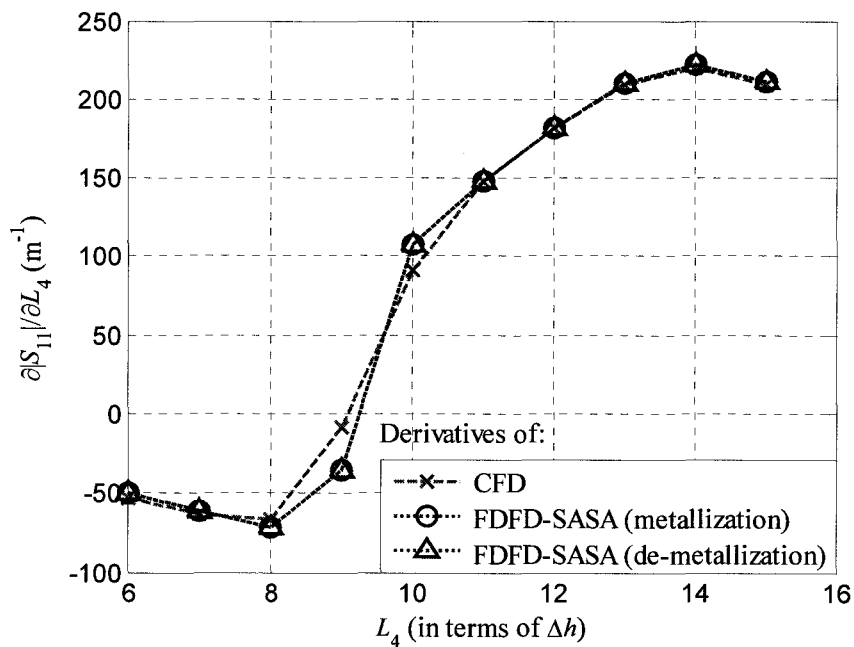


Figure 3.33 Comparison of 3-D sensitivity analyses with forward and backward perturbation.

Finally, Figure 3.33 provides a comparison of the derivatives for metallization and de-metallization cases with our 3-D self-adjoint sensitivity analyses for the parameter L_4 . We note that our 3-D FDFD-SASA approach yields identical derivatives for assumed forward (metallization) and backward (de-metallization) perturbations. Our FDFD-SASA approach is inherently 2nd-order accurate and is thus superior to forward finite-difference (FFD) and backward finite-difference (BFD) derivative estimates both in terms of accuracy and computational efficiency.

REFERENCES

- [1] D. G. Cacuci, *Sensitivity & Uncertainty Analysis, Volume 1: Theory*. Boca Raton, FL: Chapman & Hall/CRC, 2003.
- [2] A. D. Belegundu and T. R. Chandrupatla, *Optimization Concepts and Applications in Engineering*. Upper Saddle River, NJ: Prentice Hall, 1999.
- [3] E. J. Haug, K. K. Choi and V. Komkov, *Design Sensitivity Analysis of Structural Systems*. Orlando: Academic Press Inc., 1986.
- [4] H. Akel and J. P. Webb, "Design sensitivities for scattering-matrix calculation with tetrahedral edge elements," *IEEE Trans. Magnetics*, vol. 36, pp. 1043-1046, July 2000.
- [5] N. K. Nikolova, J. W. Bandler, and M. H. Bakr, "Adjoint techniques for sensitivity analysis in high-frequency structure CAD," *IEEE Trans. Microwave Theory Tech.*, vol. 52, pp. 403-419, Jan. 2004.
- [6] N. K. Georgieva, S. Glavic, M. H. Bakr and J. W. Bandler, "Feasible adjoint sensitivity technique for EM design optimization," *IEEE Trans. Microwave Theory Tech.*, vol. 50, pp. 2751-2758, Dec. 2002.
- [7] S. M. Ali, N. K. Nikolova, and M. H. Bakr, "Recent advances in sensitivity analysis with frequency-domain full-wave EM solvers," *Applied Computational Electromagnetics Society Journal*, vol. 19, pp. 147-154, Nov. 2004.
- [8] N. K. Nikolova, J. Zhu, D. Li, M. H. Bakr and J. W. Bandler, "Sensitivity analysis of network parameters with electromagnetic frequency-domain simulators," *IEEE Trans. Microwave Theory and Tech.*, vol. 54, pp. 670-681, Feb. 2006.
- [9] D. Li, J. Zhu, N. K. Nikolova, M. H. Bakr, and J. W. Bandler, "Electromagnetic optimization using sensitivity analysis in the frequency domain," *IET Proc. Microwaves, Antennas & Propagation*, vol. 1, No. 4, pp. 852-859, Aug. 2007.
- [10] Ansoft HFSS ver. 11, Ansoft Corporation, 225 West Station Square Drive, Suite 200, Pittsburgh, PA 15219, USA, 2006, www.ansoft.com

- [11] N. K. Nikolova, H. W. Tam, and M. H. Bakr, "Sensitivity analysis with the FDTD method on structured grids," *IEEE Trans. Microwave Theory and Tech.*, vol. 52, pp. 1207-1216, Apr. 2004.
- [12] N. K. Nikolova, Ying Li, Yan Li, and M.H. Bakr, "Sensitivity analysis of scattering parameters with electromagnetic time-domain simulators," *IEEE Trans. Microwave Theory Tech.*, vol. 54, pp. 1598-1610, 2006.
- [13] J. Jin, *The Finite Element Method in Electromagnetics*, 2nd ed. New York: John Wiley & Sons, 2002.
- [14] Y. Song and N.K. Nikolova, "Central-node approach for accurate self-adjoint sensitivity analysis of dielectric structures," *IEEE MTT-S Int. Microwave Symposium*, pp. 895-898, June 2007.
- [15] X. Zhu, A. Hasib, and N.K. Nikolova, "Electromagnetic sensitivity analysis of scattering parameters based on the FDFD method," *Int. Symp. on Signals, Systems, and Electronics (ISSSE 2007)*, pp. 165-168, July-Aug. 2007.
- [16] N. K. Nikolova, A. Hasib and X. Zhu, "Independent sensitivity solver based on the frequency domain finite difference method," *Applied Computational Electromagnetics Society (ACES 2008)*, pp. 1024-1029, March-Apr. 2008.
- [17] G. Matthaei, L. Young, and E. M. T. Jones, *Microwave Filters, Impedance-matching Networks, and Coupling Structures*. Norwood, MA: Artech House, 1980, p. 545.
- [18] X. Zhu, A. Hasib and N. K. Nikolova, "Efficient electromagnetic optimization using self-adjoint Jacobian computation based on a central-node FDFD method," *IEEE MTT-S Int. Microwave Symposium*, June 2008.

CHAPTER 4

GRADIENT BASED

OPTIMIZATION WITH

SELF-ADJOINT SENSITIVITY

ANALYSIS USING FDFD METHOD

4.1 INTRODUCTION

The optimization algorithms used in computer-aided design can be divided into two categories: those which require only objective function values during the optimization process and those which require the objective function and its derivatives with respect to the optimizable parameters. Examples of the former are the traditional pattern search [1], genetic and particle swarm algorithms [1], [2], as well as some neural-network based algorithms [3]. Some of these, such as the genetic and particle swarm algorithms, are preferable when there is little or no information about an initial design. Their drawback is that they require a large

number of system analyses. With 3-D full wave electromagnetic (EM) solvers, which require extensive simulation time, such approaches are often impractical. The second category includes gradient-based algorithms based on quasi-Newton, sequential quadratic programming (SQP) and trust-region methods. They need the objective function Jacobian and/or Hessian in addition to the objective function itself. These optimization methods search for a local optimal point. A gradient-based algorithm is expected to converge much faster, i.e., with fewer system analyses, than an algorithm in the first category. Its drawback is that a global minimum is not guaranteed, and a failure to converge is a possibility. Naturally, the solution provided by a gradient-based local optimization algorithm depends on the quality of the initial design. For a realistic 3-D EM-based design problem with an acceptable starting point, gradient-based optimization is usually preferred.

The efficiency of a successful gradient-based optimization process depends mainly on two factors: (i) the number of iterations required to achieve convergence, and (ii) the number of simulation calls per iteration. The first factor depends largely on the nature of the algorithm, on the proper formulation of the objective or cost function, and on the accuracy of the response Jacobians and/or Hessian. The second factor depends mostly on the method used to compute the Jacobians and/or Hessian, which are necessary to determine the search direction and the step in the design parameter space. The sensitivity analysis, which

provides Jacobians, is very time consuming when finite differences or higher-order approximations are used at the response level. At least $N+1$ full wave simulations are needed to obtain a Jacobian for N design parameters. This is unacceptable when N is large.

In Chapter 2, we discussed a frequency-domain self-adjoint sensitivity analysis (SASA) method for the efficient computation of network parameter sensitivities in the frequency domain. This method was later used in conjunction with optimization algorithms to investigate its efficiency [4]. In Chapter 3, we introduced a new frequency-domain sensitivity analysis technique to overcome the shortcomings of previous frequency-domain sensitivity analysis methods. We refer to this method as frequency-domain finite-difference SASA (FDFD-SASA) since it uses finite-difference grid and the self-adjoint constants and the field solutions are in the frequency-domain. The SASA produces the response and its Jacobian with a single full-wave analysis when the objective function depends on the network parameters, e.g., the S -parameters.

In this chapter, we investigate the advantages of using our FDFD-SASA method to provide the Jacobian during optimization processes [5]. With it, the sensitivity analysis has practically no computational overhead which leads to overall acceleration of the optimization process.

We validate and compare our method using a minimax optimization with a gradient-based trust-region search algorithm. It requires the Jacobian. For

comparison purposes, two separate optimization procedures are carried out: in the 1st one the S -parameter Jacobian is computed with FDFD-SASA while in the 2nd one the Jacobian is supplied by FD response-level approximations.

In Section 4.2, we discuss the FDFD-SASA implementation in gradient-based optimization. Section 4.3 gives a numerical example. We compare the performance of the optimization processes in Section 4.4.

4.2 OPTIMIZATION WITH 2-D FDFD SELF-ADJOINT SENSITIVITIES

The design problem is defined as

$$\mathbf{p}^* = \arg \min_{\mathbf{p}} F(\mathbf{R}(\mathbf{p})) \quad (4.1)$$

where \mathbf{R} is the vector of M responses, \mathbf{p} is the vector of design parameters, and \mathbf{p}^* is the optimal solution which minimizes the objective function F . In our examples, the M responses are the S -parameter magnitudes evaluated at select frequencies where design goals specify lower (L) or upper (U) bounds for the responses. F is defined as $F = \max\{e_1, \dots, e_M\}$, where the error e_m , $m = 1, \dots, M$ ($M = M_L + M_U$), is $e_m = L_m - R_m$, $m = 1, \dots, M_L$, in the case of a lower bound, and $e_m = R_m - U_m$, $m = M_L + 1, \dots, M$, for an upper bound.

The inaccuracy for finite-difference response-level approximations tends to be significant when the increment of the design parameters is very small, e.g.,

near a local minimum, as catastrophic cancellation occurs. The FDFD-SASA algorithm is free of such problems. It is simple to implement and guarantees very good accuracy regardless of the values of the increments in the design-parameter space.

4.3 EXAMPLE

We validate our algorithm with a finite-element method (FEM) solver HFSS [6] by a numerical example: an H-plane waveguide filter. In this example, we perform gradient-based optimization using the response Jacobian provided by: (1) the proposed FDFD-SASA approach and (2) the forward finite-difference approximation at the response level denoted by FFD.

4.3.1 Six-Section H-Plane Waveguide Filter

The six-section H-plane filter is shown in Figure 4.1 [7]. The rectangular waveguide is of width 3.485 cm and height 1.58 cm. The cutoff frequency of the TE₁₀ mode is 4.3 GHz. The 6 resonators are separated by 7 septa of finite thickness $\delta=0.625$ mm. The design parameters are the septa widths $L_1, L_2, L_3,$ and L_4 and the resonator lengths $S_1, S_2,$ and S_3 . A minimax objective function is used with the design specifications

$$\begin{aligned} |S_{11}| &\geq 0.85 & f &\leq 5.2 \text{ GHz}, \\ |S_{11}| &\leq 0.16 & 5.4 &\leq f \leq 9 \text{ GHz}, \\ |S_{11}| &\geq 0.5 & f &\geq 9.5 \text{ GHz}. \end{aligned} \tag{4.2}$$

We perform two optimizations with two and four variables, respectively. We choose 22 frequency points distributed in the frequency range from 5 GHz to 10.0 GHz.

In the two-variable optimization problem, the initial design is given by $\mathbf{p}^{(0)} = [L_3 \ L_4]^T = [9\Delta h \ 13\Delta h]^T = [5.6007 \ 8.0899]^T$ (all in mm). We use Madsen's minimax optimization algorithm [8], which employs a trust region and requires response Jacobians. We refer to Madsen's algorithm as TR-minimax. We provide the Jacobians with our FDFD-SASA solver. Its uniform central-node grid is set as $\Delta h = 0.6223$ mm, which is roughly equal to the shortest edge length of the FEM mesh generated by the FEM solver [6]. The initial trust-region radius is set to $r_0 = 0.05 \cdot \|\mathbf{p}^{(0)}\|$. Generally, the choice of the initial trust region radius depends on the nonlinearity of the objective function at the initial point. Many algorithms use an *ad hoc* value and the user is expected to provide an initial guess. This is the case with this particular optimization code. The value above was chosen so that it is sufficiently smaller than $0.1 \cdot \|\mathbf{p}^{(0)}\|$ —a value recommended for a weakly nonlinear problem—since from previous experience we know that the H-plane filter design problem is strongly nonlinear [9].

For comparison, we perform a separate optimization process where we do not use our sensitivity solver thereby enforcing response-level calculation of the Jacobian via forward finite differences (FFD). This optimization process is an

example of current practices in EM design optimization. When computing the FFD Jacobians, one has to carefully choose the amounts of perturbation Δp_n , $n = 1, \dots, N$. Otherwise, the FFD Jacobians are inaccurate and may result in trapping the optimization in a local minimum. After some trials, with the initial vector $\mathbf{p}^{(0)}$ given above, we found that a perturbation for each design parameter of 1% of its nominal value leads to an acceptable solution.

Figure 4.2 shows the $|S_{11}|$ of the initial design and the optimal design using both forward finite-difference (FFD) and FDFD-SASA method. The response Jacobian is calculated at all 22 frequency points of interest. Note that each of these Jacobians is a continuous function in the design-parameter space although the Jacobian of the minimax objective function is not. The minimax optimization algorithms operate with the complete set of Jacobians. Figure 4.3 and Figure 4.4 show the parameter step size and the objective function versus the iterations when using TR-minimax with both sensitivity-analysis techniques. FDFD-SASA method converges with $F = -0.0009564$, while FFD method converges with $F = -0.001$.

In the four-variable optimization, the initial design is $[L_1 \ L_2 \ L_3 \ L_4]^T = [5\Delta h \ 11\Delta h \ 9\Delta h \ 13\Delta h]^T = [3.115 \ 6.8453 \ 5.6007 \ 8.0899]^T$ (all in mm). Here, the FDFD-SASA method converges with $F = -0.01569$ and the FFD method converges with $F = -0.01381$. Figure 4.5 to 4.7 illustrate the $|S_{11}|$ of the

initial design and the optimal design, the parameter step size and the objective function versus the iterations.

In both optimization cases, we use the same termination criteria: $\Delta_p^{(k)} = \frac{\| \mathbf{p}^{(k+1)} - \mathbf{p}^{(k)} \|}{\| \mathbf{p}^{(k)} \|} \leq 0.001$ and/or $\Delta_F^{(k)} = |F^{(k+1)} - F^{(k)}| \leq \varepsilon$, where $\varepsilon = 0.009$ is the convergence error of the mesh refinement in HFSS.

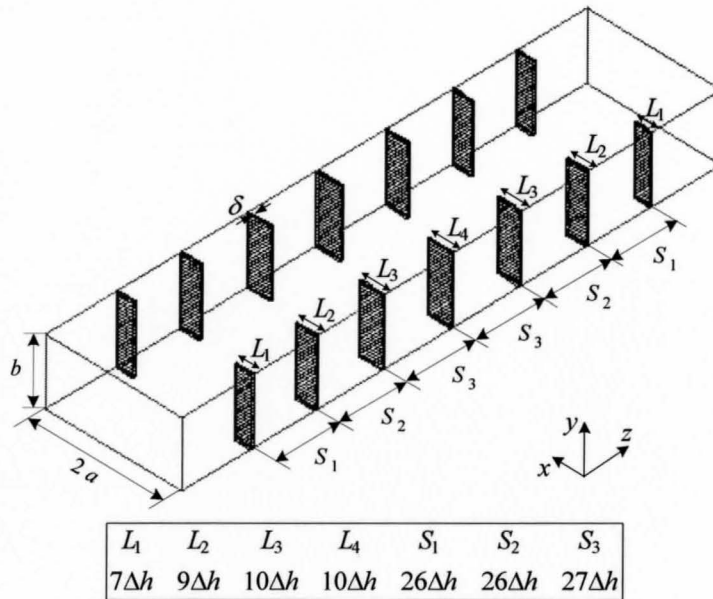


Figure 4.1 Six-section H-plane filter.

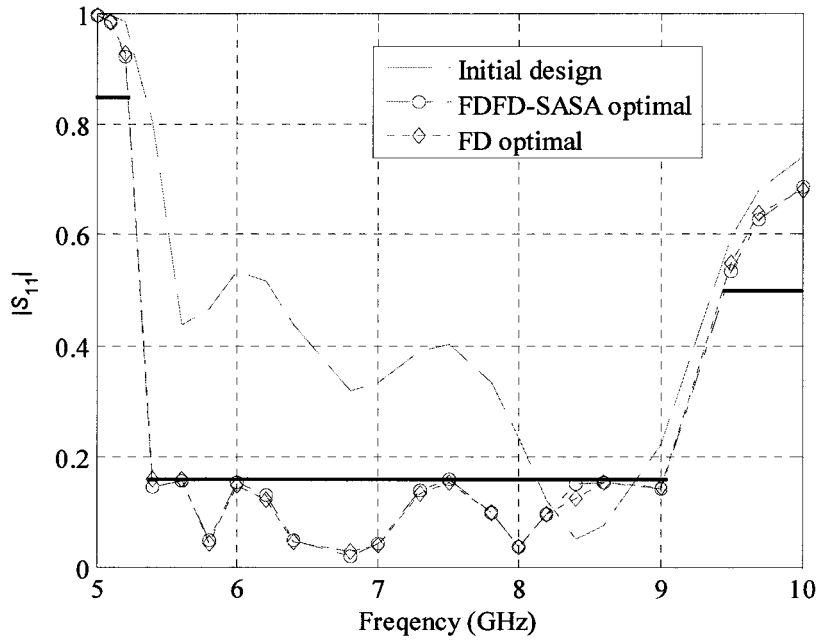


Figure 4.2 $|S_{11}|$ with respect to frequency at initial design and optimal design with two parameters.

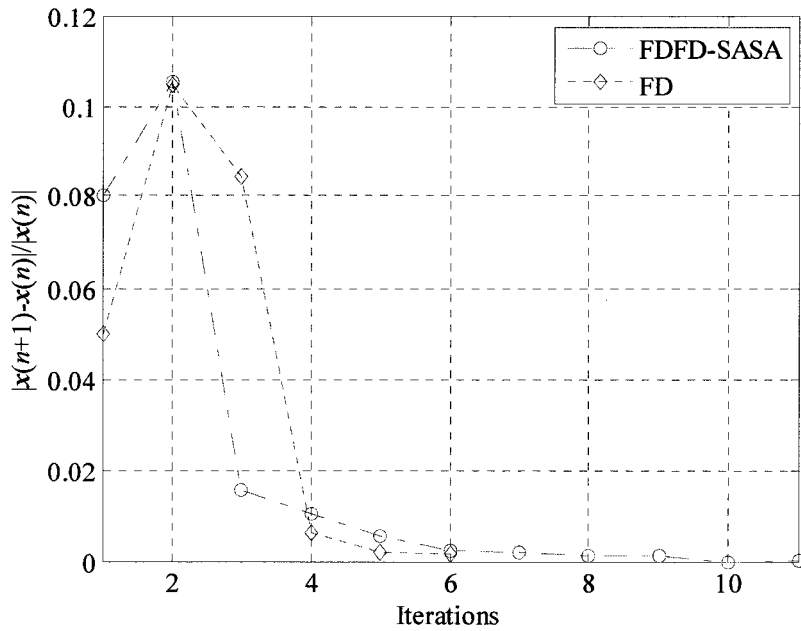


Figure 4.3 Parameter step size vs. optimization iterations in the TR-minimax optimization of the H-plane filter with two parameters.

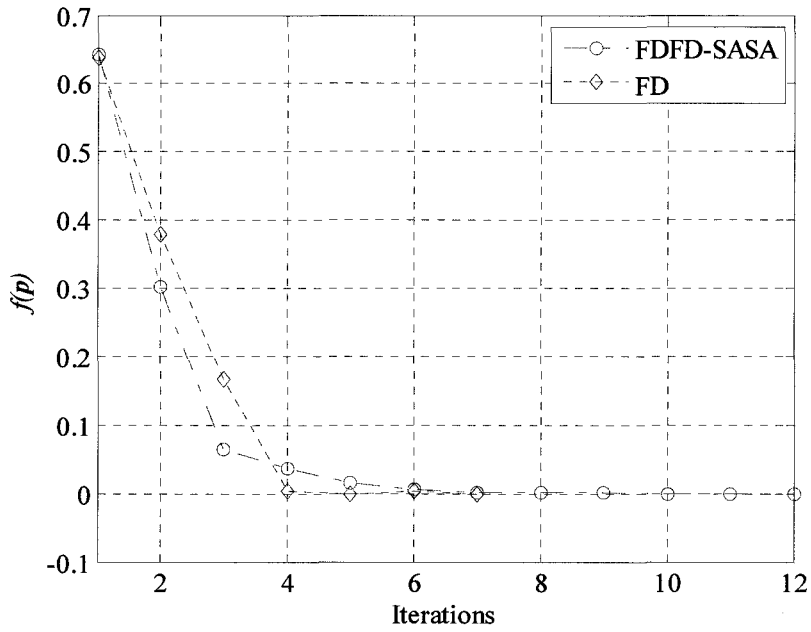


Figure 4.4 Objective function vs. optimization iterations in the TR-minimax optimization of the H-plane filter with two parameters.

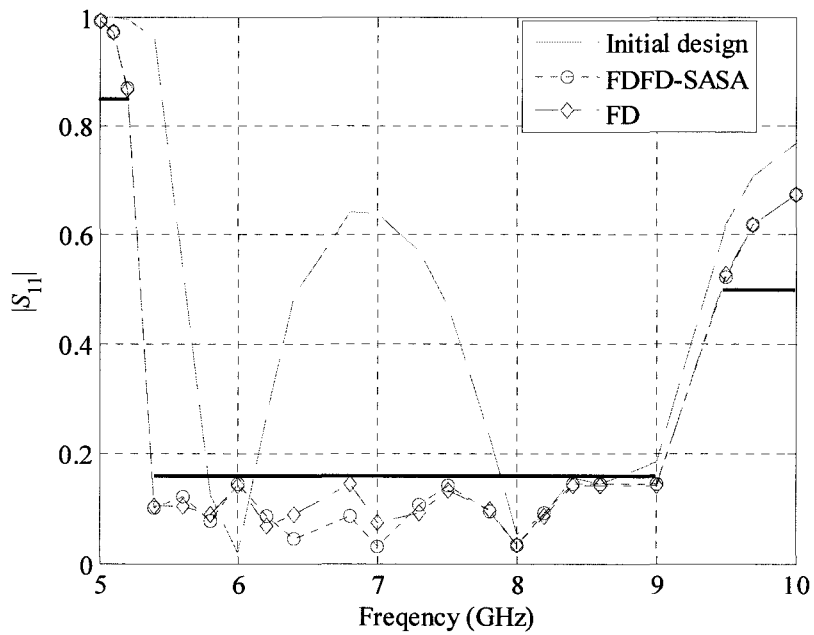


Figure 4.5 $|S_{11}|$ with respect to frequency at initial design and optimal design with four parameters.

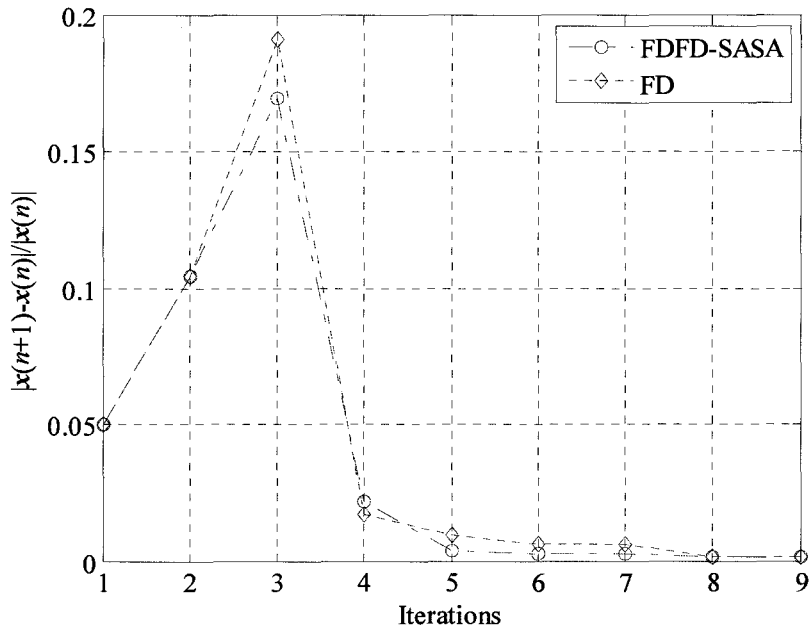


Figure 4.6 Parameter step size vs. optimization iterations in the TR-minimax optimization of the H-plane filter with four parameters.

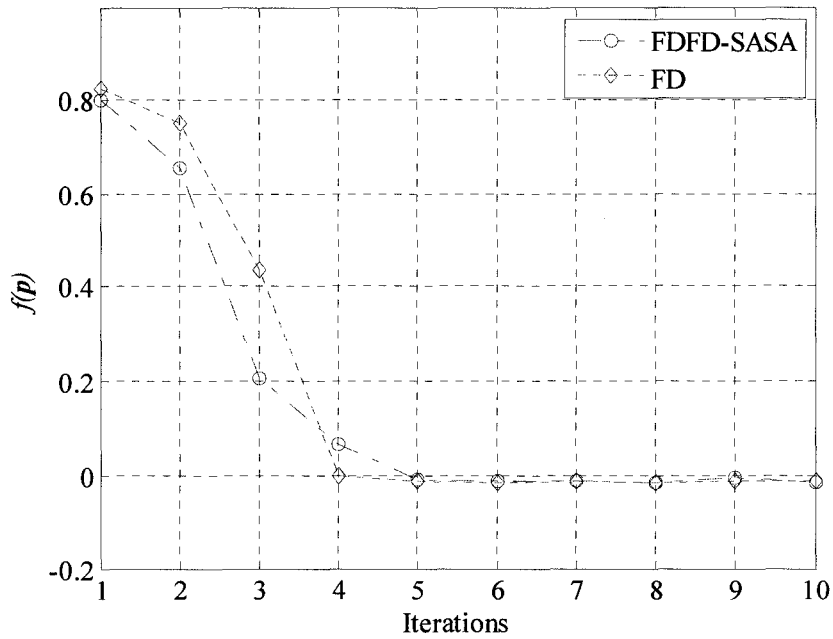


Figure 4.7 Objective function vs. optimization iterations in the TR-minimax optimization of the H-plane filter with four parameters.

4.4 COMPARISON AND CONCLUSION

We compare the efficiency of the algorithms in terms of CPU time and iteration numbers in this section.

In Table 4.1, the optimal designs achieved by the TR-minimax using FDFD-SASA and FFD approaches for two variables are compared. Table 4.2 provides the design values obtained from the optimization processes for four variables. Table 4.3 shows the number of iterations and the time cost of the two optimization processes for two variables. We notice in Table 4.3 that FFD takes longer than FDFD-SASA. This is due to the fact that FFD calls for a system analysis several times per iteration to compute the system matrix in order to determine the next step in the parameter space. FDFD-SASA needs only one system analysis per iteration. As Table 4.3 shows, TR-minimax with FFD sensitivities takes 6 iterations to converge. The time required by FDFD-SASA to compute the Jacobian is about 0.031 s. One FEM simulation (full frequency sweep) of the structure takes about 537 s. One system analysis (full frequency sweep) involves obtaining the S_{11} parameter and its 2 derivatives with respect to the design parameters. To accomplish this, 3 FEM simulations are necessary using the FFD sensitivity analysis (approximately $537 \times 3 = 1611$ s per system analysis). These times vary slightly from iteration to iteration and the above values are average. The simulation time ($7 \times 1611 = 11277$ s) accounts for almost all the time for of the optimization process. This derivative-estimation overhead is

Table 4.1 OPTIMAL DESIGNS USING DIFFERENT SENSITIVITY ANALYSIS METHODS WITH TR-MINIMAX (2 VARIABLES)

(all in mm)	L_3	L_4
FFD	5.8362	6.1957
FDFD-SASA	5.8503	6.2037

Table 4.2 OPTIMAL DESIGNS USING DIFFERENT SENSITIVITY ANALYSIS METHODS WITH TR-MINIMAX (4 VARIABLES)

(all in mm)	L_1	L_2	L_3	L_4
FFD	4.3732	5.3892	5.8185	5.9821
FDFD-SASA	4.4680	5.3042	5.9099	5.9024

Table 4.3 NUMBER OF ITERATIONS AND TIME COMPARISON BETWEEN DIFFERENT SENSITIVITY ANALYSIS METHODS (2 VARIABLES)

	FFD	FDFD-SASA
Optimization iterations	7	12
Calls for EM simulation	21	12
Response computation (s)	3759	6444
Jacobian estimation (s)	9666	668
Total optimization time (s)	16423	7380

Table 4.4 NUMBER OF ITERATIONS AND TIME COMPARISON BETWEEN DIFFERENT SENSITIVITY ANALYSIS METHODS (4 VARIABLES)

	FFD	FDFD-SASA
Optimization iterations	10	10
Calls for EM simulation	50	10
Response computation (s)	5370	5370
Jacobian estimation (s)	21480	1536
Total optimization time (s)	32063	7216

reduced to 668 s in FDFD-SASA. However, a significant portion of this time (666s) is spent in exporting field information from HFSS and then reading back the files. Similar trends can be noticed in the optimization with 4 parameters.

Our method offers more than 10 times reduction of the time required by the Jacobian calculation. The reduction of the overhead of the sensitivity calculation as well as the overall time of the optimization process becomes increasingly pronounced as the number of optimizable parameters increase.

We conclude from this example that the time cost reduction offered by the FDFD-SASA method is significant when compared with the optimization exploiting response-level sensitivities, where finite differences are used to compute the system matrix derivatives. At the same time, the optimization results are nearly the same as those obtained by the optimization algorithms based on the finite-difference response level approximation. The time savings depend on the optimization algorithms, as well as the numerical size of the problem. The computational gain increases as the number of optimizable parameters increases and the size of the FEM system matrix increases. For electrically large 3-D problems with many design parameters, the time savings are very significant.

REFERENCES

- [1] A. D. Belegundu and T. R. Chandrupatla, *Optimization Concepts and Applications in Engineering Optimization*. Upper Saddle River, NJ: Prentice Hall, 1999, pp. 56-91, 259-278.
- [2] J. Robinson and Y. Rahmat-Samii, "Particle swarm optimization in electromagnetics," *IEEE Trans. Antennas Propagat.*, vol. 52, pp. 397-407, Feb. 2004.
- [3] J. E. Rayas-Sanchez, "EM-based optimization of microwave circuits using artificial neural networks: the state-of-the-art," *IEEE Trans. Microwave Theory Tech.*, vol. 52, pp. 420-435, Jan. 2004.
- [4] N. K. Nikolova, J. Zhu, D. Li, M. H. Bakr and J. W. Bandler, "Sensitivity analysis of network parameters with electromagnetic frequency-domain simulators," *IEEE Trans. Microwave Theory Tech.*, vol. 54, pp. 670-681, Feb. 2006.
- [5] X. Zhu, A. Hasib, N.K. Nikolova and M. H. Bakr, "Efficient electromagnetic optimization using self-adjoint jacobian computation based on a central-node FDFD method," *Int. Microwave Symposium (IMS 2008)*, June. 2008.
- [6] Ansoft HFSS ver. 10.1.2, Ansoft Corporation, 225 West Station Square Drive, Suite 200, Pittsburgh, PA 15219, USA, 2006, www.ansoft.com
- [7] G. Matthaei, L. Young and E. M. T. Jones, *Microwave Filters, Impedance-Matching Networks, and Coupling Structures*. Norwood, MA: Artech House, 1980, pp. 545-547.
- [8] J. W. Bandler, W. Kellerman and K. Madsen, "A superlinearly convergent minimax algorithm for microwave circuit design," *IEEE Trans. Microwave Theory Tech.*, vol. MTT-33, pp. 1519-1530, Dec. 1985.
- [9] D. Li, J. Zhu, N. K. Nikolova, M. H. Bakr, and J. W. Bandler, "Electromagnetic optimization using sensitivity analysis in the frequency domain," *IET Proc. Microwaves, Antennas & Propagation*, vol. 1, No. 4, pp. 852-859, Aug. 2007.

CHAPTER 5

CONCLUSIONS

In this thesis, we propose a general approach to the sensitivity analysis of the network parameters based on full-wave electromagnetic solvers. The approach is referred to as the finite-difference frequency-domain self-adjoint sensitivity analysis (FDFD-SASA). Compared with the traditional finite-difference (FD) approximation, the traditional exact adjoint-variable method (AVM), and our previous frequency-domain SASA formulations described in Chapter 2, our method is significantly more efficient. It requires only one full-wave simulation to compute the responses and their sensitivities with respect to all design parameters. There is no need for system matrix derivatives or any other manipulation of the system matrix. The FDFD-SASA computational overhead is negligible in comparison with a full-wave simulation. We also investigate applications of the FDFD-SASA method with gradient-based optimization.

In Chapter 2, we review the theory of the traditional AVM, both with real and complex linear systems. We compare the required computational resources of the AVM and the response-level FD method. Also, we point out the difficulties in

the implementation of the classical AVM with commercial electromagnetic simulators. We then discuss the self-adjoint sensitivity method in the frequency domain and delineate its advantages over the AVM.

We introduce the FDFD-SASA method in Chapter 3. We mention the problems with previous SASA method and also discuss how FDFD-SASA overcomes them. We validate the FDFD-SASA method using numerical examples and compare its computational efficiency with that of the CFD method. In this implementation, our FDFD-SASA algorithm uses finite-difference grid and field solutions in the frequency domain. The results indicate that the FDFD-SASA is at least 10 times faster than the CFD method, depending on the size of the problem. We investigate both Yee-cell and central-node implementations for our user defined grids and test their accuracy. We also conclude from the error estimation that both approaches have comparable accuracy. We notice that as opposed to FD estimates, our approaches yield identical results regardless of the direction of perturbation. We also develop a new 3-D sensitivity analysis method for metallic objects based on our central-node implementations. This implementation completes our investigation of sensitivity analysis of metallic structures. We discuss both metallization and de-metallization cases for 3-D analysis. We then provide an outline for software algorithm to implement these cases with high-level programming languages.

In Chapter 4, we investigate the application of the FDFD-SASA in gradient-based optimization processes where it provides the Jacobian. We test the method with both response-level FD and FDFD-SASA as Jacobian providers. The numerical results suggest significant time saving when using FDFD-SASA and in comparison with the response-level finite differences.

Further research should focus on complex metallic structures and structures with both metallic and dielectric elements in them.

Also, further investigation regarding the implementation of the FDFD-SASA with various optimization engines should be conducted to further strengthen its contribution to time savings.

Future studies can also examine the implementation of FDFD-SASA with other PDE based frequency-domain solvers besides HFSS.

Finally, a full-fledged CAD framework incorporating our newly proposed sensitivity method should be developed. Such a framework will bring about a breakthrough in microwave CAD automation.

COMPLETE REFERENCE LIST

Chapter 1

- [1] D. G. Cacuci, *Sensitivity & Uncertainty Analysis, Volume 1: Theory*. Boca Raton, FL: Chapman & Hall/CRC, 2003.
- [2] A. D. Belegundu and T. R. Chandrupatla, *Optimization Concepts and Applications in Engineering*. Upper Saddle River, NJ: Prentice Hall, 1999.
- [3] E. J. Haug, K. K. Choi and V. Komkov, *Design Sensitivity Analysis of Structural Systems*. Orlando: Academic Press Inc., 1986.
- [4] S. W. Director and R. A. Rohrer, "The generalized adjoint network and network sensitivities," *IEEE Trans. Circuit Theory*, vol. CT-16, pp.318-323, Aug. 1969.
- [5] J. W. Bandler and R. E. Seviara, "Current trends in network optimization," *IEEE Trans. Microwave Theory Tech.*, vol. MTT-18, pp.1159-1170, Dec. 1970.
- [6] V. A. Monaco and P. Tiberio, "Computer-aided analysis of microwave circuits," *IEEE Trans. Microwave Theory Tech.*, vol. MTT-22, pp.249-263, Mar. 1974.
- [7] J. W. Bandler, "Computer-aided circuit optimization," in *Modern Filter Theory and Design*, G. C. Temes and S. K. Mitra, Eds. New York: Wiley, 1973, ch. 6.
- [8] K. C. Gupta, R. Garg, and R. Chadha, *Computer-Aided Design of Microwave Circuits*. Norwood, MA: Artech House, 1981.
- [9] J. Vlach and K. Singhal, *Computer Methods for Circuit Analysis and Design*. New York: Van Nostrand, 1983.
- [10] J. W. Bandler and R. E. Seviara, "Wave sensitivities of networks," *IEEE Trans. Microwave Theory Tech.*, vol. MTT-20, pp. 138-147, Feb. 1972.

- [11] M. H. Bakr and N. K. Nikolova, "An adjoint variable method for time-domain TLM with wide-band Johns matrix boundaries," *IEEE Trans. Microwave Theory Tech.*, vol. 52, pp. 678-685, Feb. 2004.
- [12] N. K. Nikolova, H. W. Tam, and M. H. Bakr, "Sensitivity analysis with the FDTD method on structured grids," *IEEE Trans. Microwave Theory Tech.*, vol. 52, pp. 1207-1216, Apr. 2004.
- [13] M. H. Bakr and N. K. Nikolova, "An adjoint variable method for frequency domain TLM problems with conducting boundaries," *IEEE Microwave and Wireless Component Letters*, vol. 13, pp. 408-410, Sept. 2003.
- [14] S. M. Ali, N. K. Nikolova, and M. H. Bakr, "Central adjoint variable method for sensitivity analysis with structured grid electromagnetic solvers," *IEEE Trans. Magnetics*, vol. 40, pp. 1969-1971, Jul. 2004.
- [15] N. K. Georgieva, S. Glavic, M. H. Bakr and J. W. Bandler, "Feasible adjoint sensitivity technique for EM design optimization," *IEEE Trans. Microwave Theory Tech.*, vol. 50, pp. 2751-2758, Dec. 2002.
- [16] H. Akel and J. P. Webb, "Design sensitivities for scattering-matrix calculation with tetrahedral edge elements," *IEEE Trans. Magnetics*, vol. 36, pp. 1043-1046, Jul. 2000.
- [17] Hong-bae Lee and T. Itoh, "A systematic optimum design of waveguide-to-microstrip transition," *IEEE Trans. Microwave Theory Tech.*, vol. 45, pp. 803-809, May 1997.
- [18] N. K. Nikolova, J. Zhu, D. Li, M. Bakr, and J. Bandler, "Sensitivities of network parameters with electromagnetic frequency domain simulator," *IEEE Trans. Microwave Theory Tech.* vol. 54, pp. 670-681, Feb. 2006.
- [19] S. M. Ali, N. K. Nikolova and M. H. Bakr, "Recent advances in sensitivity analysis with frequency-domain full-wave EM solvers," *Appl. Comput. Electromagn. Soc. J.*, vol. 19, pp. 147-154, Nov. 2004.
- [20] N. K. Nikolova, J. Zhu, D. Li, M. Bakr, and J. Bandler, "Sensitivities of network parameters with electromagnetic frequency domain simulator," *IEEE Trans. Microwave Theory Tech.* vol. 54, pp. 670-681, Feb. 2006.
- [21] N. K. Nikolova, Ying Li, Yan Li, and M. H. Bakr, "Sensitivity analysis of scattering parameters with electromagnetic time-domain simulators," *IEEE Trans. Microw. Theory Tech.*, vol. 54, pp. 1589-1610, Apr. 2006.
- [22] Y. Song and N. K. Nikolova, "Central-node approach for accurate self-adjoint sensitivity analysis of dielectric structures," *IEEE MTT-S Int. Microwave Symposium*, pp. 895-898, June 2007.

- [23] X. Zhu, A. Hasib, and N. K. Nikolova, "Electromagnetic sensitivity analysis of scattering parameters based on the FDFD method," *Int. Symp. on Signals, Systems, and Electronics (ISSSE 2007)*, pp. 165-168, July-Aug. 2007.
- [24] N. K. Nikolova, R. Safian, E. A. Soliman, M. H. Bakr and J. Bandler, "Accelerated gradient based optimization using adjoint sensitivities," *IEEE Trans. Antenna Propagat.*, vol. 52, pp. 2147-2157, Aug. 2004.
- [25] N. K. Nikolova, A. Hasib and X. Zhu, "Independent sensitivity solver based on the frequency domain finite difference method," *Applied Computational Electromagnetics Society (ACES 2008)*, pp. 1024-1029, March-Apr. 2008.
- [26] X. Zhu, A. Hasib, N. K. Nikolova and M. H. Bakr, "Efficient electromagnetic optimization using self-adjoint jacobian computation based on a central-node FDFD method," *Int. Microwave Symposium (IMS 2008)*, June 2008.
- [27] Ansoft HFSS ver. 11, Ansoft Corporation, 225 West Station Square Drive, Suite 200, Pittsburgh, PA 15219, USA, 2006, www.ansoft.com.

Chapter 2

- [1] N. K. Nikolova, *et al.*, "Accelerated gradient based optimization using adjoint sensitivities," *IEEE Trans. Antenna Propagat.*, vol. 52, pp. 2147-2157, Aug. 2004.
- [2] D. G. Cacuci, *Sensitivity & Uncertainty Analysis, Volume 1: Theory*. Boca Raton, FL: Chapman & Hall/CRC, 2003.
- [3] A. D. Belegundu and T. R. Chandrupatla, *Optimization Concepts and Applications in Engineering*. Upper Saddle River, NJ: Prentice Hall, 1999.
- [4] E. J. Haug, K. K. Choi and V. Komkov, *Design Sensitivity Analysis of Structural Systems*. Orlando: Academic Press Inc., 1986.
- [5] J. W. Bandler, "Computer-aided circuit optimization," in *Modern Filter Theory and Design*, G. C. Temes and S. K. Mitra, Eds. New York: Wiley, 1973, ch. 6.

- [6] S. M. Ali, N. K. Nikolova, and M. H. Bakr, "Recent advances in sensitivity analysis with frequency-domain full-wave EM solvers," *Applied Computational Electromagnetics Society Journal*, vol. 19, pp. 147-154, Nov. 2004.
- [7] M. H. Bakr and N. K. Nikolova, "An adjoint variable method for frequency domain TLM problems with conducting boundaries," *IEEE Microwave and Wireless Components Letters*, vol. 13, pp. 408-410, Sept. 2003.
- [8] N. K. Georgieva, S. Glavic, M. H. Bakr, and J. W. Bandler, "Feasible adjoint sensitivity technique for EM design optimization," *IEEE Trans. Microwave Theory Tech.*, vol. 50, pp. 2751-2758, Dec. 2002.
- [9] H. Akel and J. P. Webb, "Design sensitivities for scattering-matrix calculation with tetrahedral edge elements," *IEEE Trans. Magnetics*, vol. 36, pp. 1043-1046, July 2000.
- [10] N. K. Nikolova, J. W. Bandler, and M. H. Bakr, "Adjoint techniques for sensitivity analysis in high-frequency structure CAD," *IEEE Trans. Microwave Theory Tech.*, vol. 52, No. 1, pp. 403-419, Jan. 2004.
- [11] M. D. Greenberg, *Advanced Engineering Mathematics*. Upper Saddle River, NJ: Prentice Hall, 1998, pp. 605.
- [12] J. Ureel and D. De Zutter, "Shape sensitivities of capacitances of planar conducting surfaces using the method of moments," *IEEE Trans. Microwave Theory Tech.*, vol. 44, pp. 198-207, Feb. 1996.
- [13] J. Ureel and D. De Zutter, "A new method for obtaining the shape sensitivities of planar microstrip structures by a full-wave analysis," *IEEE Trans. Microwave Theory Tech.*, vol. 44, pp. 249-260, Feb. 1996.
- [14] N. K. Georgieva, S. Glavic, M. H. Bakr, and J. W. Bandler, "Feasible adjoint sensitivity technique for EM design optimization," *IEEE Trans. Microwave Theory Tech.*, vol. 50, pp. 2751-2758, Dec. 2002.
- [15] E. B. Saff and A. D. Snider, *Fundamentals of Complex Analysis*. Englewood Cliffs, NJ: Prentice Hall, Inc., 1976.
- [16] O. C. Zienkiewicz and Y. K. Cheung, "Finite elements in the solution of field problems," *The Engineer*, vol. 200, pp. 507-510, 1965.

- [17] J. Jin, *The Finite Element Method in Electromagnetics*, 2nd ed. New York: John Wiley & Sons, 2002.
- [18] N. K. Nikolova, J. Zhu, D. Li, M. H. Bakr, and J. W. Bandler, "Sensitivity analysis of network parameter with electromagnetic frequency-domain simulators," *IEEE Trans. Microwave Theory Tech.*, vol. 54, pp. 670-681, Feb. 2006.
- [19] M. Salazar-Palma, T. K. Sarkar, L.-E. García-Castillo, T. Roy, A. Djordjević, *Iterative and Self-Adaptive Finite-Elements in Electromagnetic Modeling*. Norwood, MA: Artech, 1998, pp. 465-466.
- [20] E. A. Soliman, M. H. Bakr, and N. K. Nikolova, "Accelerated gradient-based optimization of planar circuits," *IEEE Trans. Antennas Propagat.*, vol. 53, pp. 880-883, Feb. 2005.

Chapter 3

- [1] D. G. Cacuci, *Sensitivity & Uncertainty Analysis, Volume 1: Theory*. Boca Raton, FL: Chapman & Hall/CRC, 2003.
- [2] A. D. Belegundu and T. R. Chandrupatla, *Optimization Concepts and Applications in Engineering*. Upper Saddle River, NJ: Prentice Hall, 1999.
- [3] E. J. Haug, K. K. Choi and V. Komkov, *Design Sensitivity Analysis of Structural Systems*. Orlando: Academic Press Inc., 1986.
- [4] H. Akel and J. P. Webb, "Design sensitivities for scattering-matrix calculation with tetrahedral edge elements," *IEEE Trans. Magnetics*, vol. 36, pp. 1043-1046, July 2000.
- [5] N. K. Nikolova, J. W. Bandler, and M. H. Bakr, "Adjoint techniques for sensitivity analysis in high-frequency structure CAD," *IEEE Trans. Microwave Theory Tech.*, vol. 52, pp. 403-419, Jan. 2004.
- [6] N. K. Georgieva, S. Glavic, M. H. Bakr and J. W. Bandler, "Feasible adjoint sensitivity technique for EM design optimization," *IEEE Trans. Microwave Theory Tech.*, vol. 50, pp. 2751-2758, Dec. 2002.

- [7] S. M. Ali, N. K. Nikolova, and M. H. Bakr, "Recent advances in sensitivity analysis with frequency-domain full-wave EM solvers," *Applied Computational Electromagnetics Society Journal*, vol. 19, pp. 147-154, Nov. 2004.
- [8] N. K. Nikolova, J. Zhu, D. Li, M. H. Bakr and J. W. Bandler, "Sensitivity analysis of network parameters with electromagnetic frequency-domain simulators," *IEEE Trans. Microwave Theory and Tech.*, vol. 54, pp. 670-681, Feb. 2006.
- [9] D. Li, J. Zhu, N. K. Nikolova, M. H. Bakr, and J. W. Bandler, "Electromagnetic optimization using sensitivity analysis in the frequency domain," *IET Proc. Microwaves, Antennas & Propagation*, vol. 1, No. 4, pp. 852-859, Aug. 2007.
- [10] Ansoft HFSS ver. 11, Ansoft Corporation, 225 West Station Square Drive, Suite 200, Pittsburgh, PA 15219, USA, 2006, www.ansoft.com.
- [11] N. K. Nikolova, H. W. Tam, and M. H. Bakr, "Sensitivity analysis with the FDTD method on structured grids," *IEEE Trans. Microwave Theory and Tech.*, vol. 52, pp. 1207-1216, Apr. 2004.
- [12] N. K. Nikolova, Ying Li, Yan Li, and M.H. Bakr, "Sensitivity analysis of scattering parameters with electromagnetic time-domain simulators," *IEEE Trans. Microwave Theory Tech.*, vol. 54, pp. 1598-1610, 2006.
- [13] J. Jin, *The Finite Element Method in Electromagnetics*, 2nd ed. New York: John Wiley & Sons, 2002.
- [14] Y. Song and N.K. Nikolova, "Central-node approach for accurate self-adjoint sensitivity analysis of dielectric structures," *IEEE MTT-S Int. Microwave Symposium*, pp. 895-898, June 2007.
- [15] X. Zhu, A. Hasib, and N.K. Nikolova, "Electromagnetic sensitivity analysis of scattering parameters based on the FDFD method," *Int. Symp. on Signals, Systems, and Electronics (ISSSE 2007)*, pp. 165-168, July-Aug. 2007.
- [16] N. K. Nikolova, A. Hasib and X. Zhu, "Independent sensitivity solver based on the frequency domain finite difference method," *Applied Computational Electromagnetics Society (ACES 2008)*, pp. 1024-1029, March-Apr. 2008.

- [17] G. Matthaei, L. Young, and E. M. T. Jones, *Microwave Filters, Impedance-matching Networks, and Coupling Structures*. Norwood, MA: Artech House, 1980, p. 545.
- [18] X. Zhu, A. Hasib and N. K. Nikolova, "Efficient electromagnetic optimization using self-adjoint Jacobian computation based on a central-node FDFD method," *IEEE MTT-S Int. Microwave Symposium*, June 2008.

Chapter 4

- [1] A. D. Belegundu and T. R. Chandrupatla, *Optimization Concepts and Applications in Engineering Optimization*. Upper Saddle River, NJ: Prentice Hall, 1999, pp. 56-91, 259-278.
- [2] J. Robinson and Y. Rahmat-Samii, "Particle swarm optimization in electromagnetics," *IEEE Trans. Antennas Propagat.*, vol. 52, pp. 397-407, Feb. 2004.
- [3] J. E. Rayas-Sanchez, "EM-based optimization of microwave circuits using artificial neural networks: the state-of-the-art," *IEEE Trans. Microwave Theory Tech.*, vol. 52, pp. 420-435, Jan. 2004.
- [4] N. K. Nikolova, J. Zhu, D. Li, M. H. Bakr and J. W. Bandler, "Sensitivity analysis of network parameters with electromagnetic frequency-domain simulators," *IEEE Trans. Microwave Theory Tech.*, vol. 54, pp. 670-681, Feb. 2006.
- [5] X. Zhu, A. Hasib, N.K. Nikolova and M. H. Bakr, "Efficient electromagnetic optimization using self-adjoint jacobian computation based on a central-node FDFD method," *Int. Microwave Symposium (IMS 2008)*, June. 2008.
- [6] Ansoft HFSS ver. 10.1.2, Ansoft Corporation, 225 West Station Square Drive, Suite 200, Pittsburgh, PA 15219, USA, 2006, www.ansoft.com
- [7] G. Matthaei, L. Young and E. M. T. Jones, *Microwave Filters, Impedance-Matching Networks, and Coupling Structures*. Norwood, MA: Artech House, 1980, pp. 545-547.

- [8] J. W. Bandler, W. Kellerman and K. Madsen, "A superlinearly convergent minimax algorithm for microwave circuit design," *IEEE Trans. Microwave Theory Tech.*, vol. MTT-33, pp. 1519-1530, Dec. 1985.
- [9] D. Li, J. Zhu, N. K. Nikolova, M. H. Bakr, and J. W. Bandler, "Electromagnetic optimization using sensitivity analysis in the frequency domain," *IET Proc. Microwaves, Antennas & Propagation*, vol. 1, No. 4, pp. 852-859, Aug. 2007.